Felipe Ramirez Cortes

Gesture Recognition for Prosthesis Control using Electromyography and Force Myography based on Optical Fiber Sensors

Vitória - ES

2025

Felipe Ramirez Cortes

Gesture Recognition for Prosthesis Control using Electromyography and Force Myography based on Optical Fiber Sensors

Federal University of Espírito Santo

Technological Center

Graduate Program in Electrical Engineering

Supervisor: Prof. Dr. Camilo Arturo Rodríguez Díaz

Co-supervisor: Prof. Dr. Marcelo Eduardo Vieira Segatto

Vitória - ES

2025

Ficha catalográfica disponibilizada pelo Sistema Integrado de Bibliotecas - SIBI/UFES e elaborada pelo autor

---

Ramirez Cortes, Felipe, 2000-
R173g Gesture recognition for prosthesis control using electromyography and force myography based on optical fiber sensors / Felipe Ramirez Cortes. - 2025.
89 f. : il.

Orientador: Camilo Arturo Rodríguez Díaz.
Coorientador: Marcelo Eduardo Vieira Segatto.
Dissertação (Mestrado em Engenharia Elétrica) - Universidade Federal do Espírito Santo, Centro Tecnológico.

1. Prótese. 2. Eletromiografia. 3. Fibras ópticas. 4. Instrumentos ópticos. 5. Realidade virtual. I. Rodríguez Díaz, Camilo Arturo. II. Vieira Segatto, Marcelo Eduardo. III. Universidade Federal do Espírito Santo. Centro Tecnológico. IV. Título.

CDU: 621.3

Dissertation approved. Vitória - ES, September 17, 2025:

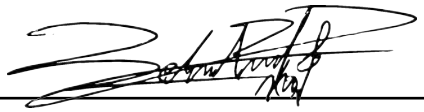

Prof. Dr. Camilo Arturo Rodríguez Díaz
Advisor
Graduate Program in Electrical Engineering/
Federal University of Espírito Santo

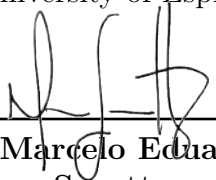

Prof. Dr. Marcelo Eduardo Vieira Segatto
Co-advisor
Graduate Program in Electrical Engineering/
Federal University of Espírito Santo

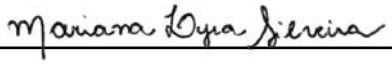

Prof. Dr. Mariana Lyra Silveira
Member of the review board
Graduate Program in Electrical Engineering/
Federal University of Espírito Santo

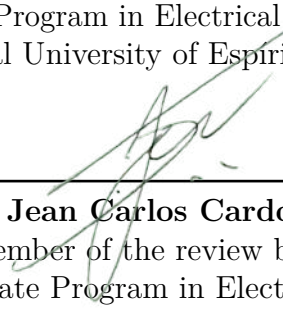

Prof. Dr. Jean Carlos Cardozo da Silva
Member of the review board
Graduate Program in Electrical and
Computer Engineering/ Federal University
of Technology, Paraná

Vitória - ES
2025

Acknowledgements

I am deeply grateful to everyone who contributed to making this work a reality. First and most important, I thank my family for their unconditional love and support through this journey. To my father, Oscar Ramirez, whose dedication and effort have always been for my happiness, and to my mother, Lina López, who taught me that love knows no conditions. To my grandmother, Mery Robayo, A pillar in my growth, and to my grandmother, Zoyla Ortega, whose memory and light from heaven continue to inspire me every day.

I want to thank my advisor, Prof. Camilo A. Rodriguez Diaz, whose patience, guidance, and judgment made this achievement possible, and my co-advisor, Prof. Marcelo E. Vieira Segatto, for providing the right environment for this work to be carried out. In addition, I would like to thank all the professors at UFES who were teaching me, as the knowledge they provided was crucial to this work.

I am thankful to the LabTel group and my colleagues for their invaluable collaboration and warm welcome from the very first day. My most sincere gratitude also goes to my friends, Juan C. Maldonado and Rosa Puentes, for their emotional support in challenging moments, and to Bianca Paulino and her family for opening their home and hearts to me.

Finally, I gratefully acknowledge the financial support provided by the funding agencies: FAPES (EXTRATO ATA DA 6ª REUNIAO CCAF/2022 – "CPID 2.2", FAPES/CNPq/Decit – PPSUS 17/2024), CNPq (306323/2024-9, 404111/2023-8, and 402739/2024-8), Finep (Tec Assistiva 2 – 2132/22), and IEEE RAS SPARX.

Resumo

A amputação é a perda parcial ou total de um membro. É um evento desafiador que afeta pessoas em todo o mundo, com uma prevalência estimada de 552,45 milhões em 2019 e uma taxa crescente. A perda de um membro superior, em particular, afeta fortemente a capacidade de uma pessoa realizar atividades da vida diária (AVD), comunicar-se e interagir com seu ambiente. Para restaurar a funcionalidade perdida, foram desenvolvidos dispositivos auxiliares conhecidos como próteses. As próteses ativas modernas podem ser controladas interpretando a intenção de movimento do usuário por meio de vários sinais biológicos, como a eletromiografia de superfície (sEMG), que mede a atividade elétrica dos músculos. Embora a sEMG seja um método de controle estabelecido e predominante, ela tem limitações. A forcemiografia (FMG) é uma técnica que mede as mudanças no volume e na pressão muscular durante a contração. Ela surgiu como uma alternativa promissora, oferecendo vantagens como maior estabilidade do sinal e menor sensibilidade a condições da pele, como suor.

Esta dissertação de mestrado propõe e avalia um sistema de sensores híbrido que combina FMG e sEMG para criar um método mais robusto e preciso para a classificação de gestos com as mãos. O sistema integra um sensor FMG desenvolvido sob medida, que usa uma rede de Bragg de fibra (FBG) incorporada em uma estrutura flexível impressa em 3D, com um sensor sEMG comercial. O objetivo principal é melhorar o controle de próteses de mãos reais e virtuais para amputados. O estudo envolveu a gravação de sinais de indivíduos sem deficiências físicas enquanto realizavam tarefas envolvendo diferentes ângulos das mãos e forças de preensão. Os dados do sEMG, FMG e do sistema híbrido combinados foram usados para treinar e testar sete algoritmos diferentes de aprendizado de máquina, com o conjunto de dados dividido em 80% para treinamento e 20% para teste.

Os resultados mostraram que a estratégia de detecção ideal depende da tarefa. Para a classificação de ângulos, o sensor híbrido FMG-sEMG alcançou a maior precisão de 85,62% com o classificador K-Nearest Neighbors (KNN). Para a classificação de força, o sensor sEMG sozinho foi superior, atingindo uma precisão de 92,53% com uma Support Vector Machine (SVM). Além disso, a viabilidade do sistema híbrido para aplicação em tempo real foi validada em um ambiente de Realidade Virtual (VR), onde atingiu 99,83% de precisão na classificação de gestos binários de abrir/fechar a mão. Esta pesquisa demonstra a natureza complementar dos sinais FMG e sEMG, concluindo que uma abordagem multimodal pode ser usada para desenvolver sistemas de controle mais sofisticados, confiáveis e intuitivos para próteses de membros superiores, selecionando a melhor modalidade de detecção para a tarefa desejada.

Palavras-chave: Identificação de gestos, força-miografia, eletromiografia de superfície,

grade de Bragg de fibra, controle de próteses, aprendizado de máquina, realidade virtual.

Abstract

Amputation is the partial or total loss of a limb. It is a challenging event that affects people worldwide, with an estimated prevalence of 552.45 million in 2019 and a growing rate. The loss of an upper limb, in particular, strongly affects a person's ability to perform activities of daily living (ADL), communicate, and interact with their environment. To restore lost functionality, assistive devices known as prostheses have been developed. Modern active prostheses can be controlled by interpreting the user's movement intention through various biological signals, such as Surface Electromyography (sEMG), which measures the electrical activity of muscles. While sEMG is an established and predominant control method, it has limitations. Forcemyography (FMG) is a technique that measures changes in muscle volume and pressure during contraction. It has emerged as a promising alternative, offering advantages such as greater signal stability and reduced sensitivity to skin conditions like sweat.

This master's dissertation proposes and evaluates a hybrid sensor system combining FMG and sEMG to create a more robust and precise method for hand gesture classification. The system integrates a custom-developed FMG sensor, which uses a Fiber Bragg Grating (FBG) embedded within a flexible 3D-printed structure, with a commercial sEMG sensor. The primary goal is to improve the control of real and virtual prosthetic hands for amputees. The study involved recording signals from able-bodied subjects while they performed tasks involving different hand angles and grip forces. Data from the sEMG, FMG, and the combined hybrid system were used to train and test seven different machine learning algorithms, with the dataset split into 80% for training and 20% for testing.

Results showed that the optimal sensing strategy is task-dependent. For angle classification, the hybrid FMG-sEMG sensor achieved the highest accuracy of 85.62% with the K-Nearest Neighbors (KNN) classifier. For force classification, the sEMG sensor alone was superior, reaching an accuracy of 92.53% with a Support Vector Machine (SVM). Furthermore, the hybrid system's feasibility for real-time application was validated in a Virtual Reality (VR) environment, where it achieved 99.83% accuracy in classifying binary open/close hand gestures. This research demonstrates the complementary nature of FMG and sEMG signals, concluding that a multimodal approach can be used to develop more sophisticated, reliable, and intuitive control systems for upper-limb prostheses by selecting the best sensing modality for the desired task.

Keywords: Gesture Identification, Forcemyography, Surface Electromyography, Fiber Bragg Grating, Prosthesis Control, Machine Learning, Virtual Reality.

List of Figures

List of abbreviations and acronyms

AA	Amputee
AAC	Average Amplitude Change
ABS	Acrylonitrile Butadiene Styrene
ADC	Analog-to-Digital Converter
ADL	Activities of Daily Living
ANN	Artificial Neural Networks
AR	Able-bodied
AR	Augmented Reality
AR	Auto-Regressive
AR-PHAM	Prosthetic Hand Assessment Measure in AR
ASS	Absolute value of the Summation of Square root
BD	B-distribution
CAD	Computer-Aided Design
DOF	Degrees of Freedom
DT	Decision Tree
EDC	Extensor Digitorum Communis
EEG	Electroencephalography
EIT	Electrical Impedance Tomography
EMG	Electromyography
FBG	Fiber Bragg Grating
FD	Frequency Domain
FDM	Fused Deposition Modeling
FDS	Flexor Digitorum Superficialis

FIR	Finite Impulse Response
FL	Fuzzy Logic Classifier
FMG	Forcemyography
FR	Frequency Ratio
FSR	Force-Sensing Resistor
HMI	Human-Machine Interfaces
iEMG	Integrated Electromyography
IMU	Inertial Measurement Unit
KNN	k-Nearest Neighbors
KRLS	Kernel Regularized Least Squares
KUR	Kurtosis
LD	Log Detector
LDA	Linear Discriminant Analysis
LSSVM	Least Squares Support Vector Machine
MAV	Mean Absolute Value
MAVS	MAV slope
MCP	Metacarpophalangeal
MdF	Median Frequency
mDWT	Discrete wavelet transform
MHW	Multiple Hamming Windows
ML	Machine learning
MLP	Multi-Layer Perceptrons
MMAV	Modified Mean Absolute Value
MNF	Mean Frequency
MP	Mean Power
MR	Mixed Reality

MU	Motor Unit
MVC	Maximal Voluntary Contraction
NIRS	Near-Infrared Spectroscopy
OFS	Optical Fiber Sensor
OvR	One-vs-Res
PF	Peak Frequency
PIP	Proximal Interphalangeal
PLA	Polylactic Acid
PS	Power Spectrum
PSD	Power Spectral Density
QDA	Quadratic Discriminant Analysis
RDA	Regularized Discriminant Analysis
RF	Random Forest
RMS	Root Mean Square
sEMG	Surface Electromyography
SKW	Skewness
SM	Spectral Movements
SSC	Stretch-Shorten Cycle
SSI	Simple Square Integral
STFT	Short-Time Fourier Transform
SVM	Support Vector Machines
TD	Time Domain
ULP	Upper Limb Prosthesis
UV	Ultraviolet
VAR	Variance
Vib	Vibration

VR	Virtual Reality
VR-BBT	VR Box and Block Test
VR-SHAP	VR Southampton Hand Assessment Procedure
WAMP	Willison Amplitude
WL	Wavelength
WT	Wavelet transform
XR	Extended Reality
ZC	Zero Crossings

Contents

1 Introduction

This masterwork focuses on developing a hand gesture classification system using Forcemyography (FMG) and Surface Electromyography (sEMG) sensors. This system is designed to improve the control of real and virtual prosthetic hands, improving their functionality and usability for amputees. It also shows the construction of the sensor, which is composed of an FMG sensor based on a Fiber Bragg Grating (FBG) sensor embedded in a 3D-printed flexible structure and a commercial sEMG sensor.

The research follows two main paths: the first involves developing and characterizing the FMG sensor to identify the performed gestures accurately, and comparing the FMG with the EMG biological signal by training machine learning algorithms to extract their metrics. This allows for the comparison of the designed sensor's performance against a commercial EMG sensor. The second path centers on applying trained classifiers to control the Digital Twin (DTwin) in a Virtual Reality (VR) serious game, and the PrHand prosthesis currently under development (ARCO et al., 2022), permitting movement validation and enhancing prosthetic control through real-time instrumentation by integrating the developed FMG sensor with the commercial sEMG sensor Shimmer3 EXG.

This chapter presents the motivation for this research and describes its objectives, contributions, and publications. Finally, it describes the organization of the masterwork.

1.1 Motivation

Amputation is the partial or complete loss of a limb, often resulting from trauma, medical illnesses, or a congenital condition (CHOO; KIM; CHANG, 2022; DAS; NAGPAL; BANKURA, 2018). This event affects patients' lives in psychological, social, and physical health aspects (CALABRESE et al., 2023). A recent study highlights the growing importance of this issue, showing that the global incidence and prevalence of amputations increased from 11.37 million and 370.25 million in 1990 to 13.23 million and 552.45 million in 2019, respectively (YUAN et al., 2023).

In particular, the loss of a limb such as the hands or arms has a negative impact on the affected person (MAJOR et al., 2020; PIERRIE R. GLENN GASTON, 2018). Hands are essential for performing activities of daily living (ADLs), communicating, and interacting with the environment. Over the years, devices such as prostheses have been developed to assist patients who suffered an amputation (UNANYAN; BELOV, 2021). Prostheses are assistive devices designed to replace the missing part and restore functionality. Their history traces back to 300 B.C., and remains a vital area of study

due to their widespread use (FINCH GLYN HARVEY HEATH, 2012). Specifically, upper limb prostheses (ULPs) are focused on the missing limbs of the human arm. Technological advances and user requirements highlight the increasing importance of robotic limbs in recovering some of the lost capabilities (BRACK; AMALU, 2021; SIEGEL et al., 2024). Key characteristics used to compare these devices include prosthesis types, degrees of freedom (DOF), control type, controller, number of actuators, weight, and cost. Some of the most commonly used prostheses in academic research are Bebionics and Bebionic 3 with 6 DOF (Ottobock, Duderstadt, Germany), LUKE Arm with 6 DOF (Salt Lake, UT, USA), CyberHand with 16 DOF (Sant'Anna School of Advanced Studies, Pisa, Italy), SmartHand with 16 DOF (Lund, Sweden and Pisa, Italy) and Michelangelo with 2 DOF (Ottobock, Duderstadt, Germany) (NG; NAZARI; ALAM, 2021; KERVER et al., 2023; TAVAKOLI et al., 2015).

These complex devices can be controlled with biological signals because they allow the user's movement intention to be known. The most commonly used in active upper limb prostheses are EMG, FMG, electrical impedance tomography (EIT), electroencephalography (EEG), and near-infrared spectroscopy (NIRS) because it is possible to detect limb and nerve movements with these signals or a combination of them (ZHENG et al., 2022). EMG is predominant and is highly used in the literature because of its comprehensive documentation and early development (JIANG et al., 2023). FMG sensors represent force sensors, generally piezoresistive, capacitive, piezoelectric, optoelectronic, or pneumatic sensors placed in the muscle to measure its variations. They have less electrical interference and a lower sampling rate than EMG sensors, and do not require precise sensor placement or extensive skin preparation (SHERIF; BASSUONI; MEHREZ, 2024). EIT is an imaging technology that measures the variation in impedance of the involved muscles during the performance of a gesture. It is challenging to implement because of the lack of technologies to quantify it, the need for complex algorithms, and the high computational load (HOPE; VANHOLSBEECK; MCDAID, 2018). EEG uses the brain's electrical stimulation during a gesture's performance. It is a novel option, but it brings high costs and a lot of user preparation (ALQAHTANI; AL-NAIB; ALTHOBAITI, 2024). Near-infrared refers to measuring the perfusion level in conjunction with muscle oxygenation. This relatively new method has little adaptation and is limited to the scientific field (KERGET; ÇIL; AKSAKAL, 2024).

In addition, control methods in prostheses include biological signals to translate a user's movement intention into action. The most common methods include EMG and FMG. EMG is a signal that represents the electrical activity in muscle activation. The nervous system controls this signal, which is responsible for controlling muscle contraction and relaxation and is affected by the anatomic and physical properties of the muscle (SUPPIAH et al., 2022; REAZ; HUSSAIN; MOHD-YASIN, 2006). EMG sensors have been used extensively in research since the 1980s and are widely used in gesture identification

systems, even creating commercial solutions based on these devices (AMOR; GHOUL; JEMNI, 2023). Nowadays, gestures are identified by machine learning models, time series approaches, or deep learning architectures, obtaining highly accurate systems, such as the work done by Le Wu *et al.*, which achieved 95% accuracy in 13 motion tasks (EDDY et al., 2024; WU et al., 2022).

FMG refers to muscle activity through the change in pressure when the muscle bulges or recoils during contraction and relaxation. This signal is based on muscle volume changes that affect the pressure between the sensor and the muscle (JIANG et al., 2020). These sensors became a popular method since they are feasible, affordable, have low-level signal processing requirements, and signal stability over time (PRAKASH; SHARMA; SHARMA, 2021). The application of FMG signals for amputees can be tracked to 1966 when Lucaccini *et al.* used muscle motion to activate a pneumatic prosthesis (LUCACCINI et al., 1966; LEI et al., 2021). However, the recent improvement of force sensors triggers the development of FMG sensors with higher accuracy, considering their advantages, such as not requiring precise positioning and not being affected by skin effects such as sweat or contaminants, becoming an alternative to the traditional EMG approach (REHMAN et al., 2023).

However, FMG sensors often include force-sensing resistors (FSR), which suffer from accuracy and repeatability problems due to their creep behavior. Therefore, FMG sensors have been developed using capacitive, optical, and piezoelectric sensors (SCHAUMANN et al., 2024). The study by Yu Tzu Wu *et al.* has shown that FMG sensors based on fiber optic sensors are a good alternative to FSR-based sensors due to immunity to external electromagnetic noise (WU et al., 2020). Since the measurement of muscle deformation is the main objective of this kind of sensor, approaches based on FBG are a promising alternative, as they are highly sensitive to deformation and, thus, to force (GAN et al., 2021). These sensors have many advantages, including affordability, high sensitivity, and high accuracy. Also, their flexibility depends on the housing, which can significantly improve their adaptability for wearable applications. Additionally, unlike flexible electronic sensors, FBGs offer multiplexing (allowing multiple sensing points along a single fiber), immunity to electromagnetic noise, and galvanic isolation, which guarantees safe operation without electrical interference. These characteristics make FBG sensors a suitable option for the construction of an FMG sensor for ADLs (XIAO et al., 2024; **??**).

In addition, training in "Extended Reality" or X-Reality (XR) has improved prosthetic control. XR refers to a set of novel technologies for human-machine interaction, which are VR, augmented reality (AR), and mixed reality (MR) (GABALLA et al., 2022). VR is an immersive environment for interaction, AR is a projection of virtual elements into the real world, and MR is an overlay of virtual elements with the real world. To further enhance, serious games are incorporated, task-oriented activities have proven to be

of great utility and generate great patient engagement (LI et al., 2024; SHARMA et al., 2018).

For these reasons, integrating an FMG sensor based on FBGs and XR training can improve the control of prostheses. Particularly, the PrHand. Because of their high sensitivity to deformation and immunity to electromagnetic noise, FBG sensors will improve the accuracy and robustness of FMG-based control systems. VR serious games training will enhance the user's motor skills, accelerate learning, and improve the real-world performance of the prosthesis. Combining these technologies increases the functionality and usability of the PrHand, a low-cost, underactuated prosthesis, for daily activities by enabling it to function more reliably during flexion and extension movements, especially grasping tasks (LIU et al., 2023).

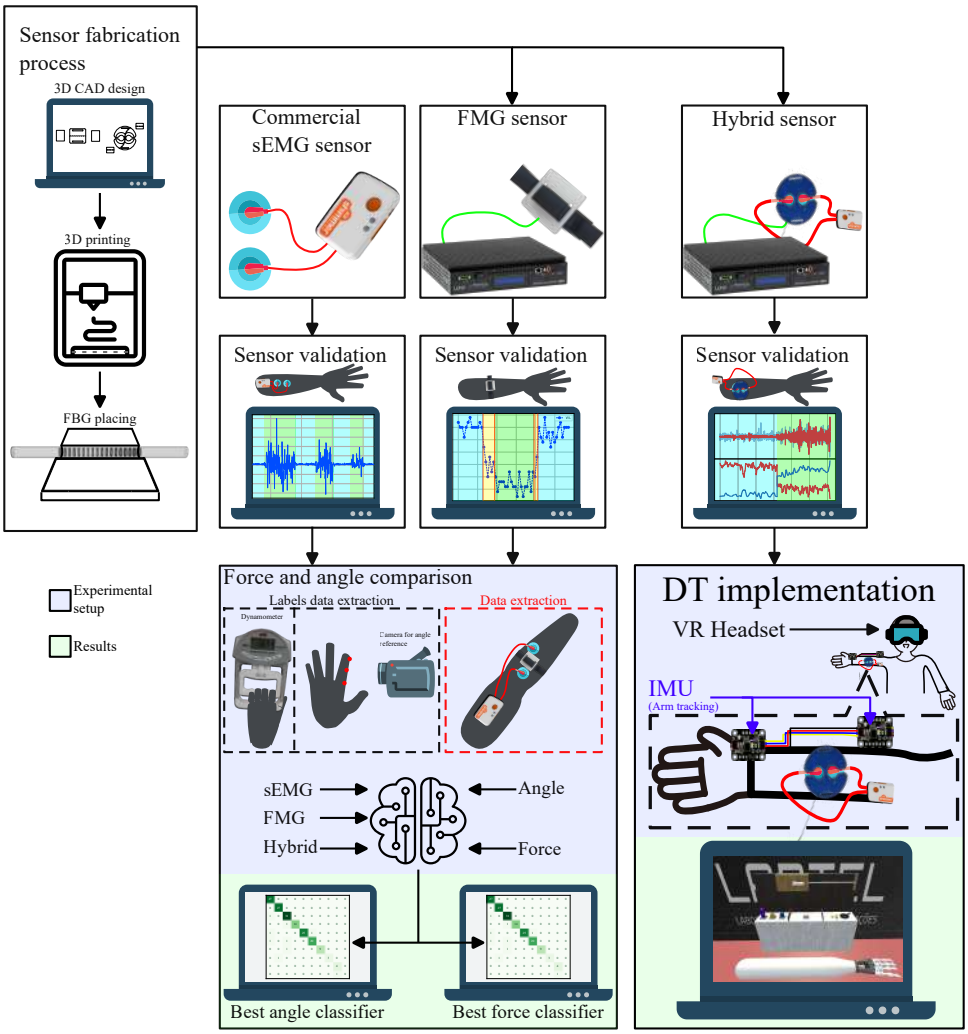

Figure 1 – Master's dissertation framework.

1.2 Framework

The framework of this master's dissertation focuses on two main validation methods for the FMG-sEMG hybrid sensor, which are illustrated in Figure 1. The first method handles a direct comparison of the precision, accuracy, and sensitivity of different machine learning algorithms in classifying grip strength and hand closure angle, utilizing sEMG, FMG, or a hybrid FMG-sEMG signals as input.

The second method utilizes a VR implementation in conjunction with a DTwin of the user's arm during the performance of some ADLs. In this approach, both the arm and the user's intention are captured using two hybrid sensors and two Inertial Measurement Unit (IMU) sensors. The hybrid sensors send information to a pre-trained machine learning model, enabling real-time implementation.

1.3 Objectives

1.3.1 General Objective

This research aims to develop a classification system for hand gestures using an FMG sensor composed of an FBG sensor embedded into a 3D-printed flexible structure and a commercial EMG sensor. This system will control real and virtual hand prostheses and improve their functionality and usability for amputees.

1.3.2 Specific

- To review the state-of-the-art related with hand gesture classification with EMG and FMG.
- To develop and characterize FMG sensors based on additive manufacturing to determine the gesture performed.
- To perform protocols for acquiring FMG and EMG biological signals during the execution of hand gestures to feed machine learning algorithms.
- To train multiple classifiers using machine learning techniques for hand gestures and compare the precision of each.
- To develop a DTwin of the PrHand prosthesis to validate movements and improve prosthesis control.
- To instrument and control the PrHand prosthesis with the commercial EMG sensor and the developed FMG sensor.

1.4 Contributions

1.4.1 The FMG and Hybrid FMG-sEMG sensors

The development of two sensors that aim to analyze the movements the user wishes to perform, facilitating control of both the PrHand physical robotic prosthesis and its DTwin. The FMG sensor uses an FBG sensor to detect physical signals that enable control of the prosthesis. The hybrid sensor integrates the mentioned technology with commercial EMG sensors to create a hybrid FMG-EMG system. This approach provides a more robust and comprehensive understanding of the user's motor intentions.

1.4.2 2D and 3D serious games

Three serious games have been explored in the Unity engine, designed to aid users in training with active prostheses. These games share a central mechanic in which the user's action of opening and closing the hand translates directly into the character's movement within the game. These are: "Flapy-hand", a 2D game in which this hand gesture provides upward propulsion; "Dino", another 2D game in which movement triggers a jump to avoid obstacles; and "Avoid", a 3D experience in which opening and closing the hand controls the horizontal movement of the character to avoid approaching obstacles.

1.4.3 Digital twin and VR serious game

The development of a DTwin of the PrHand prosthesis, giving a detailed 3D representation in VR of the physical PrHand developed in Unity. This virtual prosthesis is dynamically controlled by tracking the user's arm movements, using IMU sensors to accurately interpret the angles of abduction, adduction, flexion, and extension of the shoulder and forearm. To apply this technology, a serious VR object placement game was also created in Unity, which requires users to control the DTwin to perform tasks, such as grasping and placing virtual cubes and cylinders in designated locations within the 3D environment.

1.5 Publications

1. (Conference Proceedings) **Felipe Ramirez Cortes**, Marcelo Eduardo Vieira Segatto, Camilo A. R. Díaz. "Development of a force myography sensor for PrHand prosthesis activation using fiber bragg grating sensor and 3D printing", In 2024 Latin American Workshop on Optical Fiber Sensors (LAWOFS), Campinas, Brazil, 2024. (Presented 20/05/2024).

2. (Conference Proceedings) **Felipe Ramirez Cortes**, María Gaitán-Padilla, Marcelo E. V. Segatto, Maria José Pontes, Carlos A. Cifuentes, Camilo A. R. Díaz. "Accuracy comparison for prosthesis activation using a commercial sEMG sensor and an FMG sensor based on FBG and 3D-printing", Optical Fibers and Sensors for Medical Diagnostics, Treatment, and Environmental Applications XXV (BiOS, PW2025), San Francisco, United States, 2025. (Presented 27/01/2025).

3. (Conference Proceedings) **Felipe Ramirez Cortes**, Laura V. de Arco Barraza, Gustavo Nunes Lopes, Carlos A. Cifuentes, Marcelo Eduardo Vieira Segatto, Camilo A. R. Díaz. "Feasibility of a hybrid FMG-sEMG sensor for prosthetic training in a serious game environment", The 21st SBMO/IEEE MTT-S International Microwave and Optoelectronics Conference (IMOC), Campina Grande, Brazil, 2025. (Submitted).

1.6 Document Organization

This document is divided into five chapters. The first chapter introduces the context of this study, presenting the motivation for each chapter, along with relevant statistics and background information on different types of prostheses and actuation systems, with a particular focus on active EMG-FMG prostheses. Additionally, it discusses sensing technologies for FMG, like FBGs, and serious game implementation in prosthetics.

The second chapter consists of a literature review that discusses state-of-the-art advancements in gesture identification, fiber optic sensors, and serious games for rehabilitation. It starts by analyzing types of prostheses and control strategies and highlighting the integration of EMG and FMG approaches. Then, it explores fiber optic sensors, their functionality, different fiber sensor types, and the relevance of FBGs for biomechanical applications. Finally, it presents an overview of Fused Deposition Modeling (FDM) for fabricating FBG-based sensors and the role of serious games and virtual reality in rehabilitation.

The third chapter outlines the study's methodology. It describes the sensor fabrication process, including material considerations such as filament-based and resin-based approaches. The chapter also presents the experimental setup for sensor validation, detailing the procedures for testing with users, including validation methods using both filament and resin sensors.

The fourth chapter presents the results obtained in this research. Covering sensor characterization using metrology techniques, evaluating precision, accuracy, linearity, and repeatability. Additionally, it discusses the classification of force and angle. Moreover, the chapter details the development and integration of virtual reality tools and 2D/3D DTwin-based serious games used to validate sensor performance with EMG, FMG, and

IMU data. Finally, the fifth chapter presents the work's conclusions and discusses future lines of research and possible improvements to the proposed framework.

2 Upper limb prostheses

Amputation is a procedure that has been used for thousands of years, and in most cases leaves patients with some form of disability (PAUDEL; SHRESTHA; BANSKOTA, 2004; DAS; NAGPAL; BANKURA, 2018). This procedure can be performed in various parts of the limb, and depending on the location, it will be classified within a level of amputation. Upper limb amputation levels are transcarpal, wrist disarticulation, transradial, elbow disarticulation, transhumeral, shoulder disarticulation, and forequarter (CORDELLA et al., 2016). These levels are illustrated in Figure 2.

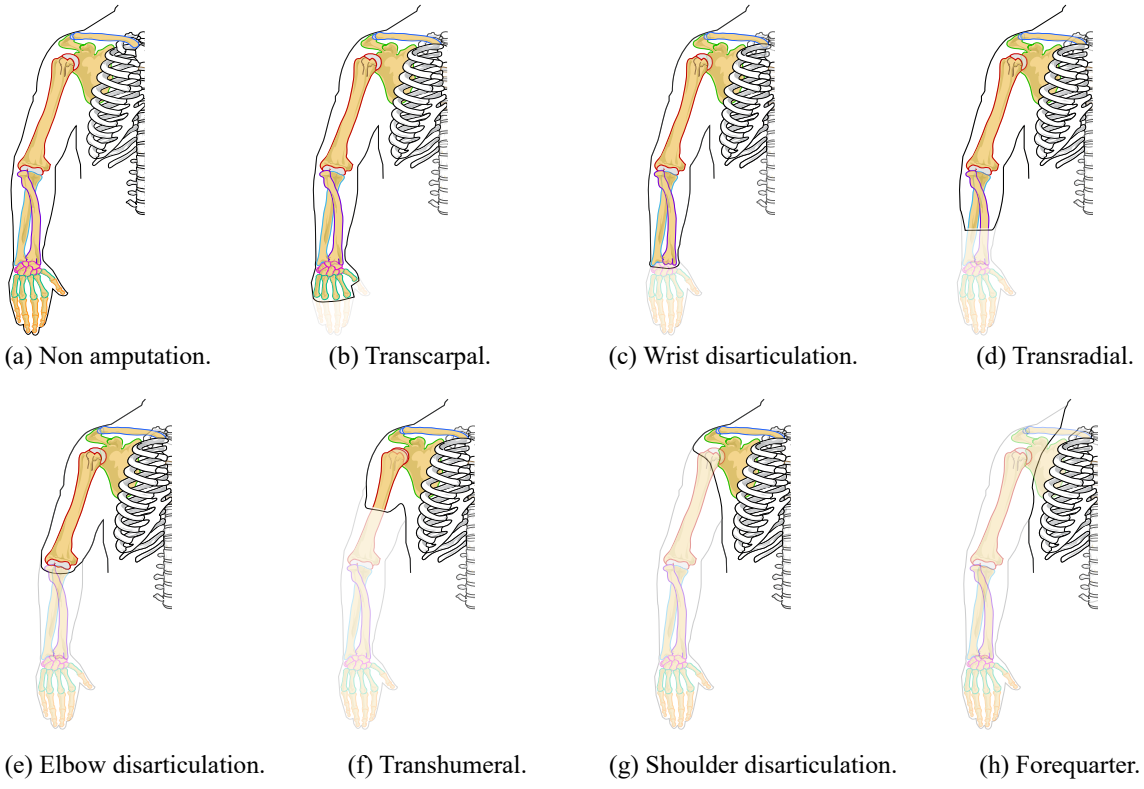

(a) Non amputation. (b) Transcarpal. (c) Wrist disarticulation. (d) Transradial.

(e) Elbow disarticulation. (f) Transhumeral. (g) Shoulder disarticulation. (h) Forequarter.

Figure 2 – Level of amputation.

2.1 Prosthesis by level of amputation

Prostheses are developed to help people with limb loss by restoring their functionality and independence. The design and functionality of upper limb prostheses depend on the level of amputation and the needs and priorities of the individual user. Each level of upper limb amputation presents unique anatomical and functional challenges, influencing the choice of prosthetic design (ZHENG et al., 2019). All the types of prostheses by level of amputation are illustrated in Figure 3.

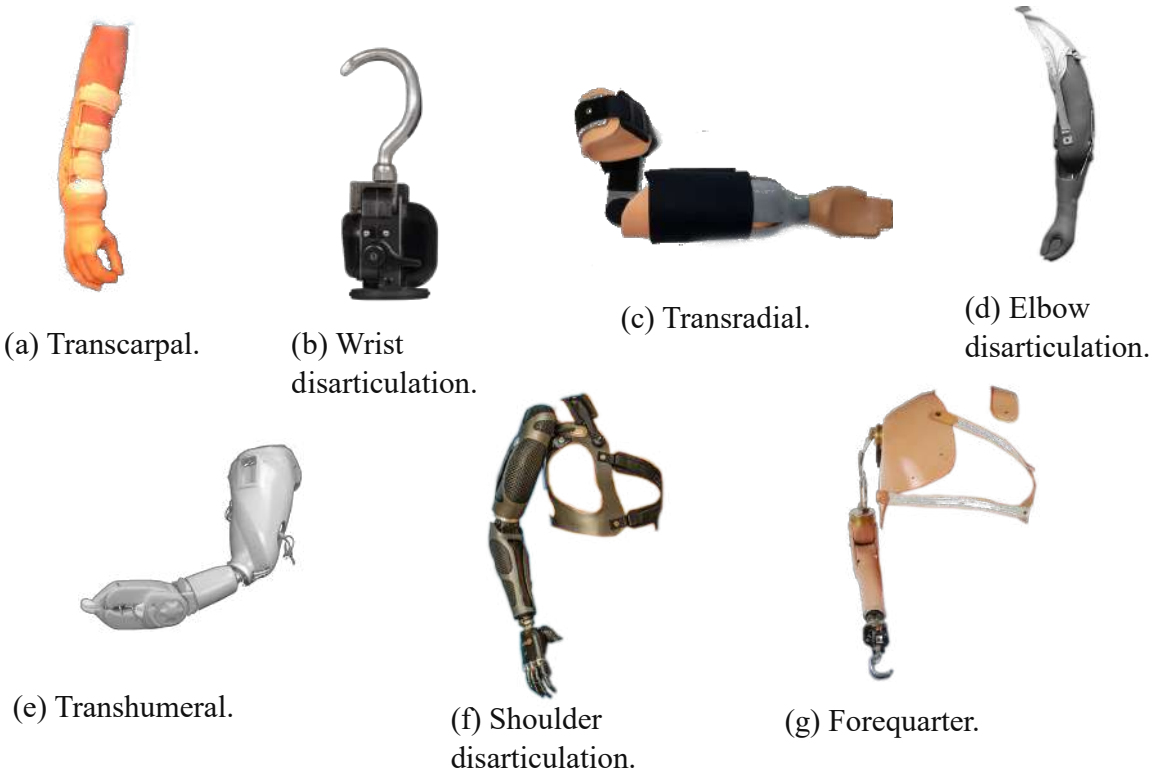

(a) Transcarpal. (b) Wrist disarticulation. (c) Transradial. (d) Elbow disarticulation.

(e) Transhumeral. (f) Shoulder disarticulation. (g) Forequarter.

Figure 3 – Types of prostheses by level of amputation.

2.1.1 Transcarpal

Transcarpal amputation is the surgical partial removal of the hand through the carpal bones, resulting in a stump that preserves the wrist joint. This type of amputation usually results from severe trauma, such as industrial accidents, explosions, or severe tear injuries, and is challenging because it severely limits the options for biological reconstruction (SALMINGER et al., 2016).

2.1.2 Wrist disarticulation

Wrist disarticulation involves amputation directly at the wrist joint, preserving the full length and full rotational capacity of the forearm. It is less common for prosthetic use because of the difficulties of prosthetic fit in the full-length residual limb. Instead, it is often selected for patients unwilling or unable to use prostheses but who benefit from preservation of length, symmetry, and limb rotation (CHOW; GASTON, 2023).

2.1.3 Transradial

Transradial amputation consists of removing the forearm below the elbow but above the wrist, usually due to trauma. It often requires shortening the forearm at least 7 cm proximal to the wrist to facilitate an optimal prosthetic fit, making it the preferred option for patients planning to use prostheses (CHOW; GASTON, 2023).

2.1.4 Elbow disarticulation

Elbow disarticulation preserves the full length of the humerus, providing excellent leverage, superior rotational control, and stable suspension capability by utilizing the elbow's natural anatomical shape. However, prosthetic fitting at this level can create aesthetic problems due to the elbow's increased width or unnatural placement, requiring specialized hinges or locking mechanisms (ANDREW, 2008).

2.1.5 Transhumeral

Transhumeral amputation often presents challenges due to reduced bone leverage, limited rotational control, and difficulties maintaining prosthetic suspension and stability. Anatomically contoured sockets for transhumeral amputations aim to provide dynamic stability, rotational control, suspension, and comfort through precise compression of soft tissue and bony structures (ANDREW, 2008).

2.1.6 Shoulder disarticulation

Shoulder disarticulation is a high-level amputation that involves the complete removal of the arm at the shoulder joint. It presents extreme prosthetic fit and control challenges, as all the arm's natural joints and muscle control points are lost. For people with this level of amputation, prosthetic devices must replace multiple complex functions, including the functioning of the end device (hand), wrist, elbow, and shoulder joint (KUIKEN et al., 2004).

2.1.7 Forequarter

Forequarter amputation is a radical surgical procedure that involves the removal of the entire upper extremity and shoulder girdle. It is indicated mainly in cases of advanced malignant neoplasms, trauma, or post-radiation lesions, when it is not possible to preserve the limb (EHRL et al., 2022).

2.2 Prosthesis by actuation system

Another widely used classification is the prosthesis actuation system, which can be divided into two main groups: passive and active. The active prosthesis can be divided into mechanical, pneumatic, and electric. Finally, electric prostheses are divided into the signals used to know the user's intention: EMG, EEG, FMG, NIRS, externally triggered, and the hybrid ones (SEGURA et al., 2024; RIBEIRO et al., 2019). These divisions are illustrated in Figure 4.

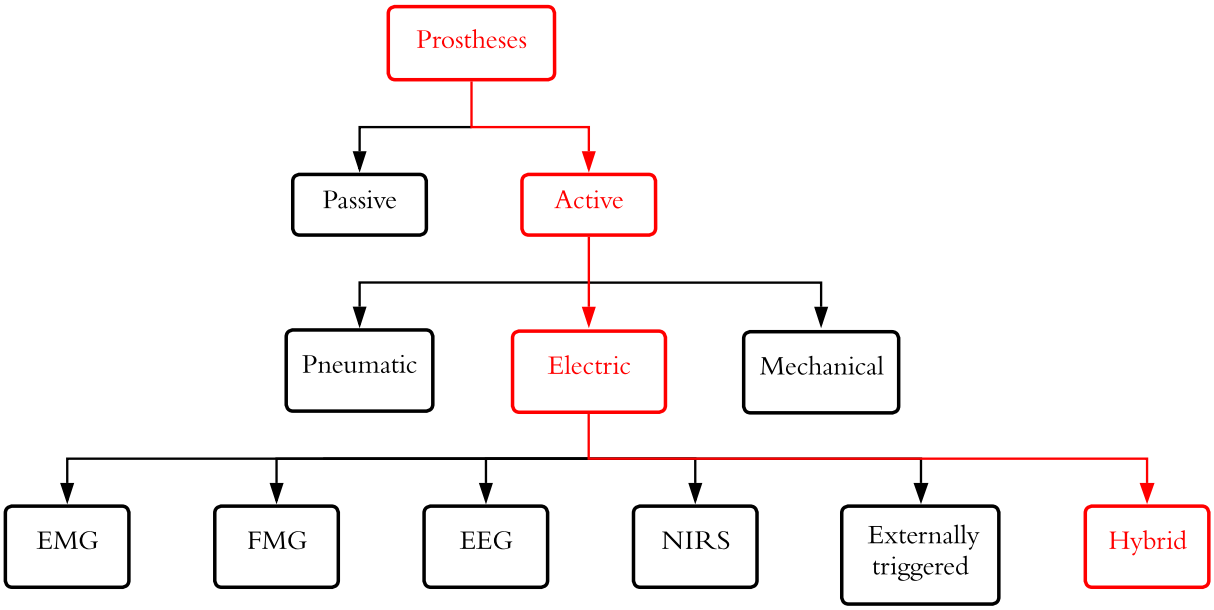

Figure 4 – Type of prosthesis by actuation system, highlighting in red the actuation system used in this work.

2.2.1 Passive

Passive prostheses are devices without internal active mechanisms, such as electric motors or body-driven systems. Instead, any movement or adjustment is applied externally, usually by the unaffected hand of the user or through interaction with the environment. In the case of upper limb prostheses, they can be classified into prosthetic hands and prosthetic tools. Prosthetic hands are designed primarily for aesthetic purposes, and prosthetic tools are mechanical devices often optimized for specific tasks such as sports, hobbies, or driving. Both can be static (fixed in position) or adjustable (manually adjustable), as can be seen in Figure 5 (MAAT et al., 2018).

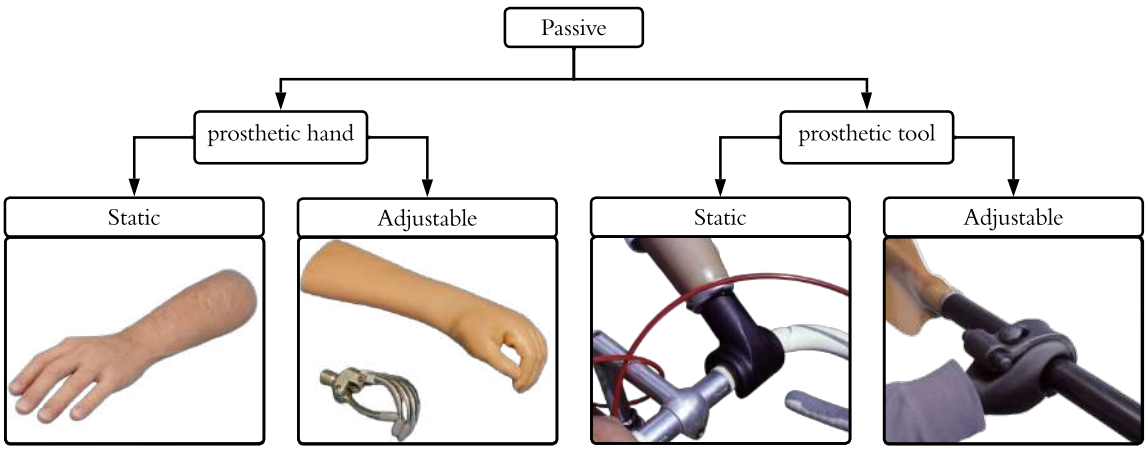

Figure 5 – Types of passive prosthesis, adapted from (MAAT et al., 2018).

2.2.2 Active

An active prosthesis is a device that restores or assists movement by generating force or motion through an internal mechanism. Unlike passive prostheses, which rely on external manipulation, active prostheses include components that can be directly controlled by the user, allowing for voluntary and functional movement (KANNENBERG, 2017).

2.2.2.1 Pneumatic

Pneumatic prostheses are active prostheses that utilize pressurized air to generate movement, effectively mimicking the action of muscles and tendons in a human limb. Pneumatic artificial muscles (PAMs) are used as the actuators, they contract and relax like biological muscles, providing a more natural and flexible movement compared to other prostheses (GONG et al., 2020).

2.2.2.2 Mechanical

Also known as body-powered, these systems use the user's body movements to power mechanical devices through a harness and cable system. It is durable, low-cost, and provides a proprioceptive response, making it especially useful in low-resource settings. These prostheses may include hooks that offer great functionality but are considered less aesthetically pleasing, or hands that appear more natural but are often inefficient. Common drawbacks include sling discomfort, high physical effort, and limited grip strength, resulting in relatively high user dissatisfaction and rejection (UELLENDAHL, 2017; KENNEY et al., 2018).

2.2.2.3 Electric

An electric prosthesis is a device that uses battery-powered electromechanical actuators to perform grasping or other movements. Unlike passive or body-powered systems, electric prostheses rely on internal motors to generate motion in the terminal device (such as a hand), providing active functionality with minimal physical effort on the user's part. These devices can be designed to support multiple grip configurations, allowing for more versatile and functional use in everyday tasks (BATTRAW et al., 2022).

2.3 Control of Active Electric Prosthesis

2.3.1 Electromyography

It is a technique used to measure the electrical activity generated by muscles when they contract. When someone thinks about moving a limb, the brain sends signals to the muscles via motor neurons, creating small electrical impulses. EMG sensors, which can be

placed on the skin surface EMG (sEMG) or implanted within the muscles (intramuscular EMG), detect these signals and interpret the user's intent to move. Therefore, EMG is vital in biomedical applications, particularly for controlling prosthetics (STANGO et al., 2016).

In upper limb prosthetics, EMG enables users to operate artificial hands or arms using muscle contractions from the residual limb. Basic systems employ two surface electrodes to capture signals from opposing muscles, facilitating simple movements like hand opening and closing. More sophisticated prostheses utilize multiple electrodes and advanced pattern recognition algorithms to discern intricate muscle activity patterns, controlling various gestures and ranges of motion, such as wrist rotation or finger flexion. These systems aim to enhance the intuitiveness and responsiveness of prosthesis control (HAHNE et al., 2021; SAMUEL et al., 2019).

2.3.2 Forcemyography

It is a sensing technology that captures the mechanical activity of muscles by detecting pressure changes on the skin's surface during muscle contractions. FMG employs force sensors, typically force-sensitive resistors (FSRs), which record the physical deformation or strain on the residual limb when muscles contract. The advantages of this technology include reduced sensitivity to sweat noise, decreasing electrode displacement or motion artifacts, and the provision of more consistent signals over time (PRAKASH et al., 2020).

In prosthetic applications, it has demonstrated significant potential as an alternative or complement to EMG-based control systems. Its capacity to provide stable, cost-effective, and intuitive user input renders it particularly suitable for controlling robotic hands with multiple DoF. Empirical studies have indicated that FMG-based systems can achieve high classification accuracy across various hand gestures and grips, particularly when integrated with advanced pattern recognition algorithms. Moreover, when coupled with machine learning techniques, FMG can discern varying grip intensities and translate them into corresponding motor commands for precise motor control, thereby establishing itself as a practical interface for everyday use by amputees (AHMADIZADEH et al., 2017).

2.3.3 Electroencephalography

It is a technique that records the brain's electrical activity using sensors placed on the scalp. In prosthetic control, EEG is used in brain-computer interfaces (BCI) to infer the user's intentions, especially through motor imagery (MI), where the user imagines moving a limb without any actual physical movement. This is particularly valuable for individuals with high-level amputations or severe motor impairments, where traditional muscle signals, such as EMG, may not be available or reliable (BAKSHI et al., 2018).

EEG monitoring allows for the noninvasive control of neuroprosthetic devices, such as functional electrical stimulation (FES) systems that can stimulate muscles to restore movement. The potential of using EEG for prosthetic control is significant, but it also presents practical challenges, especially regarding the equipment needed to capture and process brain signals. Typically, EEG systems require numerous electrodes placed on the scalp, often involving conductive gels, wired caps, and large amplifiers. Although these configurations work well in research settings, they are unsuitable for everyday use (VIDAURRE et al., 2016).

2.3.4 Near-infrared spectroscopy

It is a non-invasive technique that uses near-infrared light between 730-850 nm to measure changes in blood oxygenation and muscle circulation. When muscles contract, they consume oxygen and alter local blood flow, changing how near-infrared light is absorbed. NIRS sensors on the skin detect these changes and convert them into signals reflecting underlying muscle activity and motor intention (SATTAR et al., 2021b).

In the context of upper extremity prosthetic control, NIRS allows the detection of movement intention by analyzing these hemodynamic responses. This method is useful when conventional mechanical or electrical control signals are limited or unavailable. Although its response is somewhat slower than electrical systems and may be affected by optical noise or muscle fatigue, it offers a promising control modality for improving the responsiveness and adaptability of advanced prosthetic devices (GUO et al., 2017).

2.3.5 Externally triggered

Externally triggered prostheses are active prosthetic devices that are actuated by signals that do not originate from the user's biological systems, such as muscle contractions or brain activity. Instead, these devices are controlled via external triggers, including buttons, computer commands, or predetermined sequences, thereby facilitating movement without dependence on physiological signals from the user.

2.3.6 Hybrid

Hybrid control signals integrate two or more categories of user-derived inputs to actuate prosthetic devices. This multimodal approach employs the advantages of each signal type to get over individual deficiencies, thus enhancing reliability and control across multiple degrees of freedom. Hybrid signal systems facilitate a more intuitive, responsive, and functionally comprehensive control mechanism, particularly in intricate or advanced amputations where a singular control source may prove inadequate (RUHUNAGE et al., 2017; BLANA et al., 2016).

Some of the prostheses used in the literature are listed in Table Appendix 1.1, 52 prostheses were listed, 46 (88.46%) were Transradial, 4 (7.69%) were Transhumeral, 1 (1.92%) were Wrist disarticulation, and 1 (1.92%) were Transcarpal, as illustrated in Figure 6(a). By its type, 38 (73.08%) were Active-Electric, 10 (19.23%) were Active-Mechanical, 1 (1.92%) were Active-Pneumatic, and 3 (5.77%) were Passive, as shown in Figure 6(b).

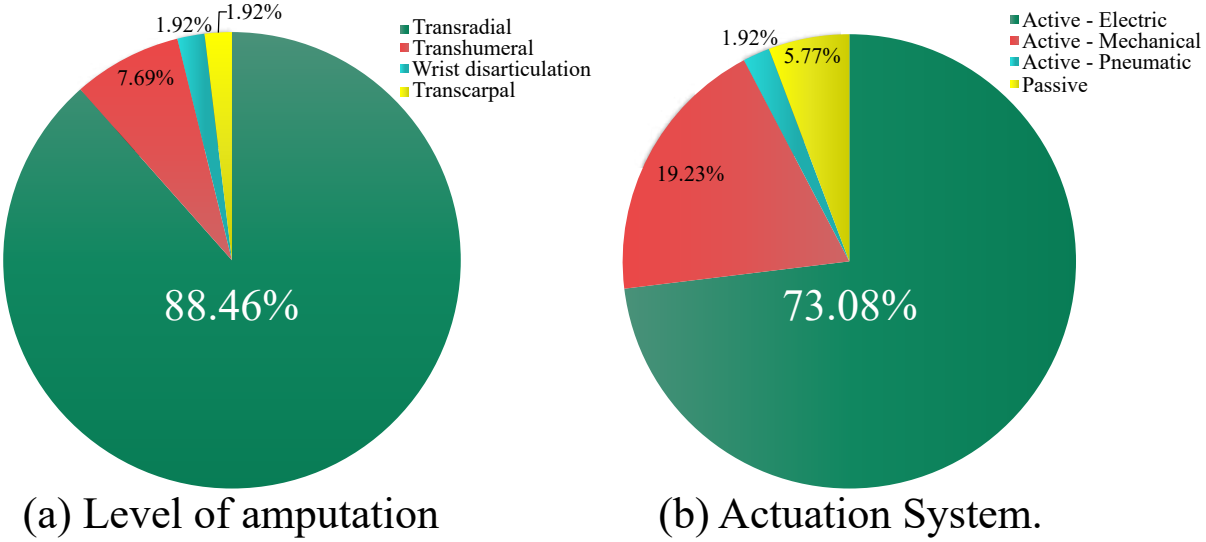

(a) Level of amputation (b) Actuation System.

Figure 6 – Percentage of prosthesis found in the literature by its category.

3 Materials

3.1 Optical fiber sensors

Optical fiber sensors (OFS) represent a promising alternative to conventional sensing technologies due to the inherent advantages of optical fibers. Their small size and lightweight structure facilitate integration into tiny or fragile environments with minimal structural disruption. Moreover, OFS exhibits significant resistance to extreme temperatures and pressures, besides immunity to electromagnetic interference (EMI), making it a suitable choice for challenging operating conditions. These characteristics are particularly valuable in settings characterized by strong electromagnetic fields, in which traditional electronic sensors may fail. Furthermore, OFS can function as sensors and data transmission channels, thus avoiding the need for separate communication systems and reducing overall system complexity and associated costs (PENDãO; SILVA, 2022).

Using the interaction between light and fiber, fiber optic sensing techniques allow accurate and reliable measurements. These sensors can measure various physical, chemical, and biomedical parameters, making them highly useful in many fields. Fiber optic sensors have advanced significantly since their establishment in the 1980s (KHONINA; KAZANSKIY; BUTT, 2023). Particularly, FBGs have become a widely used configuration due to their accuracy in detecting physical changes. FBGs are key in civil and aerospace engineering, biomedical, and automotive systems today (QU et al., 2024).

3.1.1 Fiber Bragg Grating

They are highly efficient optical sensors due to their ability to reflect specific wavelengths of light that are shifted in correspondence with strains and temperature variations. Each FBG is based on a periodic modulation of the refractive index within the optical fiber core, which selectively reflects a narrow band of wavelengths called the Bragg wavelength (λ_B) as can be seen in Figure 7. The determination of this wavelength depends on the grating period (Λ) and the effective refractive index (n_{eff}) of the core, the relationship of which is expressed by the Equation 3.1.

$$\lambda_B = 2 \times n_e f f \times \Lambda \tag{3.1}$$

When external physical factors, such as deformation or temperature, induce changes in Λ or n_{eff}, the Bragg wavelength shifts accordingly, making the FBG an accurate and passive sensing element (NAYAK, 2024).

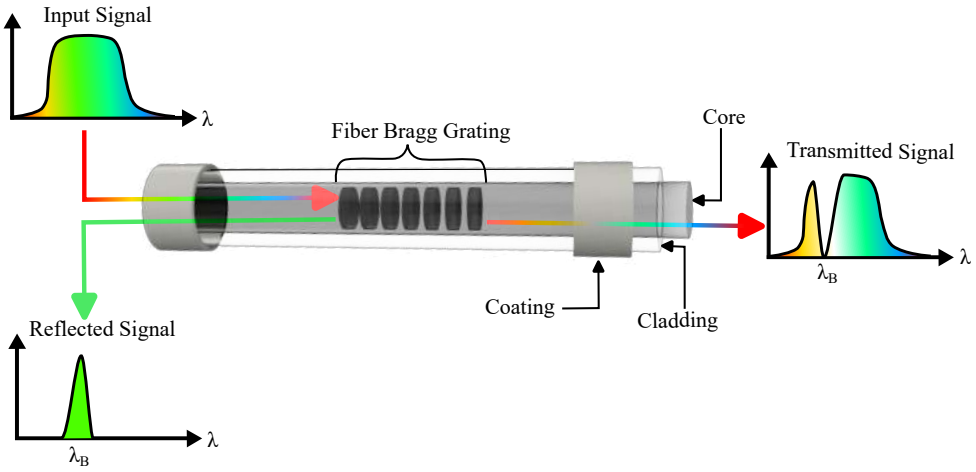

Figure 7 – Principle of FBGs.

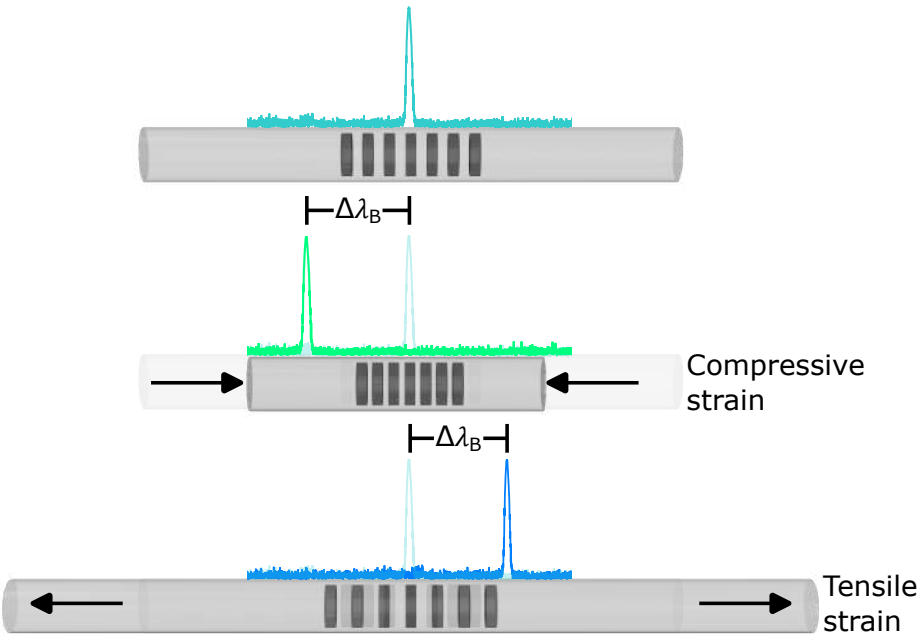

Figure 8 – FBG shifting principle.

The sensitivity of the λ_B to strain and temperature allows FBGs to function as sensors in various environments. When the optical fiber is subjected to stretching, compression, or temperature changes, the periodic grating spacing and refractive index change, resulting in a measurable shift of the reflected wavelength ($\Delta\lambda_B$), as is shown in Figure 8. This shift exhibits a linear relationship with both strain ($\Delta\varepsilon$) and temperature variation (ΔT), as illustrated in Equation 3.2.

$$\Delta\lambda_B = 2\left[\Lambda\frac{\partial n}{\partial l} + \frac{\partial\Delta}{\partial l}\right]\Delta l + 2\left[\Lambda\frac{\partial n}{\partial T} + \frac{\partial\Delta}{\partial T}\right]\Delta T, \tag{3.2}$$

where l is the length of the FBG and Δl is the change in the length caused by strain, n is the effective refractive index, and ΔT is the temperature change (AL-FAKIH; OSMAN; ADIKAN, 2012). Since FBGs respond simultaneously to both parameters, in various applications it is common to employ compensation or multiple grating techniques to

effectively isolate and measure the different effects, especially in contexts such as structural health monitoring or temperature-compensated strain assessments (HEGDE; ASOKAN; HEGDE, 2022).

FBGs are classified into several types depending on their structural characteristics and fabrication methods. The main types are simple Bragg gratings, characterized by uniform periodicity, chirped FBGs, in which the period of the grating varies monotonically, tilted FBGs, which are inscribed at an oblique angle to the fiber axis, and superstructured FBGs, which employ modulated exposure to ultraviolet (UV) light along the fiber to achieve complex reflective properties. This classification is illustrated in Figure 9. External techniques, such as interferometry, known for their sensitivity and high tunability, are mainly used to fabricate these gratings. Another widely adopted technique is the phase mask, which is stable and less sensitive to vibrations. Finally, the point-by-point method, which allows precise registration by exposing the slit and translating the fiber. Each method has distinct advantages adapted to specific applications such as sensing, telecommunications, or structural health monitoring (KORI et al., 2019).

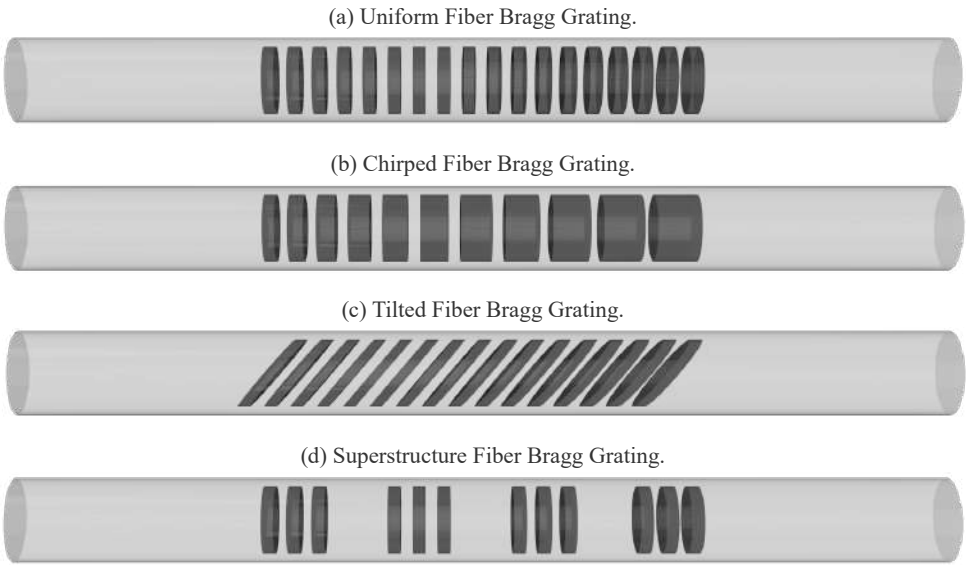

Figure 9 – Types of FBGs.

3.2 Fused deposition modeling

Fused deposition modeling (FDM) constitutes a widely recognized additive manufacturing process where a polymeric filament is heated until it attains a semi-liquid state, then is extruded through a nozzle to construct 3D objects layer-by-layer. This technique, categorized under material extrusion, is known for its simplicity, cost-effectiveness, and compatibility with various polymers, including polylactic acid (PLA), acrylonitrile butadiene styrene (ABS), and composite materials. Computer-aided design (CAD) software is employed to conceptualize the object, which is then partitioned into layers and converted

into G-code instructions for execution by the 3D printer. Its capacity to generate elaborate geometries without the necessity for molds makes it suitable for rapid prototyping and small-scale production (BAECHLE-CLAYTON et al., 2022; MWEMA; AKINLABI, 2020).

FDM has gained widespread popularity in various industries, such as aerospace, automotive and biomedical engineering, due to its cost-effectiveness, design flexibility and material versatility. However, problems such as layer adhesion, porosity and material limitations persist, especially when integrating reinforcements such as natural fibers or composite materials.

An emerging area of research focuses on the integration of FBGs within FDM structures, which has been widely studied (LEAL-JUNIOR et al., 2018; LEAL-JUNIOR et al., 2019). Particularly in biomedical applications, they have been used for monitoring heart and respiratory rates (TAVARES et al., 2022b; FAJKUS et al., 2024), back pain (LAVORGNA et al., 2025), and forearm flexion angles (CHENG-YU et al., 2021). Table 1 summarizes the physical properties of the sensors mentioned.

Table 1 – Different physical properties of the sensors embedded in 3d printed pieces.

Measurement	**Material**	**Infill**	**Sensitivity**	**Authors**
Strain, transversal force, and temperature	TPU	70%	1.1 pm/$\mu\epsilon$, -0.3 pm/N, and 14.1 pm/°C	(LEAL-JUNIOR et al., 2019)
Temperature, and transversal force	ABS	20%, 65%, and 99%	7.8 pm/°C, 14.0 pm/C, and 120.6 pm/°C, 2.22 pm/N, 2.21 pm/N, and 0.6 pm/N	(LEAL-JUNIOR et al., 2018)
Temperature, and strain	ABS	15%	55.35 pm/°C, and 1.249 pm/$\mu\epsilon$	(FAJKUS et al., 2024)
Displacement	TPU	20%	0.190 ± 0.001 pm/μm	(TAVARES et al., 2022a)
Temperature, and strain	TPU	100%	0.034 nm/°C, and 0.81 nm/mϵ	(LAVORGNA et al., 2025)
Angle	PLA	80%	0.0056 nm/Elbow°, and 0.0276 nm/Knee°	(CHENG-YU et al., 2021)

3.3 Gesture identification

Hand gestures are a fundamental component of human communication and interaction, making them a natural choice for control within human-machine interfaces (HMI). As technology advances, gesture identification has become an increasingly vital tool for facilitating intuitive, non-invasive interaction with digital systems. This is especially important in applications such as virtual reality, robotics, and assistive devices like prosthetics. Gesture-based control allows users to interact with machines in a way that strongly simulates natural movement, thus improving accessibility and user experience. Research in this field emphasizes the accurate decoding of hand movements using various sensing and machine learning methodologies to develop reliable systems in different environments and conditions of use. Among the many detection strategies that have been developed, techniques such as EMG and FMG are frequently employed. However, the overall goal

remains to improve gesture recognition performance to provide accurate and efficient HMI solutions (YOUNG et al., 2025; XIAO; MENON, 2019).

In the application of machine learning techniques for gesture recognition, a critical component is feature extraction. This procedure consists of identifying and selecting the most relevant elements of the raw input signals to represent the intentional movement patterns in a compact and meaningful way. Feature extraction significantly influences the accuracy and efficiency of the pattern recognition system, as it condenses high-dimensional data into practical inputs for the classifiers. Commonly used techniques include time-domain, frequency-domain, and time-frequency domain methods, each capturing distinct features of muscle signals, as seen in Table 2. Efficient feature extraction improves classification performance and eases the computational burden, making real-time control of prosthetic and other assistive systems more practical and reliable (PARAJULI et al., 2019).

Table 2 – Features used on gesture identification, adapted from (KHAN; KHAN; FAROOQ, 2020).

Feature	Features Names	Significance
Time-domain features	Mean Absolute Value (MAV); Root Mean Square (RMS); Variance (VAR); Wavelength (WL), mean Zero Crossings (ZC), Slope Sign Changes (SSC), Kurtosis (KUR), and Skewness (SKW)	Advantages: • Simple to compute. • Quick. • More often used in force-EMG relations. Disadvantages: • Noise sensitive.
Frequency-domain features	Mean Frequency (MNF); Median Frequency (MdF); Power Spectrum (PS); Mean Power (MP); Spectral Movements (SM{[}k{]}); Frequency Ratio (FR); Power Spectral Density (PSD) and Peak Frequency (PF).	Advantages: • More often used in fatigue estimation. Disadvantages: • Computationally complex. • Information loss due to spectral leakage.
Time-frequency features	Wavelet transform (WT); Discrete wavelet transform (mDWT);	Advantages: • Regarded best for information extraction. • High-dimensional output. Disadvantages: • Computationally expensive.

3.3.1 Features extraction

Feature extraction consists of identifying or collecting relevant information or features from a signal. This process reduces complexity and stores vital information for further analysis (KUMAR; YADAV; KUMAR, 2025). All the feature equations were extracted from the works of (GOUDA et al., 2023), (PHINYOMARK; PHUKPATTARANONT; LIMSAKUL, 2012), (PHINYOMARK et al., 2010), (KARTHICK; GHOSH; RAMAKRISHNAN, 2018), (NAZARPOUR et al., 2013), (SAMUEL et al., 2018), (BROEK et al., 2006), (SUBASI; KIYMIK, 2009), (PHINYOMARK et al., 2014) and (PHINYOMARK et al., 2013), and are illustrated in Table Appendix 2.2, Table Appendix 2.3 and Table

Appendix 2.4. Some important time domain features are summarized in Table 3 (KIM et al., 2022).

Table 3 – Time-Domain features.

Feature	**Equation**	**Characteristic**
Mean	$Mean = \frac{1}{T}\sum_{t=1}^{T} x_t$	DC offset of the signal.
MAV	$MAV = \frac{1}{T}\sum_{t=1}^{T} \lvert x_t \rvert$	Signal magnitude, average signal strength.
RMS	$RMS = \sqrt{\frac{1}{T}\sum_{t=1}^{T} x_t^2}$	Measure of signal power, related to muscle contraction force.
VAR	$VAR = \frac{1}{T-1}\sum_{t=1}^{T} (x_t - \mu)^2$	Measures the dispersion of the signal amplitude around its mean.
WL	$WL = \sum_{t=2}^{T} \lvert x_t - x_{t-1} \rvert$	Length of the signal, contains information about its complexity.
ZC	$ZC = \sum_{t=1}^{T-1} [sgn(x_t x_{t+1}) \wedge \lvert x_t - x_{t+1} \rvert \geq 0]$	Measure how many times the signal polarity changes.
SSC	$SSC = \sum_{i=2}^{N-1} sgn((x_i - x_{i-1}) \times (x_i - x_{i+1}))$	Counts the number of times the slope of the signal changes sign.
KUR	$KUR = \frac{1}{T}\sum_{t=1}^{T} \left(\frac{x_t - \mu}{\sigma}\right)^4 - 3$	Measures sharpness relative to a normal distribution.
SKW	$SKW = \frac{1}{T}\sum_{t=1}^{T} \left(\frac{x_t - \mu}{\sigma}\right)^3$	Indicates asymmetry of the signal distribution.

3.3.2 Machine learning

Machine learning (ML) algorithms can classify muscle activation patterns into several motion commands, including but not limited to hand opening, wrist rotation, and elbow flexion. In addition to mere gesture recognition, ML can estimate the force levels during grasps, adapt control mechanisms to diverse arm positions, and mitigate signal variability induced by electrode displacements or muscle fatigue (AHMADIZADEH et al., 2017; PANCHOLI; JOSHI, 2019).

Among the most commonly used are Linear Discriminant Analysis (LDA), Regularized Discriminant Analysis (RDA), Quadratic Discriminant Analysis (QDA), Support Vector Machines (SVMs), k-Nearest Neighbors (KNN), Decision Tree (DT), Random Forest (RF), and Artificial Neural Networks (ANNs), especially Multi-Layer Perceptrons (MLPs). Other classifiers in the literature are Fuzzy Logic Classifier (FL), MU Drive, Kernel Regularized Least Squares (KRLS), and Least Squares Support Vector Machine (LSSVM). The result of this analysis can be seen in Table 4.

Table 4 – Review of gesture classification methods using various sensor and classifiers. AR = Able-bodied; AA = Amputee. TD = Time Domain, FD = Frequency Domain, Vib = Vibration, MU = Motor Unit

Author	Type	#Gest	Classifier	Accuracy	Features	Participants	Year
(VIDOVIC et al., 2016)	EMG	8	LDA	>92% (offline), +25% (online)	logVar	11 (7 AR + 4 AA)	2015
(PANCHOLI; JOSHI, 2018)	EMG	5	RF	99.9% (offline)	9 TD + 7 FD	29 (25 AR + 4 AA)	2018
(BAKSHI et al., 2018)	EMG + EEG	21	KRLS	84.3% (offline)	12 EMG TD + 5 EEG FD	6 (5 AR + 1 AA)	2018
(GUéMANN et al., 2022)	EMG + Vib	1 DOF	(No) Velocity control	83.3%	MVC-based	23 (16 AR + 7 AA)	2022
(FAN et al., 2021)	sEMG	17	CNN	85.3%	mDWT	DB2 → DB3 (20 → 11 AA)	2023
(MASSON et al., 2016)	Myo (EMG)	5	k-NN	>90% (offline), 84% (online)	VAR	8 AR (offline), 1 (online)	2016
(BLANA et al., 2016)	EMG + IMU	4	TD-ANN	98.2% (offline), 90.9% (online)	TW mean	10 AR	2016
(AMSUESS et al., 2016)	EMG	11	CSP-PE + LR	SHAP: 58–71	4 TD	7 (5 AR + 2 AA)	2016
(TAVAKOLI; BENUSSI; LOURENCO, 2017)	EMG	4	SVM	90.1% (real-time)	TD (1-ch)	3 (1 expert + 2 beg.)	2017

(GUO et al., 2017)	EMG + NIRS	13/11	SVM	AR: 94%, AA: 87.7%	EMG+NIRS TD	16 (13 AR + 3 AA)	2017
(WILSON; VAIDYANATHAN, 2017)	MMG + IMU	7/5	(No) Template match	83.5% / 93.3%	MMG energy + gyro	6 (5 AR + 1 AA)	2017
(RESNIK et al., 2018)	EMG	5	LDA	Not reported	4 TD	2	2018
(PANCHOLI; JOSHI, 2019)	EMG	6	LDA	95.4% (offline), 94.14% (real-time), 91.65% (amputee, real-time)	RMS, WL, ZC, SSC	4 (3 AR + 1 AA)	2019
(PRAKASH et al., 2020)	FMG	6	FLC	97.8% (offline), 95.1% (online)	MAV, RMS, IFMG, MAX	13 (8 AR + 5 AA)	2020
(SATTAR et al., 2021a)	EMG	4	kNN	AR: 95.8%, AA: 68.1%	11 TD/FD features	19 (15 AR + 4 AA)	2021
(AL-TIMEMY et al., 2016)	EMG	6	LDA	82–93% (by force)	TD-PSD	9 AA	2016
(CHO et al., 2016)	FMG	8	LDA	80% (resid.), 95% (sound limb)	Proc. FSR	4 AA	2016
(RADMAND; SCHEME; ENGLEHART, 2016)	HD - FMG	8	LDA	99.7%	Raw pressure map	10 AR	2016
(AHMADIZADEH et al., 2017)	FMG + EMG	10	LDA	81.1%	Raw FSR + EMG	1 AA (pilot)	2017

(GAILEY; ARTEMIADIS; SANTELLO, 2017)	EMG	6	SVM+RF	60–99% pose, 74–78% force	6 TD	8 AR	2017
(GIGLI et al., 2018)	EMG + Vision	10	KRLS + CNN	sEMG: 80%, +Vision: 84%	mDWT + VGG-16	5 AR	2018
(TWARDOWSKI et al., 2018)	EMG (MU)	4	MU Drive	72.9%	MU firings	23 (13 AA + 10 AR)	2019
(HA; WITHANACHCHI; YIHUN, 2019)	FMG	4	SVM	85.8%	Raw voltages	3 AR	2019
(PANCHOLI; JOSHI; JOSHI, 2021)	sEMG	49	CNN	AA: 81.7%, DB1: 91.1%, DB2: 89.4%	Spectral Moments	NinaPro DB1–5	2021
(KRASOULIS; VIJAYAKUMAR; NAZARPOUR, 2020)	EMG + IMU	5	RDA	AR: 95%, AA: 85%	EMG+IMU TD	14 (12 AR + 2 AA)	2020
(UNANYAN; BELOV, 2021)	EMG	3 levels	(No) Amp.-based win.	97.9%	Peak EMG (100ms win.)	29 (28 AR + 1 disabled)	2021
(SAMUEL et al., 2016)	EMG	7	LDA	91.0% ± 4.1%	4 TD	4 AR	2021

The reviewed studies demonstrate various approaches to gesture classification, going from traditional EMG-based methods to hybrid strategies that combine EMG signals with other signals, such as EEG, IMU, FMG, or NIRS. Additionally, it can be observed that the use of vibration or visual feedback is used to improve the accuracy of these devices. While many studies have been based on classical classifiers such as LDA, SVM, or kNN, recent studies have explored deep learning architectures, including CNNs. The reported accuracies vary depending on the number of gestures, the type of participants (non-disabled or amputees), and whether the evaluation was performed offline or in real-time conditions. In general, offline classification tends to achieve high accuracies (often above 90%). In contrast, real-time implementations tend to show a drop in performance, particularly in cases involving amputee participants.

3.3.3 Classification algorithms

The k-Nearest Neighbor (kNN) is a technique that classifies an input based on the classes of its nearest neighbors in the feature space. The process consists of two main steps: first, the k training examples closest to the input are identified, and second, the input is assigned a class based on the classes of those neighbors, usually by a majority vote. The algorithm's performance depends on the chosen distance metric (CUNNINGHAM; DELANY, 2021).

Gaussian Naive Bayes (GNB) is a probabilistic ML algorithm based on Bayes theorem. It assumes that the data features of each class follow a multivariate Gaussian distribution. It calculates the standard deviation (μ) and variance (σ^2) for each class to estimate the probability that a new data point belongs to a given class (CHAPLOT et al., 2023; ZHANG, 2004).

Logistic Regression (LR) is another supervised algorithm employed for classification, that uses the logistic function to convert any real input value to a value in the range of $[0, 1]$, interpretable as a probability. To prevent overfitting, LR models can be regularized by penalizing large coefficient values (BEWICK; CHEEK; BALL, 2005).

Linear Discriminant Analysis (LDA) is a supervised learning technique that reduces dimensionality by filtering redundant or noisy information. This is achieved by transforming the original data into a subspace of lower dimensionality, where the transformation is optimized to improve the separation between different classes and minimize the variance within each class (ZHAO et al., 2024).

Hierarchical models were also used, beginning with the Decision Tree (DT), a supervised model with a structure that begins with a single root node and recursively partitions the data by selecting input features at decision nodes. This process continues until a stopping criterion is met, producing a clear model where each path from the root to

a leaf represents a specific classification rule (HERNáNDEZ et al., 2021). Building on this, the Random Forest (RF) is an ensemble learning method that aggregates a large number of individual, uncorrelated decision trees to obtain higher model performance. It combines multiple weak classifiers, resulting in a more robust and accurate overall model where a majority vote of all individual trees makes a final prediction (BLANCHET et al., 2020).

Finally, the Support Vector Machine (SVM) is a learning technique that achieves high generalization by maximizing the margin between data categories. This is achieved by constructing a separating hyperplane that has the maximum possible distance to the nearest data points of any class. For data that is not linearly separable, SVMs use a kernel to efficiently map the data into a higher-dimensional feature space where a separating hyperplane can be found (YU; KIM, 2012).

3.3.4 Comparison Metrics

The performance of the classification models can be evaluated using the accuracy, precision, and recall. These metrics provide a perspective of model performance by measuring its overall correctness, its ability to avoid false positives, and its ability to identify all positive cases. These metrics are calculated using the true positives (TP), true negatives (TN), false positives (FP), and false negatives (FN) of the model, their meaning is illustrated in Figure 10 (HULLEMAN; VOS, 2019).

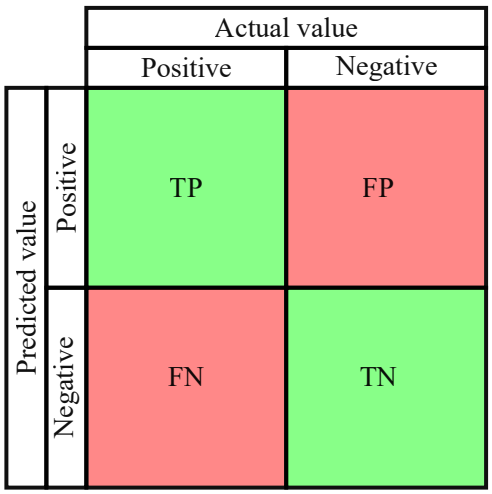

Figure 10 – Matrix showing what TP, FP, FN, and TN represent.

Accuracy is the ratio of correctly predicted samples to the total number of samples tested, and is calculated using the equation 3.3.

$$Accuracy = \frac{\sum TP + TN}{\sum TP + FP + TN + FN} \tag{3.3}$$

Precision is the ratio of correctly predicted positive samples to the total predicted positive samples, and is calculated using the equation 3.4.

$$Precision = \frac{\sum TP}{\sum TP + FP} \tag{3.4}$$

Recall or sensitivity is the ratio of correctly predicted positive samples to all actual positive samples, and is calculated using the equation 3.5.

$$Recall = \frac{\sum TP}{\sum TP + FN} \tag{3.5}$$

3.4 Serious games and extended Reality for rehabilitation

The time between surgical amputation and the acquisition of a prosthetic device is referred to as the pre-prosthetic phase. During this period, it may not always be possible to hold the training sessions with actual prosthetic limbs. Consequently, many serious games have been developed as an innovative alternative to facilitate training and rehabilitation during this crucial phase (TABOR et al., 2017; DIJK et al., 2016).

Some serious games are based on commercial games, like "Flappy Bird", Chrome Dino Runner, and Asteroids. These serious games aim to enhance user engagement and improve the adaptation process by improving their forearm muscle control (SMITH et al., 2018a; SMITH et al., 2018b; RADHAKRISHNAN et al., 2019).

Extended Reality (XR) technologies have emerged as valuable instruments in the rehabilitation of individuals utilizing electrical prostheses. XR encompasses reality (VR), augmented reality (AR), and mixed reality (MR), as can be seen in Figure 11, providing immersive, interactive environments that facilitate motor learning and engagement. In the context of prosthetic training, these systems simulate realistic control scenarios through interfaces, enabling users to practice fundamental motor commands within a controlled and adaptable setting (LI et al., 2024).

Inside the XR advancements, serious games have gained relevance in prosthesis control training. These games incorporate elements of entertainment within goal-directed rehabilitation tasks, aiming to bolster user engagement and sustain long-term participation. Serious games designed for electric prostheses typically employ abstract or gamified tasks aimed at enhancing muscle control and coordination (GARSKE et al., 2021).

The efficacy of serious games and XR-based training tools ultimately depends on their capacity to facilitate skill acquisition that generalizes to daily prosthetic use. Engagement, while advantageous for adherence, is insufficient unless accompanied by structured training that emulates real prosthetic interactions. Essential considerations for the enhancement of these systems include the integration of tasks related to ADLs, optimization of feedback mechanisms, and the assurance that virtual experiences accurately

reflect the constraints and affordances of physical prosthetic devices (MAAS; SLUIS; BONGERS, 2024).

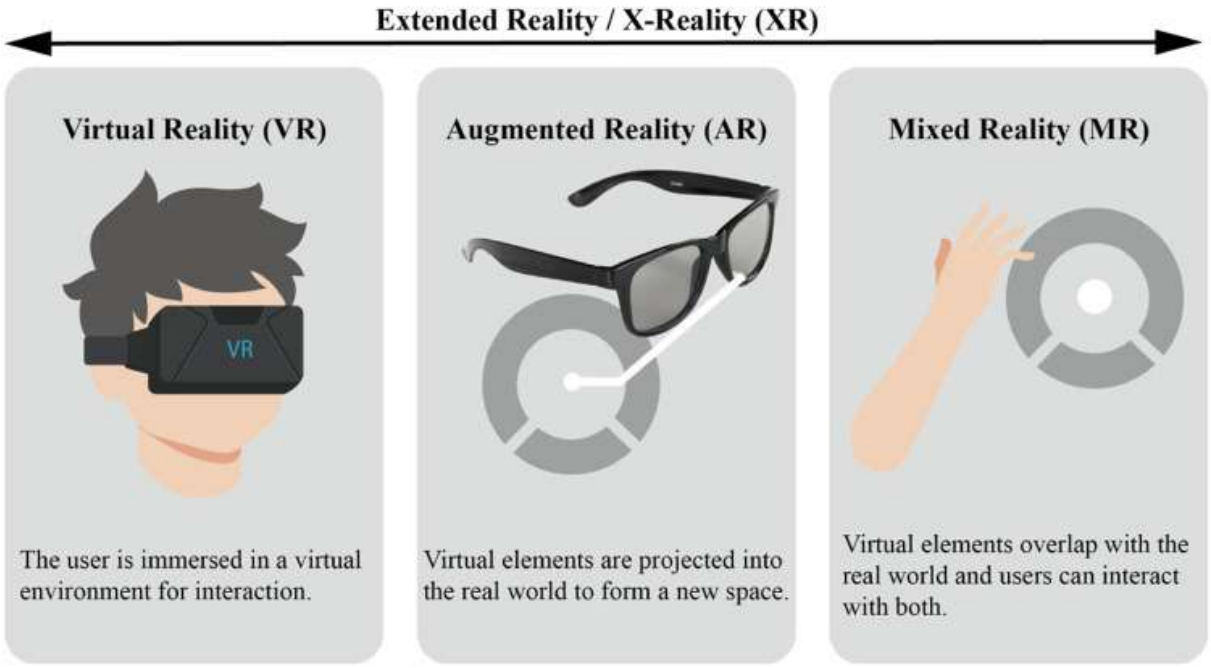

Figure 11 – Relationships and definitions between the XRs, extracted from (LI et al., 2024).

Some of the XR serious games found in the literature are based on standardized testing in the use of prostheses such as VR Box and Block Test (VR-BBT) (HASHIM et al., 2021), VR Southampton Hand Assessment Procedure (VR-SHAP) (CELLUPICA et al., 2024) or Prosthetic Hand Assessment Measure in AR (AR-PHAM) (HUNT et al., 2023). Others focus on ADL activities, such as the VR serious game proposed by Tchimino *et al.* in which the user must grab different "coffee" cups (TCHIMINO et al., 2025). And some games focus on the training of grip control (KRISTOFFERSEN et al., 2021; MAAS; SLUIS; BONGERS, 2024).

4 Methodology

This chapter details the methodology used to develop and evaluate the hybrid FMG-sEMG sensor for controlling the PrHand prosthesis and its DTwin. It will cover the research design, the participants involved, the hardware and software developed, the experimental procedure, and the statistical methods used for data analysis.

4.1 FMG and hybrid FMG-sEMG sensor development

These biosensors implement an OFS to accurately measure volumetric changes in muscle tissue during activation. It integrates an FBG sensor embedded within a flexible 3D-printed piece. Ensuring accurate readings and adaptability to the dynamic movements of the muscle, providing valuable real-time data on muscle behavior, the 3D design was based on the work of Tavares *et al.* (TAVARES et al., 2022b), where they were able to monitor respiratory and heart rates with high precision.

The FBGs used in this work were inscribed into a boron-doped photosensitive optical fiber (PS1250/1500, Fibercore) using the phase mask method. The gratings were engraved with a 265.524 nm laser (DPS-266-Q, Changchun New Industries) operating at a frequency of 10 Hz with a pulse energy of 0.37 mJ. These gratings resulted in a total length of 3 mm.

For the initial Exploratory study of the FMG sensor, a 3D-printed piece was designed to cover the FBG, ensuring direct contact with the user's muscle. Its dimensions are 50 mm in length, 50 mm in width, and 3 mm in height, as illustrated in Figure 12(a). Additionally, it features a hole at a height of 1.5 mm for the fiber, with a diameter of 0.3 mm, to ensure a proper fit. Two grooves, each with a diameter of 0.7 mm, have been added for secure glue fixation. Furthermore, the design incorporates two gaps for an elastic belt, which is used to secure the sensor to the user's arm as can be seen in Figure 12(b).

The FDM process for the sensor is detailed in Figure 13. It was produced using a flexible transparent filament (Flex, 3DFila) with a fill density of 60% following a grade pattern. The process initiates with a programmed pause in the deposition during the layer before to closing the fiber path, exposing the channel designed for fiber placement as can be seen in Figure 13(a). Then, the optical fiber is manually inserted into this designated space as ilustrated in Figure 13(b), after which a cyanoacrylate-based adhesive (Super Bonder) is applied to secure it as shown in Figure 13(c). Once the adhesive has dried up, the printing process resumes to deposit the covering layer, which entirely covers the sensing element as observed in Figure 13(d). The outcome of this fabrication scheme is

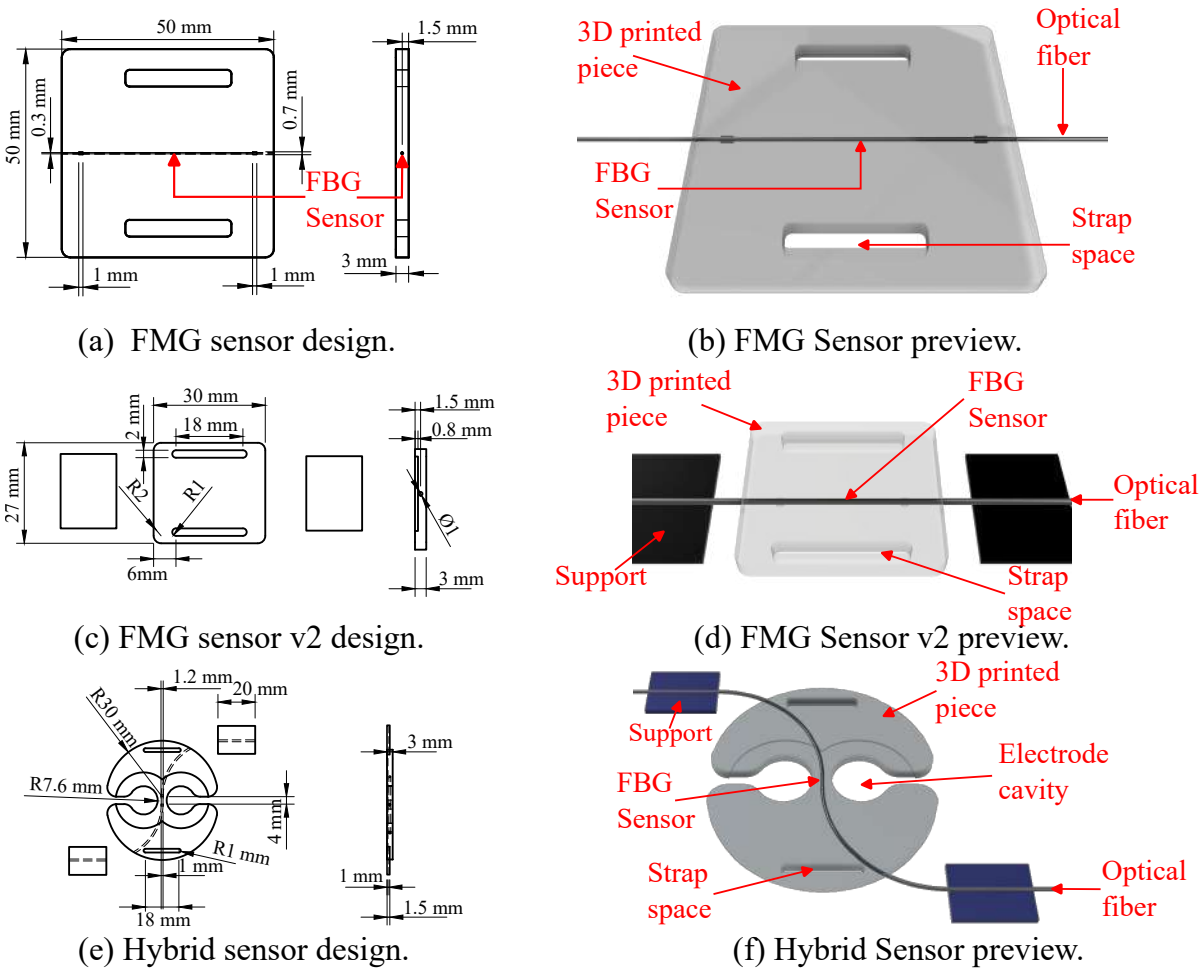

(a) FMG sensor design. (b) FMG Sensor preview.

(c) FMG sensor v2 design. (d) FMG Sensor v2 preview.

(e) Hybrid sensor design. (f) Hybrid Sensor preview.

Figure 12 – 3D design of the FMG and hybrid FMG-sEMG sensors.

ilustrated in Figure 13(e) (CORTES; SEGATTO; DíAZ, 2024).

Due to a size conflict between the FMG sensor and the sEMG sensor electrodes, it was necessary to redesign the components to allow the sensors to be placed on the same muscle for their direct comparison. The resulting 3D design is illustrated in Figure 12(c). The new piece measures 30 mm in length and 20 mm in width. It incorporates two lateral grooves, each measuring 18 mm, to better secure the device on the limb. Additionally, a centrally located path with a depth of 0.8 mm has been included to accommodate the FBG. Two supports have also been added to assist in securing the fiber to the piece, and keep the fiber straight during the gluing process, as shown in Figure 12(d).

Additionally, a new design has been developed for a feasibility study on the hybrid sensor. This design considers the dimensions of the electrode connectors measured for the Shimmer3 development kit (Consensys Bundle Development Kit) as well as the 20 mm distance between electrode centers recommended by SENIAM (STEGEMAN; HERMENS, 2007). Moreover, the minimum bend radius has been established at 30 mm, following the manufacturer's guidelines (THORLABS, 2025), as shown in Figure 12(e). This configuration grants the proper integration of the sensors, because of the gaps in the

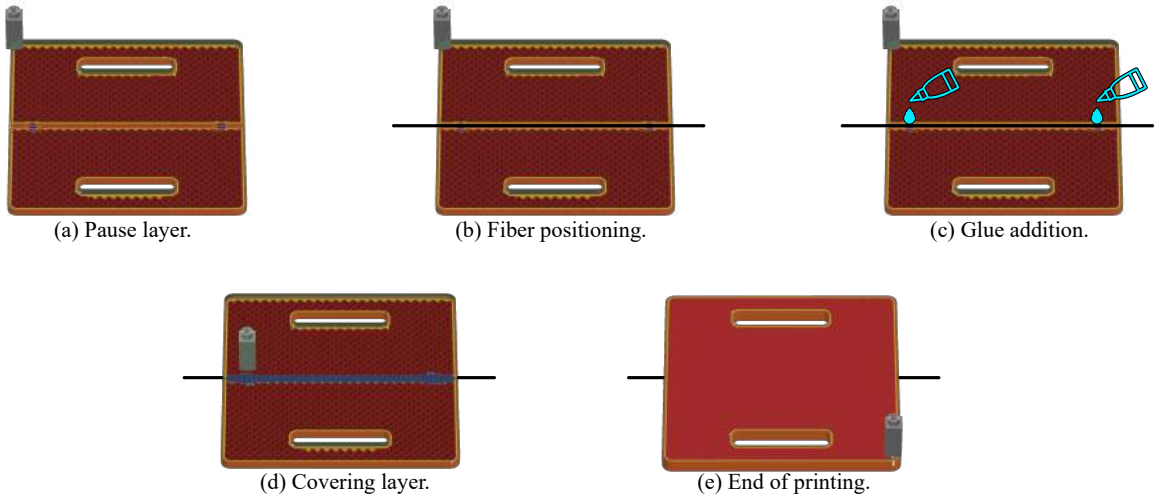

(a) Pause layer. (b) Fiber positioning. (c) Glue addition.

(d) Covering layer. (e) End of printing.

Figure 13 – Sensor building process.

electrode connectors, as illustrated in Figure 12(f).

4.2 Experimental Protocol

The experimental methodology was structured into three main protocols. The initial exploratory study of the FMG sensor developed in order to evaluate its behavior. The second protocol involved a comparative analysis between the proposed FMG sensor and a commercial sEMG. The final protocol consists of the implementation of a new FMG-sEMG hybrid sensor to assess its feasibility. This study received ethical approval from the Research Ethics Committee of the Federal University of Espírito Santo (report number: 6847995).

4.2.1 Exploratory study of the FMG sensor

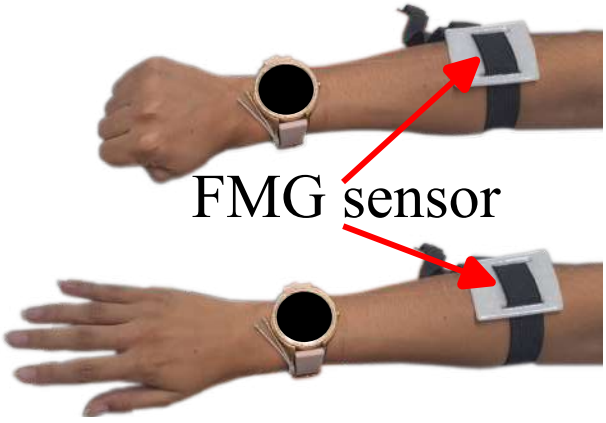

Figure 14 – Sensor placed with different gestures.

In this protocol, the sensor was attached to the Extensor Digitorum Communis (EDC) muscle, which is responsible for extending the index to little fingers (ISLAM et al., 2024). The sensor was secured using an elastic band at a comfortable contraction for the subject, as shown in Figure 14.

The user was then asked to open and close their hand three times, holding each position for approximately 15 seconds. The mean and standard deviation were then calculated for each gesture.

4.2.2 Comparison of FMG and sEMG

This protocol compares the accuracy and precision performance of the proposed FMG sensor with the performance of the commercial sEMG sensor in angle and force classification. Six volunteers, four males and two females, with a mean age of 23 ± 3 years, participated in the study. A dynamometer (DM-90, INSTRUTHERM) served as a force reference, while Kinovea software was used as an angle reference during the data collection process.

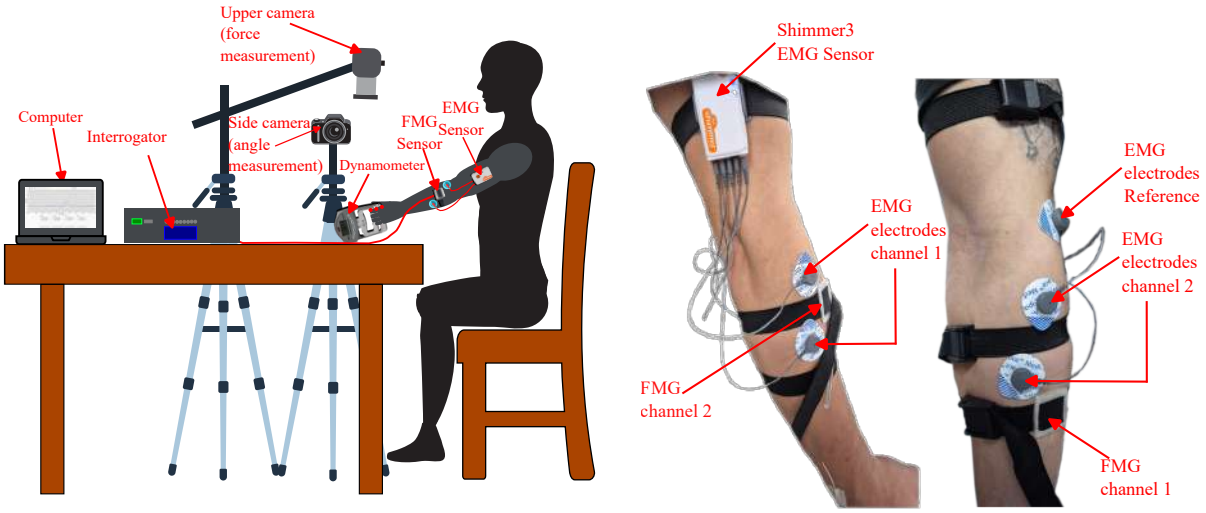

(a) Experimental layout.

(b) Sensors positioning.

Figure 15 – Protocol setup for comparison of EMG and sEMG sensors.

Initially, the protocol was detailed, and the investigators answered all the participants' questions; after which, the participants provided informed consent. Following, sEMG and FMG sensors were placed to monitor the flexor digitorum superficialis (FDS) and EDC muscles of the participants, as illustrated in Figure 15(a). Additionally, three red markers were placed on the metacarpophalangeal (MCP) joint, proximal interphalangeal (PIP) joint, and the fingertip of each participant to determine the angle. Participants were instructed to sit comfortably while performing the force effort task, which was recorded by two cameras. One camera recorded the force measured by the dynamometer, and the other

measured the angle using markers, as shown in Figure 15(b). Next, they were asked to apply three levels of force, categorized as high, medium, and low. Then, the dynamometer grip was adjusted to reduce the angle of the fingers. This was done three times for each participant. After data collection, synchronization was performed using the timestamps of the FMG and sEMG data, which were recorded simultaneously, with the timestamps extracted from the Kinovea software. It is important to note that the start time of the recording is crucial for generating accurate timestamps when using the Kinovea software.

4.2.3 Feasibility of the hybrid sensor

(a) Flappy hand. (b) Avoid.

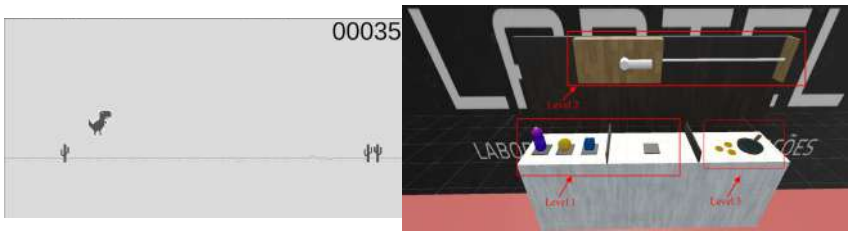

(c) Dino. (d) VR-SHAP.

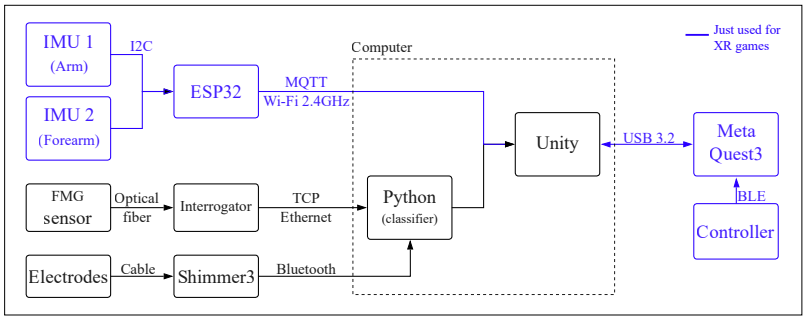

(e) Communication diagram for serious games.

Figure 16 – Serious games developed.

The main goal of this protocol was to evaluate the performance of the hybrid sensor. For this purpose, four serious games were developed. These games are: Flappy Hand, inspired by Flappy Bird; Avoid, based on Asteroids; Dino, based on the Chrome Dino game; and VR-SHAP, inspired by the SHAP test, as depicted in Figure 16(a), (b), (c), and (d), respectively. For this study, the VR-SHAP serious game was fully implemented, whereas the other serious games served only as proofs of concept and for preliminary testing of the sensors performance. The communication architecture for the serious games, shown in

Figure 16(e), consists of a combination of wired and wireless protocols to integrate data from the sensors. The data from the biosensors for gesture classification is obtained from the FMG and EMG sensors and sent via TCP/Ethernet and Bluetooth, respectively. For arm tracking in the XR games, two IMUs send data to an ESP32 using I2C. Both the Python classifier and the ESP32 publish their processed data to the Unity game engine using the MQTT protocol over Wi-Fi. Finally, the computer running Unity communicates with the Meta Quest 3 headset via USB 3.2, while the controller connects to the headset using BLE.

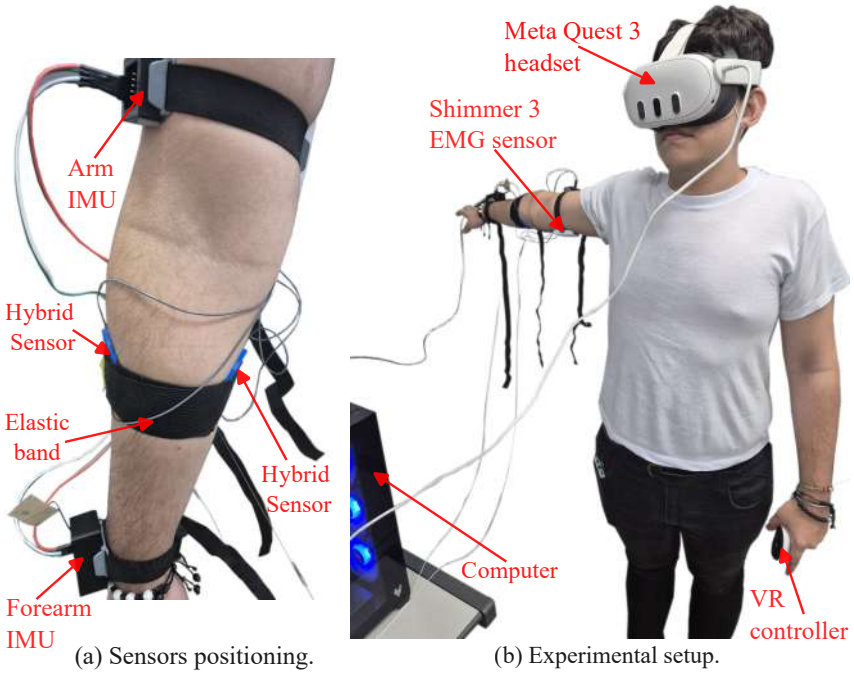

(a) Sensors positioning. (b) Experimental setup.

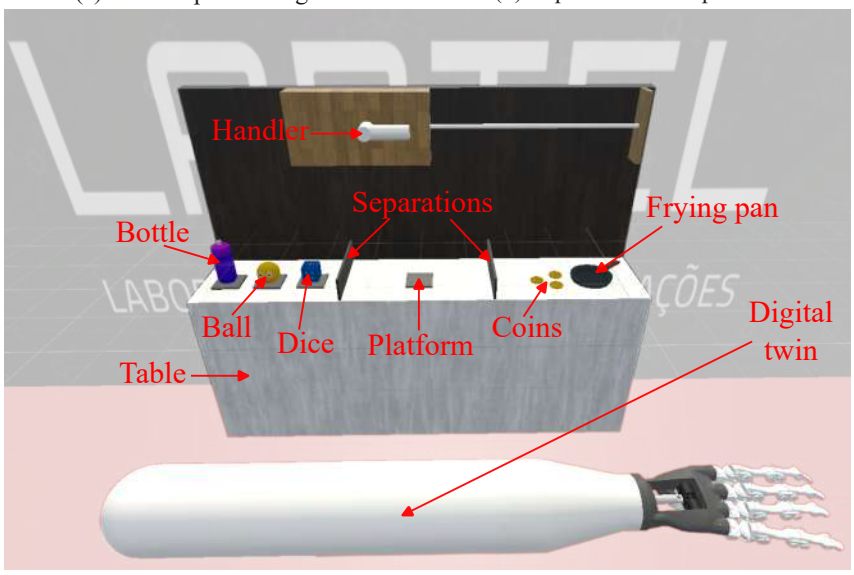

(c) VR setup.

Figure 17 – Protocol configuration for hybrid sensor feasibility.

This protocol was divided into three distinct stages: a setup phase, a classifier training phase, and an experimental task phase. The setup involved outfitting each

participant's dominant arm with the sensor array. First, two pairs of sEMG electrodes were placed over the flexor digitorum superficialis and extensor digitorum muscles. FMG sensors were then positioned between the sEMG electrodes. The entire assembly was secured to the forearm with a strap and an additional elastic band to maintain consistent pressure and ensure measurement quality. Finally, two IMUs were placed on the upper arm near the biceps brachii and on the forearm near the wrist to capture arm orientation, as can be seen in Figure 17(a) and (b). For classifier training, data was recorded for 35 seconds for each of two static gestures: a relaxed, open hand and a clenched fist, where the MVC was performed.

The protocol consists of a modified version of the VR-SHAP, initially developed by Cellupica *et al.* (CELLUPICA et al., 2024). The virtual environment consisted of a room with a table that had some interactive objects and a wall with a handle. Participants were required to complete three sequential tasks. The first phase involved grasping a bottle, a die, and a ball, and then moving them to a platform located in the middle of the table. The second phase required the user to turn the handle on the wall approximately 45°. In the final phase, the participant had to pick up three coins and drop them into a frying pan, as illustrated in Figure 17 (c).

Once the machine learning classifier was trained with the collected data, the experimental task phase began. In this phase, a Python script performed real-time gesture recognition, classifying the incoming sEMG and FMG signals and sending *open* (0) or *close* (1) commands to the Unity application. Simultaneously, data from the IMUs was sent directly to Unity to track arm movements, which were calibrated in-game prior to the tasks. To familiarize themselves with the system, the three participants first performed four trial repetitions of all tasks. Performance was then evaluated using the completion time of the fifth and final repetition. After this last trial, all sensors were removed, and participants provided subjective feedback on the system's usability.

4.3 Data recording settings and feature extraction

The data acquisition from the FBG of the FMG sensor is performed using an interrogator (HYPERION si255, Luna's, USA). This instrument operates with a sensor scan rate of 5 kHz, it features a high wavelength accuracy of 1 pm and operates within a 1500 nm to 1600 nm wavelength window, falling within its total 160 nm range capability. The interrogator interfaces with a computer via Ethernet using the TCP protocol.

For the sEMG lecture, was utilized a commercial EMG sensor (Shimmer3 ECG/EMG, Ireland). This device enables the acquisition of two EMG channels through a 24-bit analog-to-digital converter (ADC) and wirelessly transmits data at a baud rate of 1024 Hz via Bluetooth 4.2. Additionally, foam electrodes with adhesive hydrogel (Kendall, Covidien)

were employed.

For the sEMG sensor, the raw EMG signal data is passed through a digital finite impulse response (FIR) bandpass filter with a frequency range of 40 Hz to 150 Hz, as this signal exhibits maximum values within that range (EMON et al., 2024). After the filtering, the sEMG signals were normalized using maximal voluntary contraction (MVC), in which signal amplitude is expressed as a percentage of the maximum value recorded during a reference contraction (AVDAN; ONAL; SMITH, 2023). Then, the set of characteristics was defined in 10-sample moving windows, and the features chosen were RMS, MAV, SSC, WL, VAR, mean, kurtosis, skewness, and ZC.

On the other hand, FMG sensor was first smoothed using a 10-sample moving average filter. Then a min-max scaling was applied. This technique rescaled the force data to a uniform range of 0 to 1, where 0 corresponds to the minimum recorded force and 1 corresponds to the maximum recorded force (SHERIF; BASSUONI; MEHREZ, 2024). Then, the set of characteristics was defined in 10-sample moving windows, and the features chosen were RMS, MAV, SSC, WL, VAR, mean, kurtosis, and skewness.

In addition, an error handler was added for kurtosis and skewness, which cannot be calculated in small or unchanged data segments. This is because the calculation of kurtosis depends on the analysis window containing at least four data points with variation, and skewness requires at least two data points. If these conditions are not met, the system returns a value of zero.

To correlate the characteristics of EMG with their corresponding FMG, measurements must be taken during the same timeframe. While the EMG system was set up to record at a sampling frequency of 1024 Hz, and the interrogator supported a theoretical FMG transmission speed of 1 kHz, the maximum frequency achieved was 100 Hz.

For the implementation of ML, seven models were used: KNN, GNB, LR, DT, RF, SVM, and LDA. This work utilized Scikit-learn, a Python module that integrates a wide range of algorithms for supervised and unsupervised tasks. The library includes the GridSearchCV function, which systematically evaluates parameter grids using cross-validation to optimize the performance of an estimator (PEDREGOSA et al., 2011). Hyperparameter information is extracted directly from the Scikit-learn user guide (SCIKIT-LEARN, 2025b) and the Scikit-learn API (SCIKIT-LEARN, 2025a). The performance of the classification models trained in this master's work were evaluated using the accuracy, precision, and recall.

5 Results

This chapter presents the results obtained from the three main protocols used in this work. The first protocol was designed to explore the behavior of the FBG-based FMG sensor and its response to variations in muscle activity during gesture performance. The second is a direct comparison of the performance of ML algorithms trained with the optimal features obtained and also with a reduced set of features for online applications. Finally, the third shows the results of a VR application of the hybrid sensor, as measured by the system usability scale (SUS), and a comparison of the ML models used during the tests.

5.1 Exploratory study of the FMG sensor

During the three trials, the mean and standard deviation are plotted in Figure 18. Additionally, it is remarkable how the λ_B changes with every gesture, these are "Open hand," "Intermediate state," and "Closed hand".

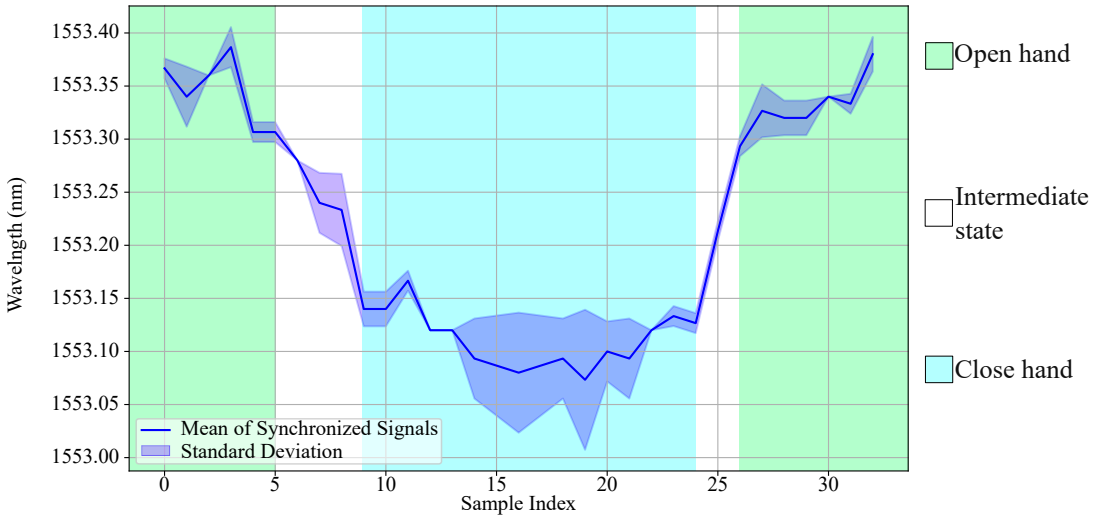

Figure 18 – FMG sensor data. (a) the mean and standard deviation. (b) λ_B of each gesture.

5.2 sEMG and FMG comparison

The data read by the sensors after the preprocessing and the regions used for the ML process are illustrated in Figure 19. Figure 19(a) illustrates the EMG-RMS values, which correlate with the force shown in Figure 19(c), but these are not linearly proportional. This nonlinearity is a characteristic of sEMG due to the complex physiological factors, including motor unit recruitment strategies. Besides, Figure 19(b) shows the normalized

FMG signal, which captures the mechanical changes in the muscles. It is important to note that, because participants held the dynamometer, the angle data shown in Figure 19(d) reflect a limited range, representing the posture required to secure the device and the adjustments made to the dynamometer grip during the protocol. Additionally, the regions used for the ML process were based on timestamps extracted from the camera that monitored the dynamometer values.

The dataset used for ML was selected based on observations of the force values recorded by the camera monitoring the dynamometer. Then, for all the participants, the features are calculated as explained in the previous chapter, resulting in a dataset containing 36 features and 4,411 records for the entire participant group. The function SelectKBest is used to determine the ten most relevant features. It applies the ANOVA F-value as a scoring function, selecting the features with the higher scores. Then the data is split 80% for training and validation, and 20% for testing. For each of the ML algorithms, the *GridSearchCV* was used with five folds to optimize the hyperparameters.

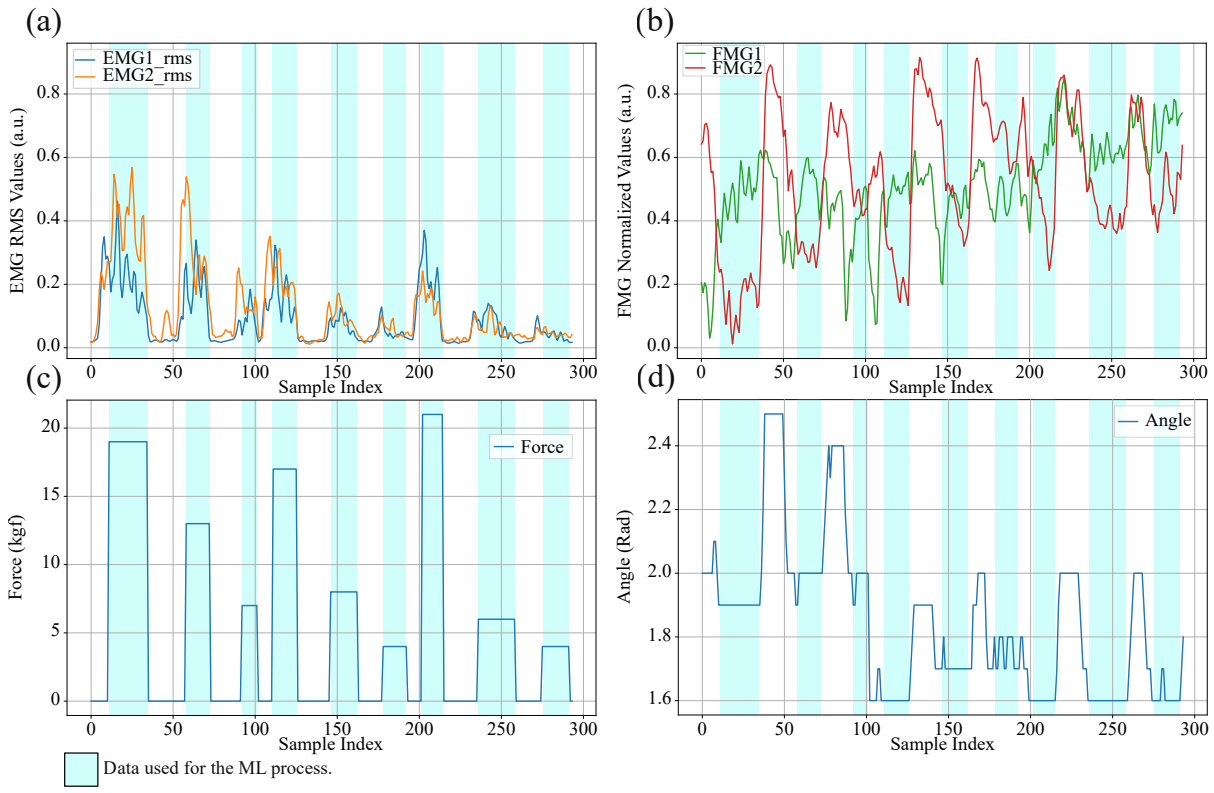

Figure 19 – Signals measured by the sensors, highlighting the data used in ML training and testing. (a) EMG-RMS data used as a feature. (b) FMG normalized data used as a feature. (c) Force values measured by the dynamometer that were used as labels. (d) Angle values extracted by the software Kinovea that were used as labels.

5.2.1 Angle classification

The features used in the angle classification were $EMG1\_MAV$, $EMG2\_RMS$, $EMG2\_MAV$, and $EMG2\_VAR$ for the sEMG. Also, For FMG signal were used $FMG1\_RMS$, $FMG1\_MAV$, $FMG1\_MEAN$, $FMG2\_RMS$, $FMG2\_MAV$, and $FMG2\_MEAN$.

The results obtained for training and testing the seven machine learning algorithms using only the sEMG features are presented in Table 5. The RF achieved the best accuracy with 56.5%. The hyperparameters were *max_depth* of 20, *min_samples_leaf* of 2, *min_samples_split* of 4, and *n_estimators* of 300. On the other hand, the results of the machine learning algorithms using only the FMG features are presented in Table 6. The RF achieved the best accuracy with 83.24%. The hyperparameters were *max_depth* of 20, *min_samples_leaf* of 2, *min_samples_split* of 2, and *n_estimators* of 300.

Table 5 – Accuracy, precision, and sensitivity comparison for ML classification of the angle using optimal EMG features.

Model	**Accuracy**	**Precision**	**Sensitivity**	**Best Estimator Params**
KNN	33.75%	35.02%	33.75%	*metric*: *manhattan*, *n_neighbors*: 2
GNB	25.71%	24.09%	25.71%	*var_smoothing*: 0.008111308307896872
LR	26.84%	21.35%	26.84%	*C*: 29.763514416313132, *penalty*: *l2*, *solver*: *lbfgs*
DT	48.24%	49.22%	48.24%	*max_depth*: 25, *min_samples_leaf*: 2, *min_samples_split*: 2
RF	56.4%	56.51%	56.4%	*max_depth*: 20, *min_samples_leaf*: 2, *min_samples_split*: 4, *n_estimators*: 300
SVM	37.94%	35.96%	37.94%	*kernel*: *rbf*, *gamma*: 1, *C*: 100
LDA	26.16%	21.33%	26.16%	*shrinkage*: None, *solver*: *svd*

Table 6 – Accuracy, precision, and sensitivity comparison for ML classification of the angle using optimal FMG features.

Model	**Accuracy**	**Precision**	**Sensitivity**	**Best Estimator Params**
KNN	43.49%	43.34%	43.49%	*metric*: *manhattan*, *n_neighbors*: 8
GNB	38.96%	39.67%	38.96%	*var_smoothing*: 0.0015199110829529332
LR	36.81%	25.23%	36.81%	*C*: 10000.0, *penalty*: *l2*, *solver*: *lbfgs*
DT	73.95%	74.44%	73.95%	*max_depth*: 25, *min_samples_leaf*: 2, *min_samples_split*: 4
RF	83.24%	83.69%	83.24%	*max_depth*: 20, *min_samples_leaf*: 2, *min_samples_split*: 2, *n_estimators*: 300
SVM	50.28%	49.8%	50.28%	*kernel*: *rbf*, *gamma*: 1, *C*: 100
LDA	36.92%	27.13%	36.92%	*shrinkage*: *auto*, *solver*: *lsqr*

When using the complete set of ten hybrid (sEMG + FMG) features, the results obtained for training and testing of the seven machine learning algorithms are presented in Table 7. For this, the best accuracy was achieved by the KNN model, with 85.62%. The optimal hyperparameters were *metric* of *minkowski*, and *n_neighbors* of 2. Showing a big increase from the best model trained with sEMG features (29.23%), and a minor increase from the model trained with FMG features (2.38%). Also, the feature permutation importance is presented in Figure 20, where it can be seen that the most important features were related to the FMG2 (EDC muscle).

Table 7 – Accuracy, precision, and sensitivity comparison for ML classification of the angle using optimal EMG and FMG features.

Model	Accuracy	Precision	Sensitivity	Best Estimator Params
KNN	85.62%	85.64%	85.62%	*metric*: *minkowski*, *n_neighbors*: 2
GNB	39.07%	39.18%	39.07%	*var_smoothing*: 0.8111308307896871
LR	43.71%	38.76%	43.71%	*C*: 1438.44988828766, *penalty*: *l2*, *solver*: *lbfgs*
DT	74.97%	75.08%	74.97%	*max_depth*: 25, *min_samples_leaf*: 2, *min_samples_split*: 2
RF	83.92%	83.98%	83.92%	*max_depth*: 20, *min_samples_leaf*: 2, *min_samples_split*: 2, *n_estimators*: 300
SVM	76.33%	76.31%	76.33%	*kernel*: *rbf*, *gamma*: *scale*, *C*: 100
LDA	41.34%	32.8%	41.34%	*shrinkage*: None, *solver*: *lsqr*

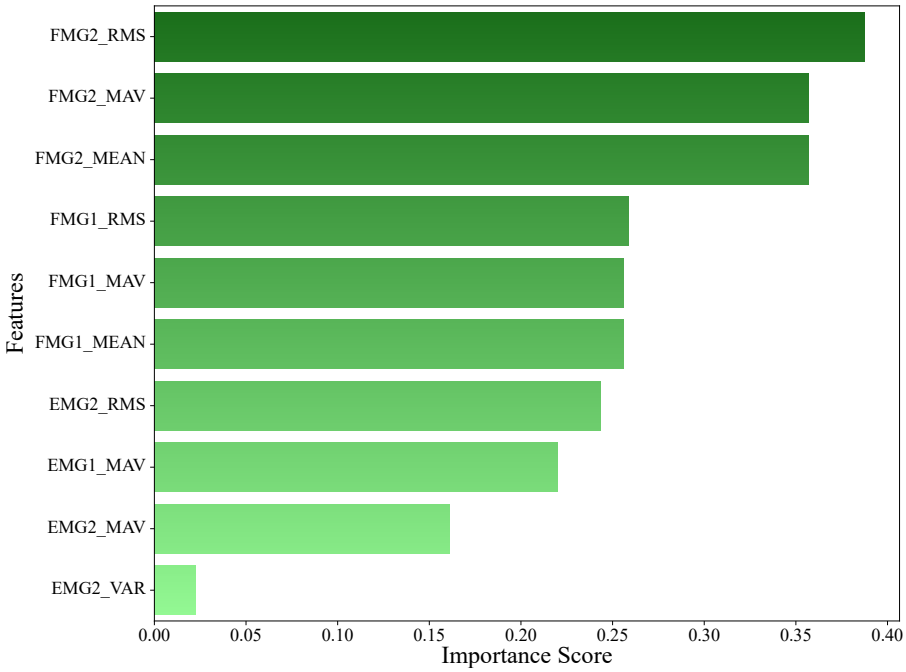

Figure 20 – Feature permutation importance for the KNN model using hybrid features.

5.2.2 Force classification

The features used in the force classification were $EMG1\_RMS$, $EMG1\_MAV$, $EMG1\_VAR$, $EMG2\_RMS$, $EMG2\_MAV$, $EMG2\_WL$, and $EMG2\_VAR$, for the sEMG. For the FMG signal, $FMG2\_RMS$, $FMG2\_MAV$, and $FMG2\_MEAN$ were used.

The result obtained for training and testing of the seven machine learning algorithms using only the sEMG features is presented in Table 8. The SVM achieved the best accuracy with 92.53%. The hyperparameters were *kernel* of *rbf*, *gamma* of 0.01, and C of 100. On the other hand, the results of the machine learning algorithms using only the FMG features are presented in Table 9. The RF achieved the best accuracy with 43.83%. The hyperparameters were max_depth of 15, $min\_samples\_leaf$ of 2, $min\_samples\_split$ of 4, and $n\_estimators$ of 300.

When using the complete set of ten hybrid (sEMG + FMG) features, the re-

Table 8 – Accuracy, precision, and sensitivity comparison for ML classification of the force using optimal EMG features.

Model	**Accuracy**	**Precision**	**Sensitivity**	**Best Estimator Params**
KNN	76.1%	78.39%	76.1%	*metric*: *manhattan*, *n_neighbors*: 2
GNB	38.84%	40.48%	38.84%	*var_smoothing*: $1.232846739442066e-08$
LR	29.56%	27.95%	29.56%	*C*: 206.913808111479, *penalty*: *l2*, *solver*: *lbfgs*
DT	83.24%	83.86%	83.24%	*max_depth*: 30, *min_samples_leaf*: 2, *min_samples_split*: 2
RF	91.17%	91.46%	91.17%	*max_depth*: 20, *min_samples_leaf*: 2, *min_samples_split*: 2, *n_estimators*: 300
SVM	92.53%	92.75%	92.53%	*kernel*: *rbf*, *gamma*: 0.01, *C*: 100

Table 9 – Accuracy, precision, and sensitivity comparison for ML classification of the force using optimal FMG features.

Model	**Accuracy**	**Precision**	**Sensitivity**	**Best Estimator Params**
KNN	23.1%	24.1%	23.1%	*metric*: *manhattan*, *n_neighbors*: 6
GNB	16.76%	6.89%	16.76%	*var_smoothing*: $1e-05$
LR	13.93%	6.96%	13.93%	*C*: 1438.44988828766, *penalty*: *l2*, *solver*: *liblinear*
DT	41.68%	42.79%	41.68%	*max_depth*: 15, *min_samples_leaf*: 2, *min_samples_split*: 4
RF	43.83%	44.44%	43.83%	*max_depth*: 15, *min_samples_leaf*: 2, *min_samples_split*: 4, *n_estimators*: 300
SVM	22.08%	20.87%	22.08%	*kernel*: *rbf*, *gamma*: *scale*, *C*: 100
LDA	13.82%	4.26%	13.82%	*shrinkage*: 0.1, *solver*: *lsqr*

sults obtained for training and testing of the seven machine learning algorithms are presented in Table 10. For this, the best accuracy was achieved by the RF model, with 78.14%. The optimal hyperparameters were *max_depth* of 20, *min_samples_leaf* of 2, *min_samples_split* of 4, and *n_estimators* of 300. Showing a moderate decrease from the best model trained with sEMG features (14.36%), and a big increase from the model trained with FMG features (34.31%). Also, the feature importance is presented in Figure 21, where it can be seen that the most important features were related to the FMG2 (EDC muscle). This suggests that the reduction in model accuracy was due to the RF model automatically attributed greater importance to FMG signals during training, which already showed lower performance compared to sEMG signals.

Table 10 – Accuracy, precision, and sensitivity comparison for ML classification of the force using optimal features.

Model	Accuracy	Precision	Sensitivity	Best Estimator Params
KNN	66.36%	67.91%	66.36%	*metric*: *manhattan*, *n_neighbors*: 2
GNB	30.24%	27.82%	30.24%	*var_smoothing*: 0.0001519911082952933
LR	30.69%	31.48%	30.69%	*C*: 10000.0, *penalty*: *l2*, *solver*: *lbfgs*
DT	66.02%	67.33%	66.02%	*max_depth*: 20, *min_samples_leaf*: 2, *min_samples_split*: 4
RF	78.14%	78.69%	78.14%	*max_depth*: 20, *min_samples_leaf*: 2, *min_samples_split*: 4, *n_estimators*: 300
SVM	64.21%	65.78%	64.21%	*kernel*: *rbf*, *gamma*: 1, *C*: 100
LDA	26.05%	24.96%	26.05%	*shrinkage*: None, *solver*: *svd*

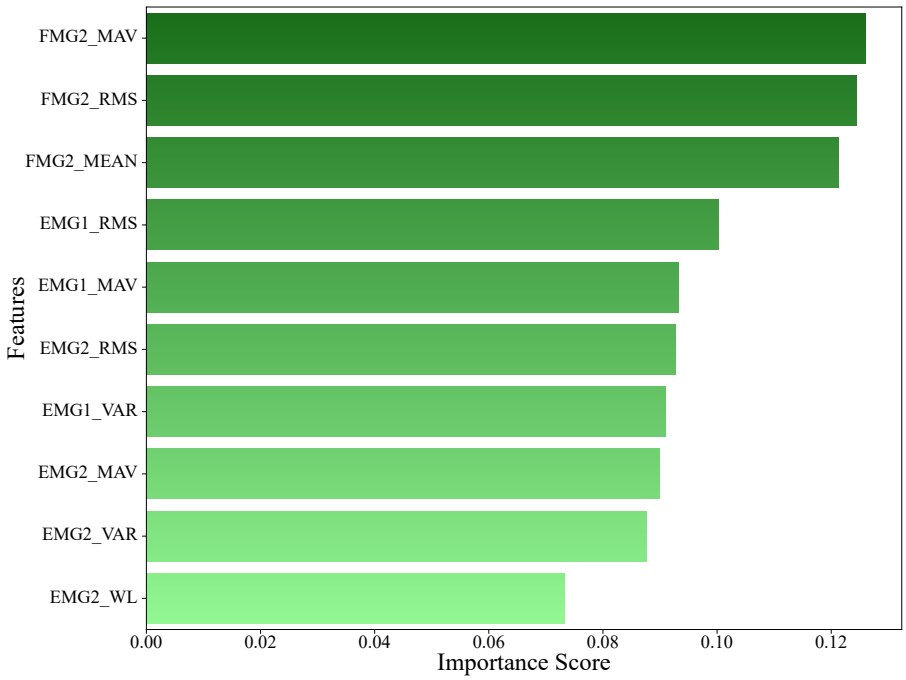

Figure 21 – Feature importance (Gini) for the RF model using hybrid features.

5.3 Feasibility of the hybrid sensor

The data read by the sensors after preprocessing is illustrated in Figure 22, where the variations in the signals can be observed when the hand is closed and opened. First, the $EMG1\_RMS$, $EMG2\_RMS$, $FMG1\_MEAN$, and $FMG2\_MEAN$ features are calculated as explained in the previous chapter, resulting in a dataset of 4 features with 7066.33 ± 6.13 samples for participant. Then the data is split 80% for training and validation, and 20% for testing. For each of the ML algorithms, the *GridSearchCV* was used with five folds to optimize the hyperparameters.

The summary of the average results from the seven machine learning algorithms from the three subjects is presented in Table 11. Among these models, the best performance was achieved by the KNN with 99.83% accuracy. For the three participants, the best *n_neighbors* was 3, and two of the three chose the best *metric* as *euclidean*, the other one chose *manhattan*.

Table 11 – Mean Performance of Machine Learning Classifiers.

Classifier	**Accuracy (%)**	**Precision (%)**	**Recall (%)**
DT	99.07 ± 1.09	99.07 ± 1.09	99.07 ± 1.09
GNB	90.61 ± 10.75	91.05 ± 10.14	90.61 ± 10.75
KNN	99.83 ± 0.11	99.83 ± 0.11	99.83 ± 0.11
LDA	92.37 ± 6.91	92.60 ± 7.02	92.37 ± 6.91
LR	93.60 ± 7.62	93.60 ± 7.62	93.60 ± 7.62
RF	99.10 ± 0.98	99.11 ± 0.98	99.10 ± 0.98
SVC	97.42 ± 2.24	97.44 ± 2.24	97.42 ± 2.24

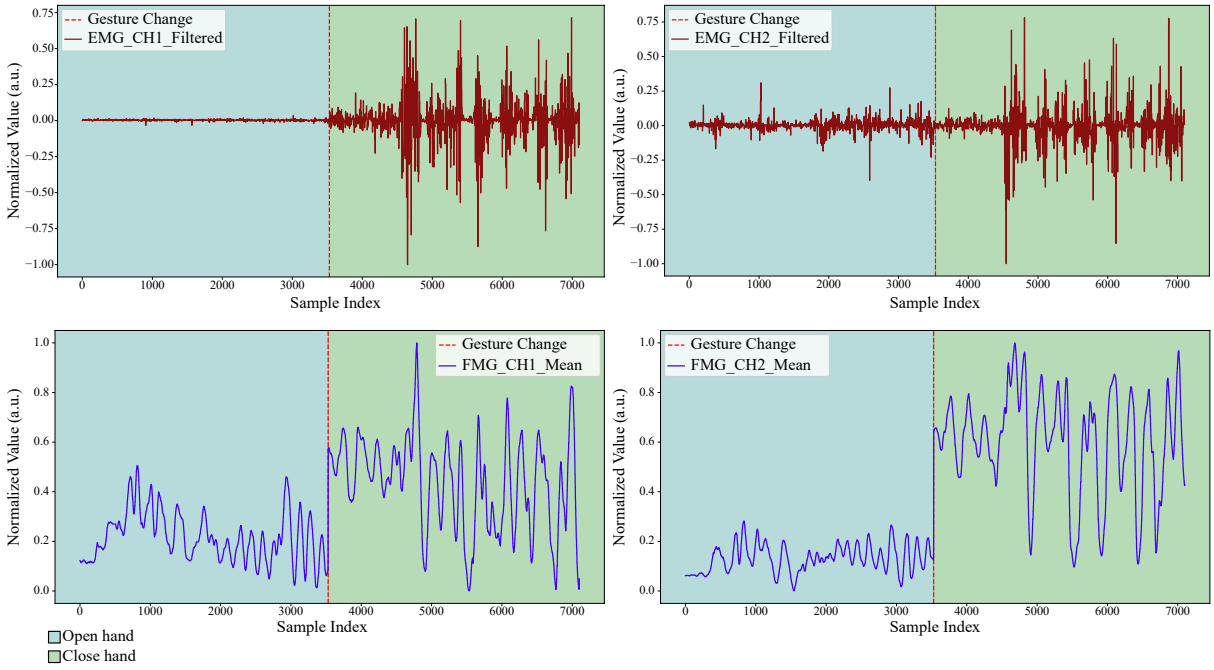

Figure 22 – Signals measured by the sensors, highlighting the variation of the data when changing the gesture. (a) Normalized EMG signal in channel 1. (b) Normalized FMG signal in channel 1. (c) Normalized EMG signal in channel 2. (b) Normalized FMG signal in channel 2.

An example of the process to move the object inside the VR serious game is illustrated in Figure 23. The duration taken to finish all stages of the experiment for the first user was 02:32.65, for User 2, it was 01:38.60, and for User 3, it was 02:06.82. The average completion time for the group was 125.92 seconds (02:05.92), with a standard deviation of 21.84 seconds.

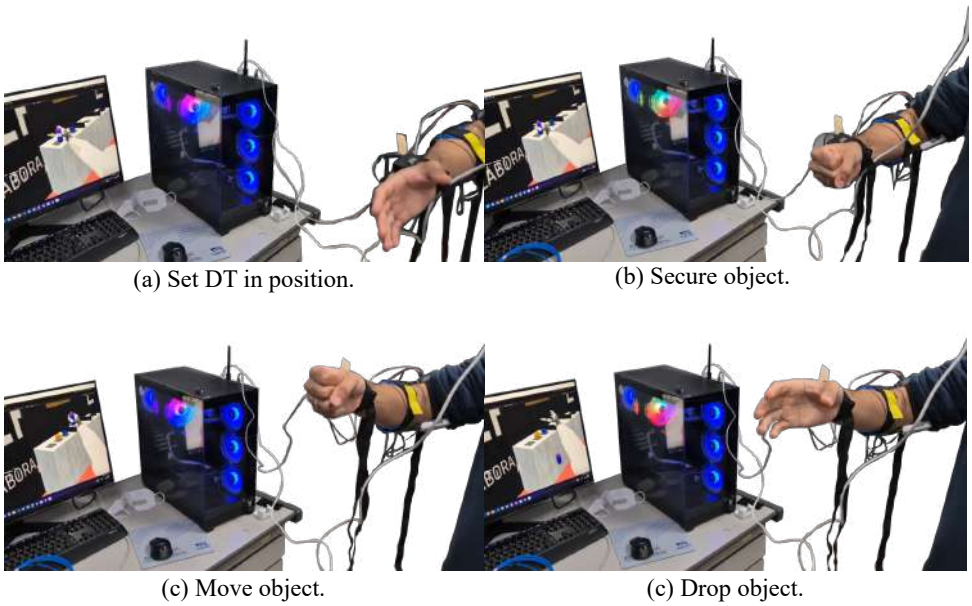

(a) Set DT in position. (b) Secure object.

(c) Move object. (c) Drop object.

Figure 23 – Process to moving a object in the VR environment.

The system usability scale (SUS) was calculated based on the answers illustrated in Figure 24, and the results were 70, 75, and 47.5, showing that two of the users validated the VR-SHAP near the average.

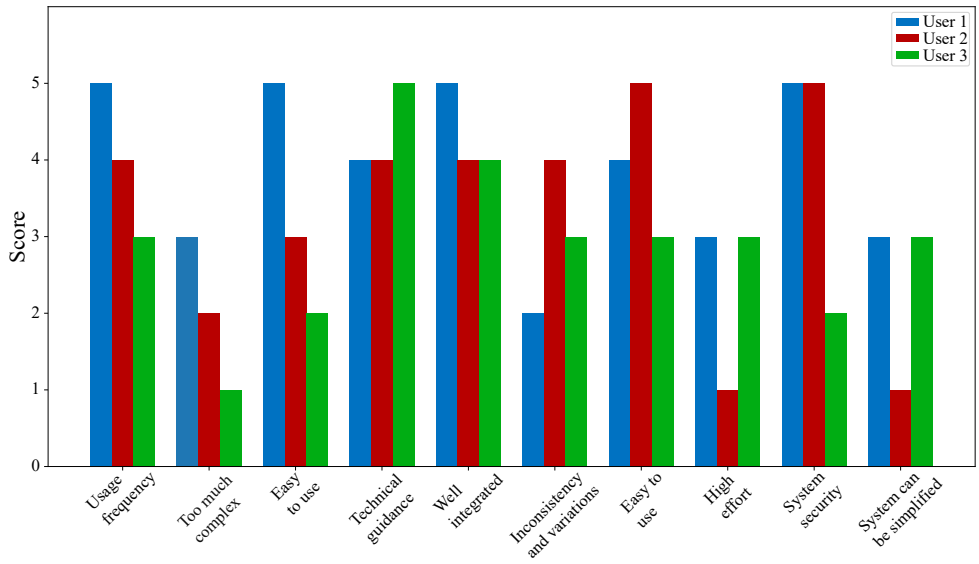

Figure 24 – System usability scale answers from zero to five.

6 Conclusions and Future Works

This master's dissertation successfully developed and evaluated a hand gesture classification system based on a hybrid sensor that combines a 3D-printed, FBG-based FMG sensor with a commercial sEMG sensor. The research achieved its specific objectives, from developing and characterizing the FMG sensor to training and comparing multiple machine learning classifiers and validating the system in a VR environment. To the best of the authors knowledge, this is the first work to demonstrate a hybrid FBG-based FMG and sEMG sensor system for hand gesture classification and its implementation in a VR environment.

The developed FBG-based FMG sensor proves to be an effective tool for gesture recognition, successfully detecting volumetric changes in muscle during contraction. Hybrid FMG-sEMG sensing highlights in angle classification, while sEMG sensing alone is most effective for force classification. Also, FMG signals have been identified as the most critical features for decoding motion intent in both angle and force classification tasks, highlighting the significance of measuring the mechanical properties of muscle contraction. This identification can be considered a significant finding, as it highlights the value of mechanical sensing for gesture recognition. The hybrid sensor system is suitable for real-time implementation, as evidenced by its accuracy of 99.83% and its control of a DTwin in a VR serious game. This research represents progress in the field of gesture identification by demonstrating the complementary behavior of FMG and sEMG signals, illustrating that different sensors can sense aspects of movement. This work contributes to the development of more sophisticated, reliable, and intuitive multimodal control systems for upper limb prostheses.

Future work must include clinical validation with amputees, which is essential to evaluate its clinical viability and adapt the models to the unique physiological signals of the target user population. In parallel, an enhancement of the usability is needed, focusing on creating a more comfortable and simpler assembly process, and a simplified calibration process to improve user acceptance.

In addition, the reduction in force classification accuracy with the hybrid sensor suggests a requirement for better sensor fusion techniques. For this reason, future research should explore advanced algorithms or deep learning architectures that can improve the interpretation of the information provided by each sensor to maximize accuracy in all tasks. To increase the system's real-world utility, an expansion of gesture and task complexity is needed, and the system should be tested with a more extensive set of complex hand gestures and functional ADLs.

For users' usage, the development of a portable system for practical application is necessary because the current configuration relies on a big FBG interrogator that is not suitable for daily use. Additionally, it is important to explore the adaptation of the system into commercially viable portable alternatives that address the challenges associated with the interrogator. Another significant improvement is the long-term performance evaluation, to investigate the system's performance over extended periods of use. This would evaluate its robustness against muscle fatigue, changes in skin impedance due to sweat, and minor sensor displacement during ADLs.

Finally, it is important to integrate the hybrid sensor with physical prostheses using the developed classification system to control these devices and provide a final validation of the system's effectiveness in a real application.

Bibliography

AHMADIZADEH, C. et al. Toward intuitive prosthetic control: Solving common issues using force myography, surface electromyography, and pattern recognition in a pilot case study. *IEEE Robotics Automation Magazine*, v. 24, n. 4, p. 102–111, 2017. Citado 3 vezes nas páginas 28, 36, and 38.

AL-FAKIH, E.; OSMAN, N. A. A.; ADIKAN, F. R. M. The use of fiber bragg grating sensors in biomechanics and rehabilitation applications: The state-of-the-art and ongoing research topics. *Sensors*, MDPI AG, v. 12, n. 10, p. 12890–12926, sep 2012. ISSN 1424-8220. Disponível em: <http://dx.doi.org/10.3390/s121012890>. Citado na página 32.

AL-TIMEMY, A. H. et al. Improving the performance against force variation of emg controlled multifunctional upper-limb prostheses for transradial amputees. *IEEE Transactions on Neural Systems and Rehabilitation Engineering*, v. 24, n. 6, p. 650–661, 2016. Citado na página 38.

ALQAHTANI, N. J.; AL-NAIB, I.; ALTHOBAITI, M. Recent progress on smart lower prosthetic limbs: a comprehensive review on using eeg and fnirs devices in rehabilitation. *Frontiers in Bioengineering and Biotechnology*, Frontiers Media SA, v. 12, aug 2024. ISSN 2296-4185. Disponível em: <http://dx.doi.org/10.3389/fbioe.2024.1454262>. Citado na página 16.

AMOR, A. B. H.; GHOUL, O. E.; JEMNI, M. Sign language recognition using the electromyographic signal: a systematic literature review. *Sensors*, MDPI, v. 23, n. 19, p. 8343, 2023. Citado na página 17.

AMSUESS, S. et al. Context-dependent upper limb prosthesis control for natural and robust use. *IEEE Transactions on Neural Systems and Rehabilitation Engineering*, v. 24, n. 7, p. 744–753, 2016. Citado na página 37.

ANDREW, J. T. Transhumeral and elbow disarticulation anatomically contoured socket considerations. *JPO: Journal of Prosthetics and Orthotics*, LWW, v. 20, n. 3, p. 107–117, 2008. Citado na página 25.

ARCO, L. D. et al. The prhand: Functional assessment of an underactuated soft-robotic prosthetic hand. In: IEEE. *2022 9th IEEE RAS/EMBS International Conference for Biomedical Robotics and Biomechatronics (BioRob)*. [S.l.], 2022. p. 1–6. Citado na página 15.

AVDAN, G.; ONAL, S.; SMITH, B. K. Normalization of emg signals: Optimal mvc positions for the lower limb muscle groups in healthy subjects. *Journal of Medical and Biological Engineering*, v. 43, n. 2, p. 195–202, Apr 2023. ISSN 2199-4757. Disponível em: <https://doi.org/10.1007/s40846-023-00782-3>. Citado na página 51.

BAECHLE-CLAYTON, M. et al. Failures and flaws in fused deposition modeling (fdm) additively manufactured polymers and composites. *Journal of Composites Science*, MDPI AG, v. 6, n. 7, p. 202, jul 2022. ISSN 2504-477X. Disponível em: <http://dx.doi.org/10.3390/jcs6070202>. Citado na página 34.

BAKSHI, K. et al. Upper limb prosthesis control: A hybrid eeg-emg scheme for motion estimation in transhumeral subjects. In: IEEE. *2018 40th Annual International Conference of the IEEE Engineering in Medicine and Biology Society (EMBC)*. [S.l.], 2018. p. 2024–2027. Citado 2 vezes nas páginas 28 and 37.

BATTRAW, M. A. et al. A review of upper limb pediatric prostheses and perspectives on future advancements. *Prosthetics and Orthotics International*, LWW, v. 46, n. 3, p. 267–273, 2022. Citado na página 27.

BEWICK, V.; CHEEK, L.; BALL, J. Statistics review 14: Logistic regression. *Critical Care*, v. 9, n. 1, p. 112, Jan 2005. ISSN 1364-8535. Disponível em: <https://doi.org/10.1186/cc3045>. Citado na página 40.

BLANA, D. et al. Feasibility of using combined emg and kinematic signals for prosthesis control: A simulation study using a virtual reality environment. *Journal of Electromyography and Kinesiology*, Elsevier BV, v. 29, p. 21–27, aug 2016. ISSN 1050-6411. Disponível em: <http://dx.doi.org/10.1016/j.jelekin.2015.06.010>. Citado 2 vezes nas páginas 29 and 37.

BLANCHET, L. et al. Constructing bi-plots for random forest: Tutorial. *Analytica Chimica Acta*, v. 1131, p. 146–155, 2020. ISSN 0003-2670. Disponível em: <https://www.sciencedirect.com/science/article/pii/S0003267020306917>. Citado na página 41.

BRACK, R.; AMALU, E. H. A review of technology, materials and ramp;d challenges of upper limb prosthesis for improved user suitability. *Journal of Orthopaedics*, Elsevier BV, v. 23, p. 88â96, jan 2021. ISSN 0972-978X. Disponível em: <http://dx.doi.org/10.1016/j.jor.2020.12.009>. Citado na página 16.

BROEK, E. L. van den et al. Computing emotion awareness through facial electromyography. In: _____. *Computer Vision in Human-Computer Interaction*. Springer Berlin Heidelberg, 2006. p. 52–63. ISBN 9783540342038. Disponível em: <http://dx.doi.org/10.1007/11754336_6>. Citado na página 35.

CALABRESE, L. et al. What is hidden behind amputation? quanti-qualitative systematic review on psychological adjustment and quality of life in lower limb amputees for non-traumatic reasons. *Healthcare*, MDPI AG, v. 11, n. 11, p. 1661, jun 2023. ISSN 2227-9032. Disponível em: <http://dx.doi.org/10.3390/healthcare11111661>. Citado na página 15.

CAPSI-MORALES, P. et al. Functional assessment of current upper limb prostheses: An integrated clinical and technological perspective. *PLOS ONE*, Public Library of Science (PLoS), v. 18, n. 8, p. e0289978, aug 2023. ISSN 1932-6203. Disponível em: <http://dx.doi.org/10.1371/journal.pone.0289978>. Citado 3 vezes nas páginas 79, 80, and 81.

CASTELLINI, C. Upper limb active prosthetic systems—overview. In: _____. *Wearable Robotics*. Elsevier, 2020. p. 365–376. ISBN 9780128146590. Disponível em: <http://dx.doi.org/10.1016/B978-0-12-814659-0.00019-9>. Citado na página 81.

CELLUPICA, A. et al. An interactive digital-twin model for virtual reality environments to train in the use of a sensorized upper-limb prosthesis. *Algorithms*, v. 17, n. 1, 2024.

ISSN 1999-4893. Disponível em: <https://www.mdpi.com/1999-4893/17/1/35>. Citado 2 vezes nas páginas 43 and 50.

CHAPLOT, N. et al. A comprehensive analysis of artificial intelligence techniques for the prediction and prognosis of genetic disorders using various gene disorders. *Archives of Computational Methods in Engineering*, Springer, v. 30, n. 5, p. 3301–3323, 2023. Citado na página 40.

CHENG-YU, H. et al. An fbg-based smart wearable ring fabricated using fdm for monitoring body joint motion. *Journal of Industrial Textiles*, v. 50, n. 10, p. 1660–1673, 2021. Disponível em: <https://doi.org/10.1177/1528083719870204>. Citado na página 34.

CHO, E. et al. Force myography to control robotic upper extremity prostheses: A feasibility study. *Frontiers in Bioengineering and Biotechnology*, Frontiers Media SA, v. 4, mar 2016. ISSN 2296-4185. Disponível em: <http://dx.doi.org/10.3389/fbioe.2016.00018>. Citado na página 38.

CHOO, Y. J.; KIM, D. H.; CHANG, M. C. Amputation stump management: A narrative review. *World Journal of Clinical Cases*, Baishideng Publishing Group Inc., v. 10, n. 13, p. 3981â3988, may 2022. ISSN 2307-8960. Disponível em: <http://dx.doi.org/10.12998/wjcc.v10.i13.3981>. Citado na página 15.

CHOW, I.; GASTON, R. G. Transradial amputation and wrist disarticulation. *Operative Techniques in Orthopaedics*, Elsevier, v. 33, n. 3, p. 101058, 2023. Citado na página 24.

CORDELLA, F. et al. Literature review on needs of upper limb prosthesis users. *Frontiers in Neuroscience*, Frontiers Media SA, v. 10, may 2016. ISSN 1662-453X. Disponível em: <http://dx.doi.org/10.3389/fnins.2016.00209>. Citado na página 23.

CORTES, F. R.; SEGATTO, M. E. V.; DíAZ, C. A. R. Development of a force myography sensor for prhand prosthesis activation using fiber bragg grating sensor and 3d printing. In: *2024 Latin American Workshop on Optical Fiber Sensors (LAWOFS)*. [S.l.: s.n.], 2024. p. 1–2. Citado na página 45.

CUNNINGHAM, P.; DELANY, S. J. k-nearest neighbour classifiers - a tutorial. *ACM Comput. Surv.*, Association for Computing Machinery, New York, NY, USA, v. 54, n. 6, jul. 2021. ISSN 0360-0300. Disponível em: <https://doi.org/10.1145/3459665>. Citado na página 40.

DAS, N.; NAGPAL, N.; BANKURA, S. S. A review on the advancements in the field of upper limb prosthesis. *Journal of Medical Engineering amp; Technology*, Informa UK Limited, v. 42, n. 7, p. 532â545, oct 2018. ISSN 1464-522X. Disponível em: <http://dx.doi.org/10.1080/03091902.2019.1576793>. Citado 2 vezes nas páginas 15 and 23.

DEIJS, M. et al. Flexible and static wrist units in upper limb prosthesis users: functionality scores, user satisfaction and compensatory movements. *Journal of NeuroEngineering and Rehabilitation*, Springer Science and Business Media LLC, v. 13, n. 1, mar 2016. ISSN 1743-0003. Disponível em: <http://dx.doi.org/10.1186/s12984-016-0130-0>. Citado 2 vezes nas páginas 79 and 80.

DEY, A.; BASUMATARY, H.; HAZARIKA, S. M. A decade of haptic feedback for upper limb prostheses. *IEEE Transactions on Medical Robotics and Bionics*, IEEE, v. 5, n. 4, p. 793–810, 2023. Citado na página 80.

DIDERIKSEN, J. et al. Investigating the benefits of multivariable proprioceptive feedback for upper-limb prostheses. *IEEE Transactions on Medical Robotics and Bionics*, IEEE, 2024. Citado na página 80.

DIJK, L. van et al. Task-oriented gaming for transfer to prosthesis use. *IEEE Transactions on Neural Systems and Rehabilitation Engineering*, v. 24, n. 12, p. 1384–1394, 2016. Citado na página 42.

EDDY, E. et al. Big data in myoelectric control: large multi-user models enable robust zero-shot emg-based discrete gesture recognition. *Frontiers in Bioengineering and Biotechnology*, Frontiers Media SA, v. 12, p. 1463377, 2024. Citado na página 17.

EHRL, D. et al. Defect coverage after forequarter amputation—a systematic review assessing different surgical approaches. *Journal of Personalized Medicine*, MDPI, v. 12, n. 4, p. 560, 2022. Citado na página 25.

EMON, M. H. M. et al. Machine learning based neuromuscular disease detection and classification using emg signal. In: *2024 IEEE International Women in Engineering (WIE) Conference on Electrical and Computer Engineering (WIECON-ECE)*. [S.l.: s.n.], 2024. p. 422–426. Citado na página 51.

FAJARDO, J. et al. Galileo hand: An anthropomorphic and affordable upper-limb prosthesis. *IEEE access*, IEEE, v. 8, p. 81365–81377, 2020. Citado na página 79.

FAJARDO, J. et al. An affordable open-source multifunctional upper-limb prosthesis with intrinsic actuation. In: IEEE. *2017 IEEE Workshop on Advanced Robotics and its Social Impacts (ARSO)*. [S.l.], 2017. p. 1–6. Citado na página 79.

FAJARDO, J. et al. User-prosthesis interface for upper limb prosthesis based on object classification. In: IEEE. *2018 Latin American Robotic Symposium, 2018 Brazilian Symposium on Robotics (SBR) and 2018 Workshop on Robotics in Education (WRE)*. [S.l.], 2018. p. 390–395. Citado na página 79.

FAJKUS, M. et al. Fbg sensor for heart rate monitoring using 3d printing technology. *IEEE Access*, IEEE, v. 12, p. 57150–57162, 2024. Citado na página 34.

FAN, J. et al. Improving semg-based motion intention recognition for upper-limb amputees using transfer learning. *Neural Computing and Applications*, Springer Science and Business Media LLC, v. 35, n. 22, p. 16101–16111, jul 2021. ISSN 1433-3058. Disponível em: <http://dx.doi.org/10.1007/s00521-021-06292-0>. Citado na página 37.

FINCH GLYN HARVEY HEATH, A. R. D. J. K. J. L. Biomechanical assessment of two artificial big toe restorations from ancient egypt and their significance to the history of prosthetics. *JPO Journal of Prosthetics and Orthotics*, Ovid Technologies (Wolters Kluwer Health), v. 24, n. 4, p. 181–191, Oct 2012. ISSN 1040-8800. Disponível em: <https://doi.org/10.1097/jpo.0b013e31826f4652>. Citado na página 16.

FRANZKE, A. W. et al. Users' and therapists' perceptions of myoelectric multi-function upper limb prostheses with conventional and pattern recognition control. *PloS one*, Public Library of Science San Francisco, CA USA, v. 14, n. 8, p. e0220899, 2019. Citado 3 vezes nas páginas 78, 79, and 80.

FRENț, C. R. et al. Concept, design, initial tests and prototype of customized upper limb prosthesis. *Applied Sciences*, MDPI AG, v. 11, n. 7, p. 3077, mar 2021. ISSN 2076-3417. Disponível em: <http://dx.doi.org/10.3390/app11073077>. Citado na página 82.

GABALLA, A. et al. Extended reality "x-reality" for prosthesis training of upper-limb amputees: A review on current and future clinical potential. *IEEE Transactions on Neural Systems and Rehabilitation Engineering*, v. 30, p. 1652–1663, 2022. Citado na página 17.

GAILEY, A.; ARTEMIADIS, P.; SANTELLO, M. Proof of concept of an online emg-based decoding of hand postures and individual digit forces for prosthetic hand control. *Frontiers in Neurology*, Frontiers Media SA, v. 8, feb 2017. ISSN 1664-2295. Disponível em: <http://dx.doi.org/10.3389/fneur.2017.00007>. Citado na página 39.

GAN, L. et al. Development of a fiber bragg grating-based force sensor for minimally invasive surgery–case study of ex-vivo tissue palpation. *IEEE Transactions on Instrumentation and Measurement*, IEEE, v. 72, p. 1–12, 2021. Citado na página 17.

GARSKE, C. A. et al. Serious games are not serious enough for myoelectric prosthetics. *JMIR Serious Games*, JMIR Publications Inc., v. 9, n. 4, p. e28079, nov 2021. ISSN 2291-9279. Disponível em: <http://dx.doi.org/10.2196/28079>. Citado na página 42.

GIGLI, A. et al. Visual cues to improve myoelectric control of upper limb prostheses. In: *2018 7th IEEE International Conference on Biomedical Robotics and Biomechatronics (Biorob)*. [S.l.: s.n.], 2018. p. 783–788. Citado na página 39.

GONG, D. et al. Bionic design of a dexterous anthropomorphic hand actuated by antagonistic pams. In: IEEE. *2020 IEEE International Conference on Real-time Computing and Robotics (RCAR)*. [S.l.], 2020. p. 493–498. Citado na página 27.

GOUDA, M. A. et al. Synthesis of semg signals for hand gestures using a 1ddcgan. *Bioengineering*, MDPI AG, v. 10, n. 12, p. 1353, nov 2023. ISSN 2306-5354. Disponível em: <http://dx.doi.org/10.3390/bioengineering10121353>. Citado na página 35.

GUO, W. et al. Toward an enhanced human–machine interface for upper-limb prosthesis control with combined emg and nirs signals. *IEEE Transactions on Human-Machine Systems*, IEEE, v. 47, n. 4, p. 564–575, 2017. Citado 2 vezes nas páginas 29 and 38.

GUéMANN, M. et al. Sensory substitution of elbow proprioception to improve myoelectric control of upper limb prosthesis: experiment on healthy subjects and amputees. *Journal of NeuroEngineering and Rehabilitation*, Springer Science and Business Media LLC, v. 19, n. 1, jun 2022. ISSN 1743-0003. Disponível em: <http://dx.doi.org/10.1186/s12984-022-01038-y>. Citado na página 37.

HA, N.; WITHANACHCHI, G. P.; YIHUN, Y. Performance of forearm fmg for estimating hand gestures and prosthetic hand control. *Journal of Bionic Engineering*, Springer Science and Business Media LLC, v. 16, n. 1, p. 88–98, jan 2019. ISSN 2543-2141. Disponível em: <http://dx.doi.org/10.1007/s42235-019-0009-4>. Citado na página 39.

HAHNE, J. et al. Control strategies for functional upper limb prostheses. In: _____. *Bionic Limb Reconstruction*. Springer International Publishing, 2021. p. 127–135. ISBN 9783030607463. Disponível em: <http://dx.doi.org/10.1007/978-3-030-60746-3_13>. Citado na página 28.

HASHIM, N. A. et al. Video game–based rehabilitation approach for individuals who have undergone upper limb amputation: case-control study. *JMIR Serious Games*, JMIR Publications Toronto, Canada, v. 9, n. 1, p. e17017, 2021. Citado na página 43.

HAVERKATE, L.; SMIT, G.; PLETTENBURG, D. H. Assessment of body-powered upper limb prostheses by able-bodied subjects, using the box and blocks test and the nine-hole peg test. *Prosthetics amp; Orthotics International*, Ovid Technologies (Wolters Kluwer Health), v. 40, n. 1, p. 109–116, feb 2016. ISSN 0309-3646. Disponível em: <http://dx.doi.org/10.1177/0309364614554030>. Citado na página 83.

HAYS, M. et al. Neuromorphic vision and tactile fusion for upper limb prosthesis control. In: IEEE. *2019 9th International IEEE/EMBS Conference on Neural Engineering (NER)*. [S.l.], 2019. p. 981–984. Citado na página 78.

HEGDE, G.; ASOKAN, S.; HEGDE, G. Fiber bragg grating sensors for aerospace applications: a review. *ISSS Journal of Micro and Smart Systems*, Springer Science and Business Media LLC, v. 11, n. 1, p. 257–275, apr 2022. ISSN 2509-7997. Disponível em: <http://dx.doi.org/10.1007/s41683-022-00101-z>. Citado na página 33.

HERNáNDEZ, V. A. S. et al. A practical tutorial for decision tree induction: Evaluation measures for candidate splits and opportunities. Association for Computing Machinery, New York, NY, USA, v. 54, n. 1, jan. 2021. ISSN 0360-0300. Disponível em: <https://doi.org/10.1145/3429739>. Citado na página 41.

HOPE, J.; VANHOLSBEECK, F.; MCDAID, A. A model of electrical impedance tomography implemented in nerve-cuff for neural-prosthetics control. *Physiological Measurement*, IOP Publishing, v. 39, n. 4, p. 044002, apr 2018. ISSN 1361-6579. Disponível em: <http://dx.doi.org/10.1088/1361-6579/aab73a>. Citado na página 16.

HUANG, H. et al. Integrating upper-limb prostheses with the human body: Technology advances, readiness, and roles in human–prosthesis interaction. *Annual Review of Biomedical Engineering*, Annual Reviews, v. 26, 2024. Citado na página 82.

HUANG, J. et al. Cross-modal integration and transfer learning using fuzzy logic techniques for intelligent upper limb prosthesis. *IEEE Transactions on Fuzzy Systems*, IEEE, v. 31, n. 4, p. 1267–1280, 2022. Citado na página 80.

HULLEMAN, W. G.; VOS, R. A. Modeling abiotic niches of crops and wild ancestors using deep learning: A generalized approach. *bioRxiv*, Cold Spring Harbor Laboratory, 2019. Disponível em: <https://www.biorxiv.org/content/early/2019/10/31/826347>. Citado na página 41.

HUNT, C. L. et al. Limb loading enhances skill transfer between augmented and physical reality tasks during limb loss rehabilitation. *Journal of NeuroEngineering and Rehabilitation*, v. 20, n. 1, p. 16, Jan 2023. ISSN 1743-0003. Disponível em: <https://doi.org/10.1186/s12984-023-01136-5>. Citado na página 43.

ISLAM, M. et al. *Impact of Electrode Position on Forearm Orientation Invariant Hand Gesture Recognition*. 2024. Citado na página 47.

IVANI, A. S. et al. Tactile perception in upper limb prostheses: mechanical characterization, human experiments, and computational findings. *IEEE Transactions on Haptics*, IEEE, 2024. Citado 2 vezes nas páginas 79 and 81.

JIANG, N. et al. Bio-robotics research for non-invasive myoelectric neural interfaces for upper-limb prosthetic control: a 10-year perspective review. *National Science Review*, Oxford University Press (OUP), v. 10, n. 5, feb 2023. ISSN 2053-714X. Disponível em: <http://dx.doi.org/10.1093/nsr/nwad048>. Citado na página 16.

JIANG, S. et al. A novel, co-located emg-fmg-sensing wearable armband for hand gesture recognition. *Sensors and Actuators A: Physical*, Elsevier, v. 301, p. 111738, 2020. Citado na página 17.

KANNENBERG, A. Active upper-limb prostheses: The international perspective. *JPO Journal of Prosthetics and Orthotics*, Ovid Technologies (Wolters Kluwer Health), v. 29, n. 4S, p. P57–P62, oct 2017. ISSN 1040-8800. Disponível em: <http://dx.doi.org/10.1097/JPO.0000000000000158>. Citado na página 27.

KARTHICK, P.; GHOSH, D. M.; RAMAKRISHNAN, S. Surface electromyography based muscle fatigue detection using high-resolution time-frequency methods and machine learning algorithms. *Computer Methods and Programs in Biomedicine*, Elsevier BV, v. 154, p. 45–56, feb 2018. ISSN 0169-2607. Disponível em: <http://dx.doi.org/10.1016/j.cmpb.2017.10.024>. Citado na página 35.

KENNEY, L. et al. Upper-limb prostheses for low and middle-income countries. *SCOPE magazine*, SCOPE Magazine, v. 2018, n. December, p. 38–40, 2018. Citado na página 27.

KERGET, B.; ÇIL, G.; AKSAKAL, A. Evaluation of the relationship between intercostal muscle oxygenation measured by near-infrared spectroscopy and exercise capacity in group e copd patients. *Pflügers Archiv-European Journal of Physiology*, Springer, v. 476, n. 10, p. 1529–1538, 2024. Citado na página 16.

KERVER, N. et al. Economic evaluation of upper limb prostheses in the netherlands including the cost-effectiveness of multi-grip versus standard myoelectric hand prostheses. *Disability and Rehabilitation*, Informa UK Limited, v. 45, n. 25, p. 4311–4321, dec 2022. ISSN 1464-5165. Disponível em: <http://dx.doi.org/10.1080/09638288.2022.2151653>. Citado 2 vezes nas páginas 81 and 82.

KERVER, N. et al. The multi-grip and standard myoelectric hand prosthesis compared: does the multi-grip hand live up to its promise? *Journal of NeuroEngineering and Rehabilitation*, Springer Science and Business Media LLC, v. 20, n. 1, feb 2023. ISSN 1743-0003. Disponível em: <http://dx.doi.org/10.1186/s12984-023-01131-w>. Citado na página 16.

KHAN, S. M.; KHAN, A. A.; FAROOQ, O. Selection of features and classifiers for emg-eeg-based upper limb assistive devices—a review. *IEEE Reviews in Biomedical Engineering*, Institute of Electrical and Electronics Engineers (IEEE), v. 13, p. 248–260, 2020. ISSN 1941-1189. Disponível em: <http://dx.doi.org/10.1109/RBME.2019.2950897>. Citado na página 35.

KHONINA, S. N.; KAZANSKIY, N. L.; BUTT, M. A. Optical fibre-based sensors—an assessment of current innovations. *Biosensors*, MDPI AG, v. 13, n. 9, p. 835, aug 2023. ISSN 2079-6374. Disponível em: <http://dx.doi.org/10.3390/bios13090835>. Citado na página 31.

KIM, J. M. et al. User recognition system based on spectrogram image conversion using emg signals. *Computers, Materials amp; Continua*, Tech Science Press, v. 72, n. 1, p. 1213–1227, 2022. ISSN 1546-2226. Disponível em: <http://dx.doi.org/10.32604/cmc.2022.025213>. Citado na página 36.

KORI, T. et al. A study on fiber bragg gratings and its recent applications. In: *Innovative Mobile and Internet Services in Ubiquitous Computing*. Springer International Publishing, 2019. p. 880–889. ISBN 9783030222635. ISSN 2194-5365. Disponível em: <http://dx.doi.org/10.1007/978-3-030-22263-5_84>. Citado na página 33.

KRASOULIS, A.; VIJAYAKUMAR, S.; NAZARPOUR, K. Multi-grip classification-based prosthesis control with two emg-imu sensors. *IEEE Transactions on Neural Systems and Rehabilitation Engineering*, v. 28, n. 2, p. 508–518, 2020. Citado na página 39.

KRISTOFFERSEN, M. B. et al. User training for machine learning controlled upper limb prostheses: a serious game approach. *Journal of NeuroEngineering and Rehabilitation*, v. 18, n. 1, p. 32, Feb 2021. ISSN 1743-0003. Disponível em: <https://doi.org/10.1186/s12984-021-00831-5>. Citado na página 43.

KUIKEN, T. A. et al. The use of targeted muscle reinnervation for improved myoelectric prosthesis control in a bilateral shoulder disarticulation amputee. *Prosthetics and orthotics international*, Taylor & Francis, v. 28, n. 3, p. 245–253, 2004. Citado na página 25.

KUMAR, A.; YADAV, S. P.; KUMAR, A. An improved feature extraction algorithm for robust swin transformer model in high-dimensional medical image analysis. *Computers in Biology and Medicine*, v. 188, p. 109822, 2025. ISSN 0010-4825. Disponível em: <https://www.sciencedirect.com/science/article/pii/S0010482525001726>. Citado na página 35.

LAVORGNA, V. et al. Dual-material 3d printed wearable sensors based on fbg technology for physiological and biomechanical monitoring in back pain assessment. *IEEE Sensors Journal*, IEEE, 2025. Citado na página 34.

LEAL-JUNIOR, A. G. et al. 3d-printing techniques on the development of multiparameter sensors using one fbg. *Sensors*, MDPI, v. 19, n. 16, p. 3514, 2019. Citado na página 34.

LEAL-JUNIOR, A. G. et al. Fbg-embedded 3-d printed abs sensing pads: The impact of infill density on sensitivity and dynamic range in force sensors. *IEEE Sensors Journal*, IEEE, v. 18, n. 20, p. 8381–8388, 2018. Citado na página 34.

LEGRAND, M. et al. Simultaneous control of 2dof upper-limb prosthesis with body compensations-based control: a multiple cases study. *IEEE Transactions on Neural Systems and Rehabilitation Engineering*, IEEE, v. 30, p. 1745–1754, 2022. Citado na página 81.

LEI, G. et al. Investigation on the sampling frequency and channel number for force myography based hand gesture recognition. *Sensors*, MDPI, v. 21, n. 11, p. 3872, 2021. Citado na página 17.

LI, W. et al. Current status and clinical perspectives of extended reality for myoelectric prostheses: review. *Frontiers in Bioengineering and Biotechnology*, Frontiers Media SA, v. 11, jan 2024. ISSN 2296-4185. Disponível em: <http://dx.doi.org/10.3389/fbioe.2023.1334771>. Citado 4 vezes nas páginas 8, 18, 42, and 43.

LIU, X. et al. A review on the usability, flexibility, affinity, and affordability of virtual technology for rehabilitation training of upper limb amputees. *Bioengineering*, MDPI, v. 10, n. 11, p. 1301, 2023. Citado na página 18.

LUCACCINI, L. et al. Evaluation of the heidelberg pneumatic prosthesis. *Bull Prosthet Res*, v. 5, n. 10, p. 58–115, 1966. Citado na página 17.

MAAS, B.; SLUIS, C. K. V. D.; BONGERS, R. M. Assessing effectiveness of serious game training designed to assist in upper limb prosthesis rehabilitation. *Frontiers in Rehabilitation Sciences*, Volume 5 - 2024, 2024. ISSN 2673-6861. Disponível em: <https://www.frontiersin.org/journals/rehabilitation-sciences/articles/10.3389/fresc.2024.1353077>. Citado na página 43.

MAAT, B. et al. Passive prosthetic hands and tools: A literature review. *Prosthetics amp; Orthotics International*, Ovid Technologies (Wolters Kluwer Health), v. 42, n. 1, p. 66–74, feb 2018. ISSN 0309-3646. Disponível em: <http://dx.doi.org/10.1177/0309364617691622>. Citado 2 vezes nas páginas 8 and 26.

MAJOR, M. J. et al. Effects of upper limb loss or absence and prosthesis use on postural control of standing balance. *American Journal of Physical Medicine amp; Rehabilitation*, Ovid Technologies (Wolters Kluwer Health), v. 99, n. 5, p. 366â371, may 2020. ISSN 0894-9115. Disponível em: <http://dx.doi.org/10.1097/PHM.0000000000001339>. Citado na página 15.

MASSON, S. et al. Integrating myo armband for the control of myoelectric upper limb prosthesis. In: *Proceedings of the XXV Congresso Brasileiro de Engenharia Biomédica*. [S.l.: s.n.], 2016. Citado na página 37.

MOHAMMADI, A. et al. A paediatric 3d-printed soft robotic hand prosthesis for children with upper limb loss. In: *2020 42nd Annual International Conference of the IEEE Engineering in Medicine Biology Society (EMBC)*. [S.l.: s.n.], 2020. p. 3310–3313. Citado na página 85.

MONTAGNANI, F.; CONTROZZI, M.; CIPRIANI, C. Exploiting arm posture synergies in activities of daily living to control the wrist rotation in upper limb prostheses: A feasibility study. In: IEEE. *2015 37th Annual International Conference of the IEEE Engineering in Medicine and Biology Society (EMBC)*. [S.l.], 2015. p. 2462–2465. Citado na página 78.

MWEMA, F. M.; AKINLABI, E. T. Basics of fused deposition modelling (fdm). In: *Fused Deposition Modeling*. Springer International Publishing, 2020. p. 1–15. ISBN 9783030482596. ISSN 2191-5318. Disponível em: <http://dx.doi.org/10.1007/978-3-030-48259-6_1>. Citado na página 34.

NAGARAJA, V. H. et al. A novel respiratory control and actuation system for upper-limb prosthesis users: clinical evaluation study. *IEEE Access*, IEEE, v. 10, p. 128764–128778, 2022. Citado na página 83.

NAYAK, N. Comprehensive review of fiber bragg grating sensors: Principles, technologies, and diverse applications across industries. *Tuijin Jishu/Journal of Propulsion Technology*, v. 45, n. 03, p. 74–85, 2024. Disponível em: <https://www.propulsiontechjournal.com/index.php/journal/article/download/7087/4602>. Citado na página 31.

NAZARPOUR, K. et al. A note on the probability distribution function of the surface electromyogram signal. *Brain Research Bulletin*, Elsevier BV, v. 90, p. 88–91, jan 2013. ISSN 0361-9230. Disponível em: <http://dx.doi.org/10.1016/j.brainresbull.2012.09.012>. Citado na página 35.

NG, K. H.; NAZARI, V.; ALAM, M. Can prosthetic hands mimic a healthy human hand? *Prosthesis*, MDPI AG, v. 3, n. 1, p. 11â23, jan 2021. ISSN 2673-1592. Disponível em: <http://dx.doi.org/10.3390/prosthesis3010003>. Citado na página 16.

OMARKULOV, N. et al. Design and analysis of an underactuated anthropomorphic finger for upper limb prosthetics. In: *2015 37th Annual International Conference of the IEEE Engineering in Medicine and Biology Society (EMBC)*. [S.l.: s.n.], 2015. p. 2474–2477. Citado na página 85.

O'BRIEN, L. et al. Real-world testing of the self grasping hand, a novel adjustable passive prosthesis: A single group pilot study. *Prosthesis*, MDPI AG, v. 4, n. 1, p. 48–59, feb 2022. ISSN 2673-1592. Disponível em: <http://dx.doi.org/10.3390/prosthesis4010006>. Citado 2 vezes nas páginas 82 and 83.

PANCHOLI, S.; JOSHI, A. M. Portable emg data acquisition module for upper limb prosthesis application. *IEEE Sensors Journal*, v. 18, n. 8, p. 3436–3443, 2018. Citado na página 37.

PANCHOLI, S.; JOSHI, A. M. Time derivative moments based feature extraction approach for recognition of upper limb motions using emg. *IEEE Sensors Letters*, v. 3, n. 4, p. 1–4, 2019. Citado 2 vezes nas páginas 36 and 38.

PANCHOLI, S.; JOSHI, A. M.; JOSHI, D. A robust and accurate deep learning based pattern recognition framework for upper limb prosthesis using semg. *arXiv preprint arXiv:2106.02463*, 2021. Citado na página 39.

PARAJULI, N. et al. Real-time emg based pattern recognition control for hand prostheses: A review on existing methods, challenges and future implementation. *Sensors*, MDPI AG, v. 19, n. 20, p. 4596, oct 2019. ISSN 1424-8220. Disponível em: <http://dx.doi.org/10.3390/s19204596>. Citado na página 35.

PAUDEL, B.; SHRESTHA, B.; BANSKOTA, A. Two faces of major lower limb amputations. *Kathmandu University medical journal (KUMJ)*, v. 3, p. 212–6, 11 2004. Citado na página 23.

PEDREGOSA, F. et al. Scikit-learn: Machine learning in python. *Journal of Machine Learning Research*, v. 12, n. 85, p. 2825–2830, 2011. Disponível em: <http://jmlr.org/papers/v12/pedregosa11a.html>. Citado na página 51.

PENDãO, C.; SILVA, I. Optical fiber sensors and sensing networks: Overview of the main principles and applications. *Sensors*, MDPI AG, v. 22, n. 19, p. 7554, oct 2022. ISSN 1424-8220. Disponível em: <http://dx.doi.org/10.3390/s22197554>. Citado na página 31.

PHINYOMARK, A. et al. Evaluation of emg feature extraction for hand movement recognition based on euclidean distance and standard deviation. In: *ECTI-CON2010: The 2010 ECTI International Confernce on Electrical Engineering/Electronics, Computer, Telecommunications and Information Technology*. [S.l.: s.n.], 2010. p. 856–860. Citado na página 35.

PHINYOMARK, A.; PHUKPATTARANONT, P.; LIMSAKUL, C. Feature reduction and selection for emg signal classification. *Expert Systems with Applications*, Elsevier BV, v. 39, n. 8, p. 7420–7431, jun 2012. ISSN 0957-4174. Disponível em: <http://dx.doi.org/10.1016/j.eswa.2012.01.102>. Citado na página 35.

PHINYOMARK, A. et al. Emg feature evaluation for improving myoelectric pattern recognition robustness. *Expert Systems with Applications*, Elsevier BV, v. 40, n. 12, p. 4832–4840, sep 2013. ISSN 0957-4174. Disponível em: <http://dx.doi.org/10.1016/j.eswa.2013.02.023>. Citado na página 35.

PHINYOMARK, A. et al. Feature extraction of the first difference of emg time series for emg pattern recognition. *Computer Methods and Programs in Biomedicine*, Elsevier BV, v. 117, n. 2, p. 247–256, nov 2014. ISSN 0169-2607. Disponível em: <http://dx.doi.org/10.1016/j.cmpb.2014.06.013>. Citado na página 35.

PIERRIE R. GLENN GASTON, B. J. L. S. N. Current concepts in upper-extremity amputation. *The Journal of Hand Surgery*, Elsevier BV, v. 43, n. 7, p. 657–667, Jul 2018. ISSN 0363-5023. Disponível em: <https://doi.org/10.1016/j.jhsa.2018.03.053>. Citado na página 15.

PRAKASH, A. et al. Force myography controlled multifunctional hand prosthesis for upper-limb amputees. *Biomedical Signal Processing and Control*, Elsevier BV, v. 62, p. 102122, sep 2020. ISSN 1746-8094. Disponível em: <http://dx.doi.org/10.1016/j.bspc.2020.102122>. Citado 3 vezes nas páginas 28, 38, and 84.

PRAKASH, A.; SHARMA, N.; SHARMA, S. An affordable transradial prosthesis based on force myography sensor. *Sensors and Actuators A: Physical*, Elsevier, v. 325, p. 112699, 2021. Citado na página 17.

QU, W. et al. Application of optical fiber sensing technology and coating technology in blood component detection and monitoring. *Coatings*, MDPI AG, v. 14, n. 2, p. 173, jan 2024. ISSN 2079-6412. Disponível em: <http://dx.doi.org/10.3390/coatings14020173>. Citado na página 31.

RADHAKRISHNAN, M. et al. Design and assessment of myoelectric games for prosthesis training of upper limb amputees. In: *2019 IEEE International Conference on Pervasive Computing and Communications Workshops (PerCom Workshops)*. [S.l.: s.n.], 2019. p. 151–157. Citado na página 42.

RADMAND, A.; SCHEME, E.; ENGLEHART, K. High-density force myography: A possible alternative for upper-limb prosthetic control. Rehabilitation Research and Development Service, 2016. Citado na página 38.

RADOSH, A. et al. Prototyping of cosmetic prosthesis of upper limb using additive manufacturing technologies. *Advances in Science and Technology Research Journal*, Wydawnictwo Naukowe Gabriel Borowski (WNGB), v. 11, n. 3, p. 102–108, sep 2017.

ISSN 2299-8624. Disponível em: <http://dx.doi.org/10.12913/22998624/70995>. Citado na página 85.

RAGHIBI, L. E. et al. Virtual reality can mediate the learning phase of upper limb prostheses supporting a better-informed selection process. *Journal on Multimodal User Interfaces*, Springer Science and Business Media LLC, v. 17, n. 1, p. 33–46, dec 2022. ISSN 1783-8738. Disponível em: <http://dx.doi.org/10.1007/s12193-022-00400-7>. Citado na página 82.

REAZ, M. B. I.; HUSSAIN, M. S.; MOHD-YASIN, F. Techniques of emg signal analysis: detection, processing, classification and applications. *Biological procedures online*, Springer, v. 8, p. 11–35, 2006. Citado na página 16.

REHMAN, M. U. et al. A wearable force myography-based armband for recognition of upper limb gestures. *Sensors*, MDPI, v. 23, n. 23, p. 9357, 2023. Citado na página 17.

RESNIK, L. et al. Evaluation of emg pattern recognition for upper limb prosthesis control: a case study in comparison with direct myoelectric control. *Journal of NeuroEngineering and Rehabilitation*, Springer Science and Business Media LLC, v. 15, n. 1, mar 2018. ISSN 1743-0003. Disponível em: <http://dx.doi.org/10.1186/s12984-018-0361-3>. Citado na página 38.

RIBEIRO, J. et al. Analysis of man-machine interfaces in upper-limb prosthesis: A review. *Robotics*, MDPI AG, v. 8, n. 1, p. 16, feb 2019. ISSN 2218-6581. Disponível em: <http://dx.doi.org/10.3390/robotics8010016>. Citado na página 25.

RUHUNAGE, I. et al. Emg signal controlled transhumerai prosthetic with eeg-ssvep based approch for hand open/close. In: IEEE. *2017 IEEE International Conference on Systems, Man, and Cybernetics (SMC)*. [S.l.], 2017. p. 3169–3174. Citado na página 29.

SALMINGER, S. et al. Prosthetic reconstruction to restore function in transcarpal amputees. *Journal of Plastic, Reconstructive & Aesthetic Surgery*, Elsevier, v. 69, n. 3, p. 305–310, 2016. Citado na página 24.

SAMUEL, O. W. et al. Intelligent emg pattern recognition control method for upper-limb multifunctional prostheses: advances, current challenges, and future prospects. *Ieee Access*, IEEE, v. 7, p. 10150–10165, 2019. Citado na página 28.

SAMUEL, O. W. et al. Examining the effect of subjects' mobility on upper-limb motion identification based on emg-pattern recognition. In: *2016 Asia-Pacific Conference on Intelligent Robot Systems (ACIRS)*. [S.l.: s.n.], 2016. p. 137–141. Citado na página 39.

SAMUEL, O. W. et al. Pattern recognition of electromyography signals based on novel time domain features for amputees' limb motion classification. *Computers amp; Electrical Engineering*, Elsevier BV, v. 67, p. 646–655, apr 2018. ISSN 0045-7906. Disponível em: <http://dx.doi.org/10.1016/j.compeleceng.2017.04.003>. Citado na página 35.

SATTAR, N. Y. et al. Emg based control of transhumeral prosthesis using machine learning algorithms. *International Journal of Control, Automation and Systems*, Springer Science and Business Media LLC, v. 19, n. 10, p. 3522–3532, jul 2021. ISSN 2005-4092. Disponível em: <http://dx.doi.org/10.1007/s12555-019-1058-5>. Citado na página 38.

SATTAR, N. Y. et al. Enhancing classification accuracy of transhumeral prosthesis: A hybrid semg and fnirs approach. Institute of Electrical and Electronics Engineers (IEEE), 2021. Citado na página 29.

SCHAUMANN, S. et al. Force myography for motion intention detection based on 3d-printed piezoelectric sensors. *IEEE Sensors Letters*, IEEE, 2024. Citado na página 17.

SCIKIT-LEARN. Api v1.7.0. 2025. Accessed on July 13, 2025. Disponível em: <https://scikit-learn.org/stable/api/index.html>. Citado na página 51.

SCIKIT-LEARN. User guide v1.7.0. 2025. Accessed on July 13, 2025. Disponível em: <https://scikit-learn.org/stable/user_guide.html>. Citado na página 51.

SEGURA, D. et al. Upper limb prostheses by the level of amputation: A systematic review. *Prosthesis*, MDPI AG, v. 6, n. 2, p. 277–300, mar 2024. ISSN 2673-1592. Disponível em: <http://dx.doi.org/10.3390/prosthesis6020022>. Citado na página 25.

SEPPICH, N. et al. Cyberlimb: a novel robotic prosthesis concept with shared and intuitive control. *Journal of NeuroEngineering and Rehabilitation*, Springer Science and Business Media LLC, v. 19, n. 1, apr 2022. ISSN 1743-0003. Disponível em: <http://dx.doi.org/10.1186/s12984-022-01016-4>. Citado 2 vezes nas páginas 79 and 81.

SHARMA, A. et al. A mixed-reality training environment for upper limb prosthesis control. In: IEEE. *2018 IEEE Biomedical Circuits and Systems Conference (BioCAS)*. [S.l.], 2018. p. 1–4. Citado na página 18.

SHERIF, O.; BASSUONI, M. M.; MEHREZ, O. A survey on the state of the art of force myography technique (fmg): analysis and assessment. *Medical & Biological Engineering & Computing*, v. 62, n. 5, p. 1313–1332, May 2024. ISSN 1741-0444. Disponível em: <https://doi.org/10.1007/s11517-024-03019-w>. Citado 2 vezes nas páginas 16 and 51.

SIEGEL, J. R. et al. A performance evaluation of commercially available and 3d-printable prosthetic hands: a comparison using the anthropomorphic hand assessment protocol. *BMC Biomedical Engineering*, Springer Science and Business Media LLC, v. 6, n. 1, dec 2024. ISSN 2524-4426. Disponível em: <http://dx.doi.org/10.1186/s42490-024-00086-w>. Citado na página 16.

SILVA, L. A. da et al. Interdisciplinary-based development of user-friendly customized 3d printed upper limb prosthesis. In: SPRINGER. *Advances in Usability, User Experience and Assistive Technology: Proceedings of the AHFE 2018 International Conferences on Usability & User Experience and Human Factors and Assistive Technology, Held on July 21–25, 2018, in Loews Sapphire Falls Resort at Universal Studios, Orlando, Florida, USA 9*. [S.l.], 2019. p. 899–908. Citado na página 79.

SMITH, P. A. et al. The impact of a custom electromyograph (emg) controller on player enjoyment of games designed to teach the use of prosthetic arms. *The Computer Games Journal*, v. 7, n. 2, p. 131–147, Jun 2018. ISSN 2052-773X. Disponível em: <https://doi.org/10.1007/s40869-018-0060-0>. Citado na página 42.

SMITH, P. A. et al. Usability testing games for prosthetic training. In: *2018 IEEE 6th International Conference on Serious Games and Applications for Health (SeGAH)*. [S.l.: s.n.], 2018. p. 1–7. Citado na página 42.

SPIERS, A. J.; RESNIK, L.; DOLLAR, A. M. Analyzing at-home prosthesis use in unilateral upper-limb amputees to inform treatment & device design. In: IEEE. *2017 International Conference on Rehabilitation Robotics (ICORR)*. [S.l.], 2017. p. 1273–1280. Citado 2 vezes nas páginas 78 and 81.

STANGO, A. et al. Characterization of in-body to on-body wireless radio frequency link for upper limb prostheses. *PloS one*, Public Library of Science San Francisco, CA USA, v. 11, n. 10, p. e0164987, 2016. Citado na página 28.

STEGEMAN, D.; HERMENS, H. Standards for surface electromyography: The european project surface emg for non-invasive assessment of muscles (seniam). *Enschede: Roessingh Research and Development*, v. 10, n. 8, 2007. Citado na página 45.

SUBASI, A.; KIYMIK, M. K. Muscle fatigue detection in emg using time–frequency methods, ica and neural networks. *Journal of Medical Systems*, Springer Science and Business Media LLC, v. 34, n. 4, p. 777–785, apr 2009. ISSN 1573-689X. Disponível em: <http://dx.doi.org/10.1007/s10916-009-9292-7>. Citado na página 35.

SUPPIAH, R. et al. Fuzzy inference system (fis)-long short-term memory (lstm) network for electromyography (emg) signal analysis. *Biomedical physics & engineering express*, IOP Publishing, v. 8, n. 6, p. 065032, 2022. Citado na página 16.

TABOR, A. et al. Designing game-based myoelectric prosthesis training. In: *Proceedings of the 2017 CHI Conference on Human Factors in Computing Systems*. New York, NY, USA: Association for Computing Machinery, 2017. (CHI '17), p. 1352–1363. ISBN 9781450346559. Disponível em: <https://doi.org/10.1145/3025453.3025676>. Citado na página 42.

TAVAKOLI, M.; BENUSSI, C.; LOURENCO, J. L. Single channel surface emg control of advanced prosthetic hands: A simple, low cost and efficient approach. *Expert Systems with Applications*, Elsevier BV, v. 79, p. 322–332, aug 2017. ISSN 0957-4174. Disponível em: <http://dx.doi.org/10.1016/j.eswa.2017.03.012>. Citado na página 37.

TAVAKOLI, M. et al. Underactuated anthropomorphic hands: Actuation strategies for a better functionality. *Robotics and Autonomous Systems*, Elsevier BV, v. 74, p. 267â282, dec 2015. ISSN 0921-8890. Disponível em: <http://dx.doi.org/10.1016/j.robot.2015.08.011>. Citado na página 16.

TAVARES, C. et al. Respiratory and heart rate monitoring using an fbg 3d-printed wearable system. *Biomed. Opt. Express*, Optica Publishing Group, v. 13, n. 4, p. 2299–2311, Apr 2022. Disponível em: <https://opg.optica.org/boe/abstract.cfm?URI=boe-13-4-2299>. Citado na página 34.

TAVARES, C. et al. 3d printed wearable fbg based devices: A proof of concept for heart rate monitoring. In: *2022 IEEE International Workshop on Metrology for Industry 4.0 IoT (MetroInd4.0IoT)*. [S.l.: s.n.], 2022. p. 366–370. Citado 2 vezes nas páginas 34 and 44.

TCHIMINO, J. et al. Effects of game design characteristics of a virtual reality serious game for upper-limb prosthesis control training on motor learning. *Frontiers in Rehabilitation Sciences*, Volume 6 - 2025, 2025. ISSN 2673-6861. Disponível em: <https://www.frontiersin.org/journals/rehabilitation-sciences/articles/10.3389/fresc.2025.1520184>. Citado na página 43.

THOMAS, N. et al. Comparison of vibrotactile and joint-torque feedback in a myoelectric upper-limb prosthesis. *Journal of NeuroEngineering and Rehabilitation*, Springer Science and Business Media LLC, v. 16, n. 1, jun 2019. ISSN 1743-0003. Disponível em: <http://dx.doi.org/10.1186/s12984-019-0545-5>. Citado na página 78.

THORLABS. Thorlabs monomode fiber recommendations. 2025. Accessed on July 13, 2025. Disponível em: <https://www.thorlabs.com/newgrouppage9.cfm?objectgroup_id=949>. Citado na página 45.

TORRES-SANMIGUEL, C. R. Modeling and simulation process via incremental methods of a production-aimed upper limb prosthesis. *Applied Sciences*, MDPI AG, v. 12, n. 6, p. 2788, mar 2022. ISSN 2076-3417. Disponível em: <http://dx.doi.org/10.3390/app12062788>. Citado na página 83.

TWARDOWSKI, M. D. et al. Motor unit drive: a neural interface for real-time upper limb prosthetic control. *Journal of Neural Engineering*, IOP Publishing, v. 16, n. 1, p. 016012, dec 2018. ISSN 1741-2552. Disponível em: <http://dx.doi.org/10.1088/1741-2552/aaeb0f>. Citado na página 39.

UELLENDAHL, J. Myoelectric versus body-powered upper-limb prostheses: a clinical perspective. In: LWW. *JPO: Journal of Prosthetics and Orthotics*. [S.l.], 2017. v. 29, n. 4S, p. P25–P29. Citado na página 27.

UNANYAN, N. N.; BELOV, A. A. Design of upper limb prosthesis using real-time motion detection method based on emg signal processing. *Biomedical Signal Processing and Control*, Elsevier BV, v. 70, p. 103062, sep 2021. ISSN 1746-8094. Disponível em: <http://dx.doi.org/10.1016/j.bspc.2021.103062>. Citado 3 vezes nas páginas 15, 39, and 81.

VIDAURRE, C. et al. Eeg-based bci for the linear control of an upper-limb neuroprosthesis. *Medical engineering &physics*, *Elsevier*, *v.* 38, *n.* 11, *p.*1195 − −1204, 2016. *Citadonapágina*29.

VIDOVIC, M. M.-C. et al. Improving the robustness of myoelectric pattern recognition for upper limb prostheses by covariate shift adaptation. *IEEE Transactions on Neural Systems and Rehabilitation Engineering*, v. 24, n. 9, p. 961–970, 2016. Citado na página 37.

WILSON, S.; VAIDYANATHAN, R. Upper-limb prosthetic control using wearable multichannel mechanomyography. In: *2017 International Conference on Rehabilitation Robotics (ICORR)*. [S.l.: s.n.], 2017. p. 1293–1298. Citado na página 38.

WU, L. et al. Rejecting novel motions in high-density myoelectric pattern recognition using hybrid neural networks. *Frontiers in Neurorobotics*, Frontiers Media SA, v. 16, p. 862193, 2022. Citado na página 17.

WU, Y. T. et al. Integrated optical fiber force myography sensor as pervasive predictor of hand postures. *Biomedical engineering and computational biology*, SAGE Publications Sage UK: London, England, v. 11, p. 1179597220912825, 2020. Citado na página 17.

XIAO, K. et al. Pdms-embedded wearable fbg sensors for gesture recognition and communication assistance. *Biomedical optics express*, Optica Publishing Group, v. 15, n. 3, p. 1892–1909, 2024. Citado na página 17.

XIAO, Z. G.; MENON, C. A review of force myography research and development. *Sensors*, MDPI AG, v. 19, n. 20, p. 4557, oct 2019. ISSN 1424-8220. Disponível em: <http://dx.doi.org/10.3390/s19204557>. Citado na página 35.

XU, G. et al. Three-dimensional-printed upper limb prosthesis for a child with traumatic amputation of right wrist: A case report. *Medicine*, Ovid Technologies (Wolters Kluwer Health), v. 96, n. 52, p. e9426, dec 2017. ISSN 0025-7974. Disponível em: <http://dx.doi.org/10.1097/MD.0000000000009426>. Citado na página 84.

YOUNG, P. R. et al. The effects of limb position and grasped load on hand gesture classification using electromyography, force myography, and their combination. *PLOS ONE*, Public Library of Science (PLoS), v. 20, n. 4, p. e0321319, apr 2025. ISSN 1932-6203. Disponível em: <http://dx.doi.org/10.1371/journal.pone.0321319>. Citado na página 35.

YU, H.; KIM, S. Svm tutorial — classification, regression and ranking. Springer Berlin Heidelberg, Berlin, Heidelberg, p. 479–506, 2012. Disponível em: <https://doi.org/10.1007/978-3-540-92910-9_15>. Citado na página 41.

YUAN, B. et al. The global burden of traumatic amputation in 204 countries and territories. *Frontiers in Public Health*, Frontiers Media SA, v. 11, oct 2023. ISSN 2296-2565. Disponível em: <http://dx.doi.org/10.3389/fpubh.2023.1258853>. Citado na página 15.

ZHANG, H. The optimality of naive bayes. *Proceedings of the Seventeenth International Florida Artificial Intelligence Research Society Conference, FLAIRS 2004*, v. 2, 01 2004. Citado na página 40.

ZHAO, S. et al. Linear discriminant analysis. *Nature Reviews Methods Primers*, v. 4, n. 1, p. 70, Sep 2024. ISSN 2662-8449. Disponível em: <https://doi.org/10.1038/s43586-024-00346-y>. Citado na página 40.

ZHENG, J. Y. et al. Priorities for the design and control of upper limb prostheses: A focus group study. *Disability and Health Journal*, Elsevier, v. 12, n. 4, p. 706–711, 2019. Citado na página 23.

ZHENG, Z. et al. A review of emg-, fmg-, and eit-based biosensors and relevant humanâmachine interactivities and biomedical applications. *Biosensors*, MDPI AG, v. 12, n. 7, p. 516, jul 2022. ISSN 2079-6374. Disponível em: <http://dx.doi.org/10.3390/bios12070516>. Citado na página 16.

ZUNIGA, J. M. et al. Remote fitting procedures for upper limb 3d printed prostheses. *Expert review of medical devices*, Taylor & Francis, v. 16, n. 3, p. 257–266, 2019. Citado na página 79.

Appendix 1: Review of prostheses used in the literature table.

Table Appendix 1.1 – Review of prostheses used in the literature.

Name	**Level of amputation**	**Type**	**Actuator**	**No. of actuators**	**DOF**	**No. of participants**	**Cost**	**Weight (g)**	**Reference**
10S17 Electric Wrist Rotator	Transradial	Active - Electric - Add-on	Electric motor	1	1				(MONTAGNANI; CONTROZZI; CIPRIANI, 2015)
Adept Prehensors	Transradial	Active - Mechanical	Cable						(SPIERS; RESNIK; DOLLAR, 2017)
Bebionic	Transradial	Active - Electric	Electric motors			4	High		(FRANZKE et al., 2019)
Bebionic3	Transradial	Active - Electric	Electric motors			1			(HAYS et al., 2019)
Custom	Transradial	Active - Electric	Electric motors	1	1	12			(THOMAS et al., 2019)

Continued on next page

Customized 3D-Printed Prosthesis	Transradial	Active - Mechanical	Body-powered (elbow flexion)	1	1	1	Low		(SILVA et al., 2019)
CyberTUM	Transradial	Active - Electric	Electric motors		3			1950	(DEIJS et al., 2016; IVANI et al., 2024; SEPPICH et al., 2022)
Cyborg Beast (3D Printed)	Transradial	Active - Mechanical	Cable				Low		(ZUNIGA et al., 2019)
Flex-wrist	Transradial	Active - Electric	Electric motor			8			(DEIJS et al., 2016)
Galileo Hand	Transradial	Active - Electric	DC gear-motors	6	15	2	<$350	<350	(FAJARDO et al., 2017; FAJARDO et al., 2018; FAJARDO et al., 2020)
Hands On	Transradial	Active - Electric	sEMG-based						(CAPSI-MORALES et al., 2023)
Hannes	Transradial	Active - Electric	2 sEMG	1					(CAPSI-MORALES et al., 2023)
I-limb (Revolution / Quantum)	Transradial	Active - Electric	Electric motors		5	5			(FRANZKE et al., 2019)

Continued on next page

Imperial ARM	Transradial	Active - Electric	Electric motors	5	5				(CAPSI-MORALES et al., 2023; DEY; BASUMATARY; HAZARIKA, 2023)
Intelligent Upper Limb Prosthesis (Huang et al., 2023)	Transradial	Active - Electric	Electric motor + fuzzy logic			2			(HUANG et al., 2022)
Maker Hand	Transradial	Active - Mechani-cal	Body-powered (NC) + stiffness disc						(CAPSI-MORALES et al., 2023)
Michelangelo	Transradial	Active - Electric	Electric motors	2	2	8			(DIDERIKSEN et al., 2024; FRANZKE et al., 2019)
Multi-flex wrist + ProPlusHand	Transradial	Active - Electric	Electric			8			(DEIJS et al., 2016)
MyoHand VariPlus Speed	Transhumeral	Active - Electric	Implanted EMG						(CAPSI-MORALES et al., 2023)
Myohand VariPlus	Transradial	Active - Electric	Electric motors			2			(DIDERIKSEN et al., 2024)

Continued on next page

Narek's Prosthesis	Transradial	Active - Electric	Electric motors			1	Low	400–500	(UNANYAN; BELOV, 2021)
Otto Bock System Hand	Transradial	Active - Mechanical	Cable						(SPIERS; RESNIK; DOLLAR, 2017)
Quantum (Touch Bionics / Össur)	Transhumeral	Active - Electric	Electric motors	3	3	4			(LEGRAND et al., 2022)
SensorHand Speed	Transradial	Active - Electric	Electric motor	1					(CASTELLINI, 2020)
SoftHand	Transradial	Active - Electric	Electric motor	1					(CASTELLINI, 2020)
SoftHand Pro	Transradial	Active - Electric	2 sEMG		18	1			(SEPPICH et al., 2022; CAPSI-MORALES et al., 2023)
SuperMotorica	Transradial	Active - Electric	2 sEMG			1			(CAPSI-MORALES et al., 2023)
Vincent	Transradial	Active - Electric	Electric motors						(KERVER et al., 2022)
Viswajyothi	Transradial	Active - Electric	Electric motor			1			(CAPSI-MORALES et al., 2023)
Cosmetic Hand (CH)	Transradial	Passive - Cosmetic	None	0	0				(IVANI et al., 2024)

Continued on next page

SmartHand	Transradial	Active - Electric	Electric motors	4	4				(KERVER et al., 2022)
Mobius Bionics LUKE Arm	Transhumeral	Active - Electric	Electric motors	>10	10				(O'BRIEN et al., 2022)
Greifer	Transradial	Active - Electric	Electric motor		1				(RAGHIBI et al., 2022)
Customized Upper Limb Prosthesis (Radu et al.)	Transradial	Active - Electric	Electric motor		5	1			(FRENț et al., 2021)
Ability Hand	Transradial	Active - Electric	Electric motors	5	5				(HUANG et al., 2024)
VINCENT - evolution4	Transradial	Active - Electric	Electric motors	6	6				(RAGHIBI et al., 2022)
ProWrist	Transradial	Active - Electric	Electric motor	1	1				(RAGHIBI et al., 2022)
MC Powered FlexionWrist	Transradial	Active - Electric	Electric motor	1	1				(RAGHIBI et al., 2022)
DEKA Arm	Transhumeral	Active - Electric	Electric motors	>10	10				(HUANG et al., 2024)

Continued on next page

Self Grasping Hand (SGH)	Transradial	Active - Mechanical	Spring mechanism (body-powered)		1			300	(O'BRIEN et al., 2022)
Upper Limb Prosthesis (Leal-Naranjo model)	Transradial	Passive - Cosmetic	None	0	1	1			(TORRES-SANMIGUEL, 2022)
Airbender	Transradial	Active - Pneumatic	Tesla turbine (air powered)	1	1	15			(NAGARAJA et al., 2022)
Motion Control ETD	Transradial	Active - Electric	Electric motor		2	30			(NAGARAJA et al., 2022)
Hosmer Hook Model 5XA	Transradial	Active - Mechanical	Cable			21		87	(HAVERKATE; SMIT; PLETTENBURG, 2016)
TRS Grip 2S Hook	Transradial	Active - Mechanical	Cable			21		318	(HAVERKATE; SMIT; PLETTENBURG, 2016)
Otto Bock VO Hand	Transradial	Active - Mechanical	Cable			21		395	(HAVERKATE; SMIT; PLETTENBURG, 2016)

Continued on next page

Customized 3D-Printed Prosthesis (Raptor Reloaded variant)	Wrist disarticulation	Active - Mechanical	Cable-driven			1 child	<$20 USD	<500	(XU et al., 2017)
Prosthetic Hand Prototype 1	Transradial	Active - Electric	Electric (Servomotors)	2	2	5 amputees	Low-cost, not precisely stated	350	(PRAKASH et al., 2020)
Prosthetic Hand Prototype 2	Transradial	Active - Electric	Electric (Servomotors)	5	16	5 amputees and 8 intact subjects	Low-cost, not precisely stated	∼1000	(PRAKASH et al., 2020)

Continued on next page

Underactuated Anthropomorphic Finger	Transcarpal	Active - Electric	Electric motor	1	1	None (engineering study, no clinical test)	Low (3D printed)	Not specified	(OMARKULOV et al., 2015)
Paediatric Soft Robotic Hand Prosthesis	Transradial	Active - Electric	3 DC micro motors, cable-driven	3	2	Prototype phase	~70 USD (materials)	230	(MOHAMMADI et al., 2020)
Cosmetic Upper Limb Prosthesis (Radosh et al.)	Transradial	Passive - Cosmetic	None	N/A	N/A	1 (female patient)	~2500 PLN (prototype)	314	(RADOSH et al., 2017)

Appendix 2: Features equations

A2.1. Features equation in time, frequency, and time-frequency domain

Table Appendix 2.2 – Time-Domain features.

Feature	Equation	Characteristic
IEMG	$IEMG = \sum_{t=1}^{T} \lvert x_t \rvert$	Total muscle activation level.
MAV	$MAV = \frac{1}{T} \sum_{t=1}^{T} \lvert x_t \rvert$	Mean signal amplitude.
MAV1	$MAV1 = \frac{1}{T} \sum_{t=1}^{T} w_t \lvert x_t \rvert$ with stepwise w_t	Weighted MAV using a window to emphasize the center portion of the signal.
MAV2	$MAV2 = \frac{1}{T} \sum_{t=1}^{T} w_t \lvert x_t \rvert$ with smooth w_t	Modified MAV with continuous weights for smoother emphasis across the window.
RMS	$RMS = \sqrt{\frac{1}{T} \sum_{t=1}^{T} x_t^2}$	Relates to muscle contraction force.
SSI	$SSI = \sum_{t=1}^{T} x_t^2$	Energy index; sum of squares.
VAR	$VAR = \frac{1}{T-1} \sum_{t=1}^{T} x_t^2$	Statistical variance.
LD	$LD = \exp\left(\frac{1}{N} \sum_{t=1}^{N} \log \lvert x_t \rvert\right)$	Log Detector (LD); geometric mean of rectified EMG, highlights small fluctuations and compresses signal amplitude range.
WL	$WL = \sum_{t=2}^{T} \lvert x_t - x_{t-1} \rvert$	Signal complexity indicator.
ZC	$ZC = \sum_{t=1}^{T-1} [sgn(x_t x_{t+1}) \wedge \lvert x_t - x_{t+1} \rvert \geq \theta]$	Zero crossings indicating frequency content.
AAC	$AAC = \frac{1}{T} \sum_{t=2}^{T} \lvert x_t - x_{t-1} \rvert$	Average absolute amplitude change.
WAMP	$WAMP = \sum_{t=1}^{T-1} f(\lvert x_t - x_{t+1} \rvert)$	Number of large amplitude variations.
SSC	$SSC = \sum_{i=2}^{N-1} sgn((x_i - x_{i-1}) \times (x_i - x_{i+1}))$	Counts slope reversals.

MAVS	$MAVS = MAV_{w+1} - MAV_w$	Difference in MAV across windows.
MHW	$MHW = \sum_{i=0}^{T} (x_i w_{i-k})^2$	Energy from multiple Hamming windows.
AR	$x_t = \sum_{p=1}^{P} a_p x_{t-p} + w_t$	Auto-regressive linear prediction model.
CC	$c_p = -a_p - \sum_{l=1}^{p-1} \left(1 - \frac{l}{p}\right) a_l c_{p-l}$	Cepstral coefficients from AR.
KUR	$KUR = \frac{1}{T} \sum_{t=1}^{T} \left(\frac{x_t - \mu}{\sigma}\right)^4 - 3$	Measures peakedness relative to a normal distribution.
SKW	$SKW = \frac{1}{T} \sum_{t=1}^{T} \left(\frac{x_t - \mu}{\sigma}\right)^3$	Indicates asymmetry of the signal distribution.
ASS	$ASS = \left\lvert \sum_{n=1}^{k} (k_n)^{\frac{1}{2}} \right\rvert$	ASS involves full-wave rectification and integration of the rectified EMG signal, reflecting overall muscle activation strength.

Table Appendix 2.3 – Frequency-Domain features.

Feature	**Equation**	**Characteristic**
MNF	$MNF = \frac{\sum_{j=1}^{M} f_j P_j}{\sum_{j=1}^{M} P_j}$	Mean frequency (spectral centroid).
MdF	$\sum_{j=1}^{MdF} P_j = \frac{1}{2} \sum_{j=1}^{M} P_j$	Frequency splitting the spectrum in half.
MP	$MP = \frac{1}{M} \sum_{j=1}^{M} P_j$	Mean power of the spectrum.
SM[k]	$SM_k = \sum_{j=1}^{M} P_j f_j^k$	k-th spectral moment.
FR	$FR = \frac{\sum_{j=LLC}^{ULC} P_j}{\sum_{j=LHC}^{UHC} P_j}$	Low-to-high frequency power ratio.
PF	$PF = \max(P_j)$	Peak frequency (dominant component).

Table Appendix 2.4 – Time-Frequency features.

Feature	**Equation**	**Characteristic**
WT	$WT[n,s] = \sum_{t=0}^{T-1} x[t] \cdot \psi^*_{s,n}[t]$	Discrete Wavelet Transform (DWT); analyzes signals at different frequency scales and time resolutions using wavelet bases.
mDWT	$mDWT_l = \sum_{\tau=0}^{T/2^l-1} \left\lvert \sum_{t=1}^{T} x_t \psi_{l,\tau}(t) \right\rvert$	Multiscale energy feature extracted from DWT decomposition level l.
sFT	$STFT[n,k] = \sum_{m=0}^{M-1} x[m] \cdot w[n-m] \cdot e^{-j2\pi km/N}$	Short-time Fourier Transform; localized spectrum using sliding window $w[n]$ for time-varying frequency analysis.
Cohen Class	$C[n,k] = 2 \sum_{\lvert m\rvert<M/2} G[n,m] \cdot (x[n+m] \cdot x^*[n-m]) e^{-j2\pi km/M}$	Bilinear time-frequency distribution; kernel $G[n,m]$ reduces cross-terms in multicomponent EMG signals.
S-transform	$S[n,k] = \sum_{m=0}^{N-1} e^{-\frac{2\pi^2 m^2}{k^2}} X[k+m] e^{-j\frac{2\pi mn}{N}}$	Scalable Gaussian window with Fourier transform; preserves time-frequency resolution and phase.
BD	$G[n,m] = \left(\frac{\lvert 2m\rvert}{\cosh(2n)} \right)^{\beta} \cdot \mathrm{sinc}(m)$	Discrete B-distribution kernel with sharp cut-off for cross-term suppression; β controls smoothing in ambiguity domain.